

**The Feasibility of  
A Human-powered Flight  
Between Crete and the Mainland of Greece**

**VOLUME II**

Collected Papers of the Daedalus Project Working Group  
April, 1986

© 1986

Department of Aeronautics and Astronautics  
Massachusetts Institute of Technology

and the

National Air and Space Museum  
Smithsonian Institution

## Contents

This volume contains an unedited, unreviewed collection of papers prepared by members of the Daedalus Project Working Group. Included are:

1. Human Factors by Steven R. Bussolari and Ethan R. Nadel.
2. Daedalus Airfoils by Mark Drela.
3. Feasibility Study on the Implementation of a Flight Control System in the Daedalus Human Powered Aircraft by Stephen L. Finberg, R. Bryan Sullivan, and Steve Hall.
4. Estimate of the Diameter Required for the Fresh-Air Intake of the Daedalus Fuselage, by Theodosios P. Korakianitis.
5. Climatological Study of the Kithira Straits for Project Daedalus by Jonathan Wyss.

## CHAPTER IV - HUMAN FACTORS

### Introduction

The design configuration of a powered aircraft, from heavy lift transport to supersonic fighter, is strongly influenced by the characteristics of its propulsion system. The technological challenge of the Daedalus flight is a direct result of the use of the human pilot as the aircraft powerplant. The aeronautical engineer, who is unable to significantly alter the design of the human engine, is faced with the problem of optimizing the airframe to effectively match the capacity of the human pilot as the source of mechanical power as well as manual controller and decision-maker. In order to perform this optimization, it is necessary to formulate engineering models for human performance that may be combined with similar models for the aircraft. The resulting pilot/aircraft combination is then subject to analysis by formal engineering methods.

Early human-powered aircraft (HPA) required a relatively high power output from the pilot for flights of a few minutes duration<sup>1</sup>. As the aircraft technology advanced, the power required of the human pilot in order to sustain flight was reduced. This resulted in a significant increase in flight duration and distance, eventually leading to the flight of the Gossamer Albatross (2 hours 49 min / 23 statute miles). Continued progress in the technology of human-powered flight has brought forth the fundamental question that faces the designer of the next generation HPA: what are the limits of the human's capacity for long duration power generation and how do those limits affect HPA duration and range?

The production of mechanical power by humans has long been the subject of study by a considerable number of investigators. An exhaustive review of these investigations is beyond the scope of this report. In lieu of such a review, a general summary of human power measurements as reported in the literature has been compiled and is presented in Figure IV-1. The power produced by human subjects is plotted against the length of time during which that power was produced. The methods employed in the investigations summarized in Figure IV-1 vary widely as do the results. It is important, however, to note that the measurements of human power limitations are extremely difficult to perform, simply because each measurement must be carried out until the test subject is exhausted. The physiological preparation and psychological motivation of the test subject becomes an important experimental variable that is difficult to control in a repeatable fashion. A further limitation of the reviewed literature was the fact that important parameters, including test subject body weight, level of training, and details of the measurement techniques are not uniformly reported. The result is that limits of human endurance as expressed in Figure IV-1, while useful for establishing rough bounds on the problem, are of little help in establishing the engineering feasibility of the Daedalus flight.

The research described in this Chapter was performed to formulate preliminary answers to the following questions:

- 1) What are the physiological mechanisms that limit the duration of human power production?

- 2) What power level (per unit of body weight) can be expected from a human pilot given a certain level of athletic ability and endurance training?
- 3) What countermeasures are available to ensure that physiological limits are not encountered during the Daedalus flight?
- 4) How large is the population pool from which appropriate pilots may be selected?

#### Background

In order to move an object over a given distance, energy must be generated and converted to mechanical work. An automobile, for instance, requires the delivery of fuel and oxygen to the cylinders, in which energy is released by combustion. Similarly, a human requires the release of chemically bound energy to provide for both the contraction and relaxation processes in skeletal muscle. Energy is released to the muscle cells by the hydrolysis of specific high-energy compounds, adenosine triphosphate and creatine phosphate. Since skeletal muscle stores these compounds in very small quantities, capable of supporting activity for a few seconds at best, continuous activity can be sustained only by providing sufficient delivery of oxygen and fuel to the muscle from elsewhere. The complete oxidation of the available fuel provides for the resynthesis of the high energy compounds, making them available for hydrolysis and release of energy. An adequate delivery of oxygen and fuel ensures that adenosine

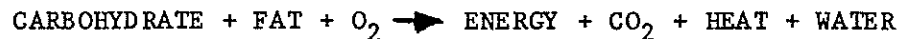
diphosphate is re-energized to adenosine triphosphate at a rate equivalent to the hydrolysis rate.

Oxygen and fuel are delivered to muscle by an integrated organ system response that is mediated by reflexes sensitive to the energy requirement. The body's fuels are stored in relatively large quantities in different sites. Most of the stored energy is in the form of triglycerides, or fats, located in adipocytes (specialized fat storage cells). An average-sized person carries 100,000 kcal of potential energy in adipose tissue (it takes only 100 kcal to run one mile). The rest of the stored energy is in the form of glycogen; around 1500 kcal of potential energy in this form is stored in the liver and skeletal muscle. Despite the tremendous supply of fuel stored in these depots, they require mobilization and transfer by nervous and endocrine reflexes in order to be available for oxidation.

Although there is an abundant store of fuel in the body, the body's oxygen store is only on the order of one liter, a volume that can support moderate exercise for 30 seconds at best. Thus, oxygen must be continuously transported from the ambient air to the muscle mitochondria in which the oxidative machinery exists in order to provide for the oxidation of fuels and the continuous release of energy. This is accomplished by increasing the rate of pulmonary ventilation to maintain a high oxygen tension in the lungs, ensuring optimal transfer of oxygen from air to blood, and by increasing cardiac output, ensuring a sufficiently high flow of oxygenated blood to the muscles. The integrated organ system response to the elevated energy requirement in muscle during physical activity involves the close coupling of the pulmonary and cardiovascular oxygen

delivery systems to the oxygen acceptor systems in muscle (Figure IV-2).

Potential factors that can limit the regeneration of energy, and therefore the ability to maintain power output, can be deduced from the energy production equation:



During activity up to 1.5 - 2.5 hours, fuel delivery is generally not a limiting factor. Oxygen delivery can be limiting if the energy demand from muscle exceeds the body's ability to deliver oxygen via, primarily, the cardiovascular system (the pulmonary system in healthy people exercising at sea level, for instance, is rarely limiting). Since anaerobic sources of energy production are inefficient in humans, and since they carry with them the penalty of decreasing the pH of muscle and thereby rendering it even less able to metabolize fuels aerobically, these need not be considered further. Finally, the build-up of the heat produced as a by-product of metabolic activity can be limiting if the body is unable to dissipate this heat at its rate of production (the rate of heat production during moderate exercise is 600-1000 watt, sufficient to raise the body core temperature 1 degree Celsius every 5-8 minutes if no increase in the rate of heat dissipation occurs).

#### Approach

In order to predict the maximal power output we would expect from a pilot during a flight of at least four hours' duration, we needed to

determine experimentally whether humans reached their limits in the oxygen, fuel or heat transport systems at a sufficiently high power output on a cycle ergometer.

The maximum oxygen uptake, or maximum aerobic power of any individual is an objective index of that person's functional capacity to generate power. In elite endurance athletes the maximum oxygen uptake ( $\text{VO}_2$ ) may be as high as 70 to 80 ml  $\text{O}_2$  per min per kg of body weight. Assuming a 20 per cent efficiency, we might expect a maximum output of mechanical work to be on the order of 4.5 W per kg of body weight from such an individual. Middle-aged, healthy adults average around 35 to 40 ml  $\text{O}_2$  per min per kg and are able to increase this maximum by up to 20 per cent within three months of beginning a moderately serious program of physical conditioning.

Increasing one's maximum aerobic power ( $\text{VO}_2$  max) provides obvious practical benefits. It allows a given work output, requiring a given rate of energy release in muscle (and therefore a given  $\text{VO}_2$ ), to occur with relatively less reliance on anaerobic process. This minimizes the production of the anaerobic metabolites, particularly excess lactic acid and hydrogen ion ( $\text{H}^+$ ). When the  $\text{VO}_2$  is less than 50 per cent of  $\text{VO}_2$  max, the net energy release in active muscle is essentially anaerobic. Above 60 per cent  $\text{VO}_2$  max in the average person, there is an increasingly greater reliance on anaerobic processes for the release of energy, with the consequent production of the anaerobic metabolites. Unless the body can adequately buffer the excess  $\text{H}^+$  in such conditions, exercise will eventually be limited by the developing acidosis in muscle. We expected that highly fit athletes, who have induced adaptations to physical activity



in both the oxygen delivery and oxygen acceptance systems, would provide nearly all of the energy release in muscle aerobically at 70 per cent of  $\text{VO}_2$  max. In such conditions there should be no disturbances in the blood (or muscle) acid-base balance, and oxygen delivery to muscle should not be a limiting factor to prolonged exercise<sup>2</sup>. Such athletes should be able to perform continuously until fuel availability or body temperature (or body fluid balance, which will affect temperature) limit further activity.

Our experimental plan was formulated as follows. The object of the feasibility study was simply to determine whether athletes could produce a high power output continuously for four hours, and to follow certain physiological variables that indicate oxygen and fuel availability to muscle throughout the test. By providing water ad libitum and controlling the environmental temperature, we expected to minimize the adverse effects of progressive dehydration and excessive hyperthermia during the test. Prior to testing, however, we needed to recruit athletes who had a high  $\text{VO}_2$  max and were motivated to participate in such a feasibility study.

We recruited volunteers by announcement through the news media. Recruitment was informal. We interviewed a number of potential volunteers by telephone and selected five for further study. These included a female national class field hockey player, a male amateur tri-athlete, a female amateur tri-athlete, a male national class wrestler, and a male national class bicyclist. We planned to perform  $\text{VO}_2$  max tests on each of these volunteers in order to determine their maximum power outputs and their power outputs at 70 per cent  $\text{VO}_2$  max. This latter determination would be an essential design criterion for the aircraft. We planned to then select

one or more of these volunteers for the long duration (four hour) test.

#### Initial Screening ( $\text{VO}_2$ max) Tests

Determination of maximal aerobic power is a standard procedure for a human physiology laboratory. We brought the five volunteers to the John B. Pierce Foundation Laboratory at Yale on a Saturday morning. After a brief orientation, we proceeded to test each of them in order to determine  $\text{VO}_2$  max.

$\text{VO}_2$  max was estimated from an incremental test (Reference Balke and Ware). Volunteers exercised using a cycle ergometer in the semi-recumbent position, with the legs nearly horizontal to the ground.  $\text{VO}_2$  was determined continuously by the open circuit method, according to the following technique. The subject breathed room air via a one-way valve. The mass flow rate of expired air was measured by a dry gas meter and the fractional concentrations of oxygen and carbon dioxide ( $f\text{O}_2$  and  $f\text{CO}_2$ ) in the expired air were determined continuously by electronic analyzers.  $\text{VO}_2$  was calculated from  $f\text{O}_2$ ,  $f\text{CO}_2$  and the volume rate of pulmonary ventilation and corrected to standard pressure, temperature and humidity.

The protocol used involved a brief, 5 min warm-up at an exercise intensity around 50 per cent  $\text{VO}_2$  max. Following a 5 min recovery period, the subject began the incremental test. The power requirement of pedaling the cycle ergometer at 60 rpm was adjusted to around 60 per cent  $\text{VO}_2$  max by adjusting the tension of the belt around the flywheel. At 2 min intervals the power requirement was increased by 180 kg-m/min, or around 30 W. The

subject maintained pedalling frequency until he or she could no longer do so, despite the encouragement offered by the investigators. The objective criteria for  $\text{VO}_2$  max included: 1) a  $\text{VCO}_2/\text{VO}_2$  ratio of greater than 1.1 (indicating excessive hyperventilation) and 2) no increase in  $\text{VO}_2$  despite an increase in power requirement (levelling off). The  $\text{VO}_2$  vs power output data are shown in Figure IV-3.

Table IV-1 shows the salient features of the initial screening tests. Four of the five volunteers had  $\text{VO}_2$  max values in the range of elite athletes. We selected the top two of these athletes, based upon their maximal power outputs, to return for the four hour tests. Computed power output at 70 per cent of maximum for these two people was around 3 W/kg. This value was transmitted to the aircraft design engineers who determined that this power level would result in a flight duration of 4 to 5 hours.

TABLE IV-1  
RESULTS OF INITIAL SCREENING TESTS

	VO <sub>2</sub> max (ml/min/kg)	Wt (kg)	Max P (watt)	100% P/Wt. (watt/kg)	70% P/Wt. (watt/kg)
Subject					
<del>LP</del> LD	55	51.2	206	4.03	2.82
LG	47	82.6	280	3.39	2.37
LM	59	55.6	235	4.24	2.97
PW	60	52.8	206	3.90	2.73
RS	66	73.0	324	4.44	3.11

### Long Duration Tests

The two selected individuals, RS and LM, were invited to volunteer for an experiment in which they would be expected to exercise on the cycle ergometer continuously at power output of 70 per cent of their maximum for four hours. This was to be a simulation of the Daedalus flight, with the proviso that we would optimize environmental conditions and allow them food and water ad libitum. We also wished to measure their metabolic status throughout the four hours by taking blood and expired air samples at frequent intervals. Both accepted and agreed to come to New Haven in late January for tests. RS was scheduled to begin the test at 8:00 am and LM at 1:00 pm.

Upon arrival in the laboratory, each had the EKG electrodes attached and had a catheter inserted in an antecubital vein in the left arm. Each was instructed to maintain cadence in synchrony with a metronome in order to maintain power output. Each had  $VO_2$  measured at intervals throughout. Blood samples were drawn at intervals for measurement of the following: glucose concentration, to assess the body's fuel status; lactate concentration, to assess the relative anaerobiosis and acid-base status; osmolality, to assess the body fluid status; and the change in plasma volume from hemoglobin and hematocrit measurements, also to assess the body fluid status. Measurements of fluid intake were also recorded.

Throughout each experiment the room temperature was adjusted to maintain the subject's comfort. A fan was directed onto the subject's upper body to optimize evaporative cooling and prevent excessive heat storage. Subjects were encouraged to drink water and eat during the bout.

Although both subjects found the test demanding during the first two hours, neither had great difficulty in maintaining cadence. Heart rates during the first two hours averaged between 150 and 160 beats per min for both and  $\text{VO}_2$  values were comparable and steady, between 40 and 43 ml  $\text{O}_2$  per min per kg body weight (Figure IV-4). Power output was maintained at a steady 3 W/kg.

After two 2 hours RS found the going increasingly difficult and was forced to stop at 3.5 hours, complaining of soreness and cramping in his legs. His blood osmolality had begun to climb at 2 hours, reaching 295 mOsm per kg plasma water by 3.5 hours (Figure IV-5), indicating progressive dehydration. His heart rate also began to climb at 2 hours, reaching 180 beats per min at 3.5 hours. Both of these changes suggest an inability to maintain an appropriate distribution of blood flow to muscle and skin. The fact that blood lactate was not elevated implies adequate muscle blood flow. We were not able to measure body core temperature at the end of exercise.

LM, on the other hand, was able to complete the four hours easily, and could have, by her own assessment, continued for another 1/2 to 1 hour. Her physiological picture supports this claim (Figure IV-4 and IV-5). She maintained a steady state in all variables throughout the bout. Of particular interest is that her blood osmolality was maintained, implying adequate replacement of fluid lost during the four hours. Her cumulative fluid intake was around 3000 ml, nearly three times that of RS. Her heart rate never climbed above 160 beats per min, implying a steady cardiac

filling and no pooling of blood in the periphery.

From the physiological measurements we are able to draw several conclusions. Fuel delivery to muscle was apparently sufficient to sustain activity, based upon the steady concentration of blood glucose in both volunteers. Although we did not measure muscle glycogen, we might have expected blood glucose to decline somewhat if muscle stores were fully depleted. Nonetheless, glycogen loading prior to the long duration test should be important to ensure adequate muscle stores. LM employed a glycogen loading regime prior to the test; RS did not. It will be important for the Daedalus pilot to do so.

The fact that blood lactate concentration was not elevated in either subject throughout supports the notion that 70 per cent  $\text{VO}_2$  max can be sustained aerobically for extended periods by endurance athletes.

One likely reason for the difference in performance between our two volunteers was the difference in body fluid status. LM drank freely throughout, maintaining her blood osmolality, while RS drank much less and shared a progressive rise in blood osmolality after 2 hours, indicating progressive dehydration. When water is lost from the body and not replaced, it must be drawn from all the body compartments. Dramatic changes in intracellular water content will have effects upon solute concentration and cellular function. Clearly, such an event must be avoided to ensure optimal performance.

We conclude that a well-trained endurance athlete can exercise at 70

per cent  $\text{VO}_2$  max for four hours in optimal conditions. It appears from this preliminary study that fluid replacement will be an extremely important factor to ensure the maintenance of the physiological steady state. Further, given optimal conditions, neither fuel transport nor oxygen transport to muscle should directly limit performance in this range.

### Conclusions

Based upon the Phase I work described above, several conclusions may be drawn concerning the feasibility of the Daedalus flight in terms of the capabilities of the human pilot. These conclusions are presented in the following paragraphs in answer to the fundamental questions posed in the Introduction to this Chapter.

- 1) The physiological mechanisms that appear to limit the production of mechanical work by humans are related to the storage, transport, and metabolism of fuel and oxygen and the rejection of waste products and heat. Endurance-trained athletes have optimized these mechanisms to maintain key physiological variables in a stable state during exercise at relatively high power output (approximately 70% of maximum oxygen uptake) for long periods of time (several hours). The limits of endurance are characterized by departures from this steady state that result in the breakdown of transport and metabolic processes, with subsequent reduction of power output.
- 2) We have demonstrated that an endurance-trained athlete exercising on a recumbent cycle ergometer is capable of producing power at 70% of



maximum oxygen uptake (corresponding, in this case, to a specific power of 3 watts/kg body weight) for a period of 4 hours. These values of power and duration correspond to the requirements for the Daedalus flight.

- 3) There are training and environmental countermeasures available to ensure that physiological limits are not encountered during the Daedalus flight. Endurance training conducted in conditions similar to those anticipated in flight will aid in the adaptation necessary to provide a robust equilibrium of the physiological mechanisms discussed above. In addition, control of the cockpit environment as well as the intake of water and food will decrease the load on these mechanisms.
- 4) The population pool from which qualified athletes may be selected appears to be sufficiently large to ensure success in locating appropriate pilots. The specificity of muscle group training by endurance cyclists make this group a likely source of pilots given the proposed use of pedaling motion to produce power in the Daedalus aircraft. This was borne out in our feasibility study, in which the two subjects selected for the long-duration ergometer test were endurance cyclists. Regional or National class cyclists appear to have the level of fitness and training necessary to prepare for the Daedalus flight. Previous experience in piloting aircraft would be desirable but not required.

#### Future Work (Phase II AND III)

The human factors study described above was designed to provide

information leading to an assessment of the feasibility of the Daedalus flight. This section outlines the follow-on research necessary during the building, testing, and flight operation activities.

The selection of one or more pilots to participate in the construction and flight test portion (Phase II) of the project should take place as early as practical in those activities. This will ensure adequate time for physiological and flight skills training as well as establishing a comfortable working relationship with all members of the Daedalus team. The members of the Working Group that are charged with pilot selection and training must generate a complete set of requirements for pilot selection and a mechanism for screening applicants at the start of Phase II.

In parallel with the pilot selection activities, the investigation of aircraft human factors should continue with ergometer testing under environmental conditions similar to those to be encountered in flight. In particular, the temperature, humidity, and airflow within the cockpit will have a significant effect on the production of power by the pilot and his/her requirements for food and water in flight. These ergometer tests will be used to fix physical aircraft parameters such as air vent size and capacity of pilot water reservoir. Physiological measurements taken during the flight testing will validate predictions made during the ergometer tests.

The results of Phase II will be incorporated into a generalized pilot training program for the Phase III activities leading to the flight operations in the Aegean. This program will include elements of

physiological and flight training as well as pilot scheduling to account for the tapering of training and diet modification in the days preceeding the long duration flights.

# HUMAN POWER GENERATION

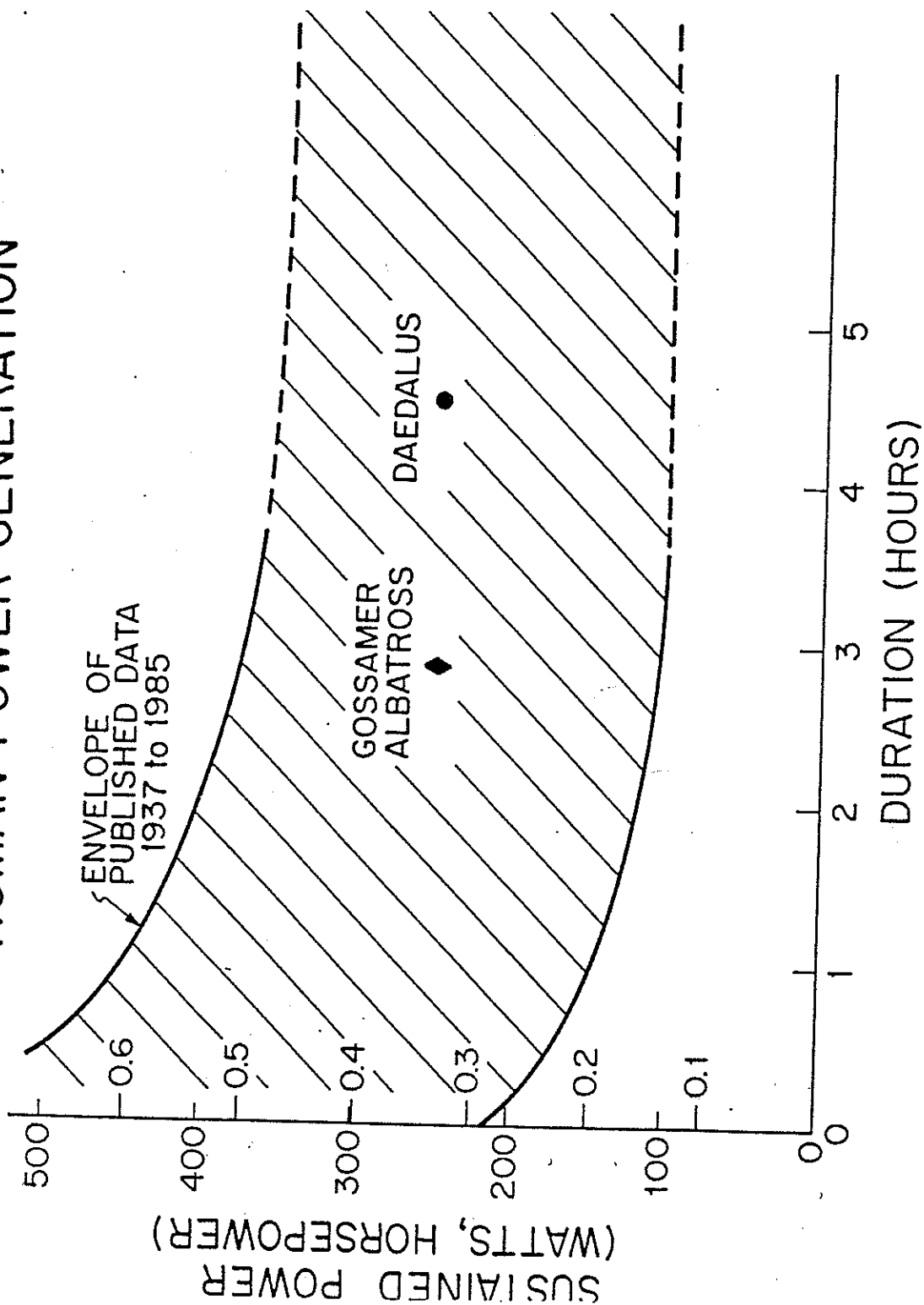
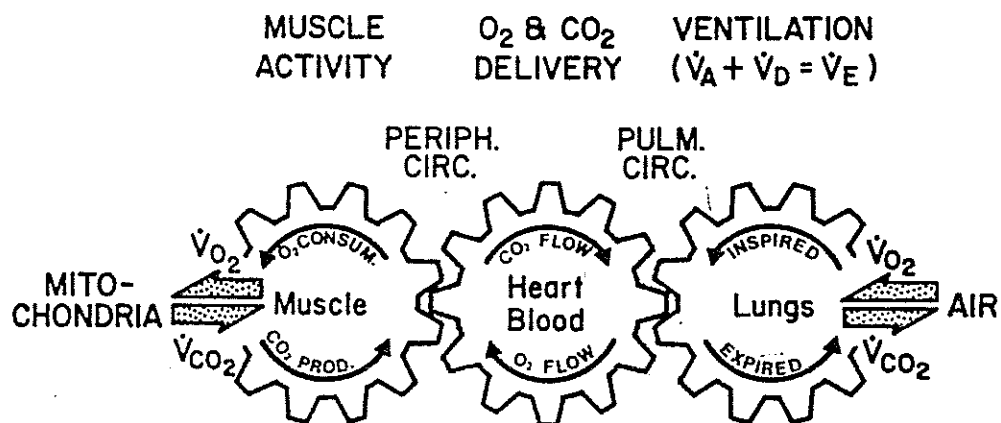
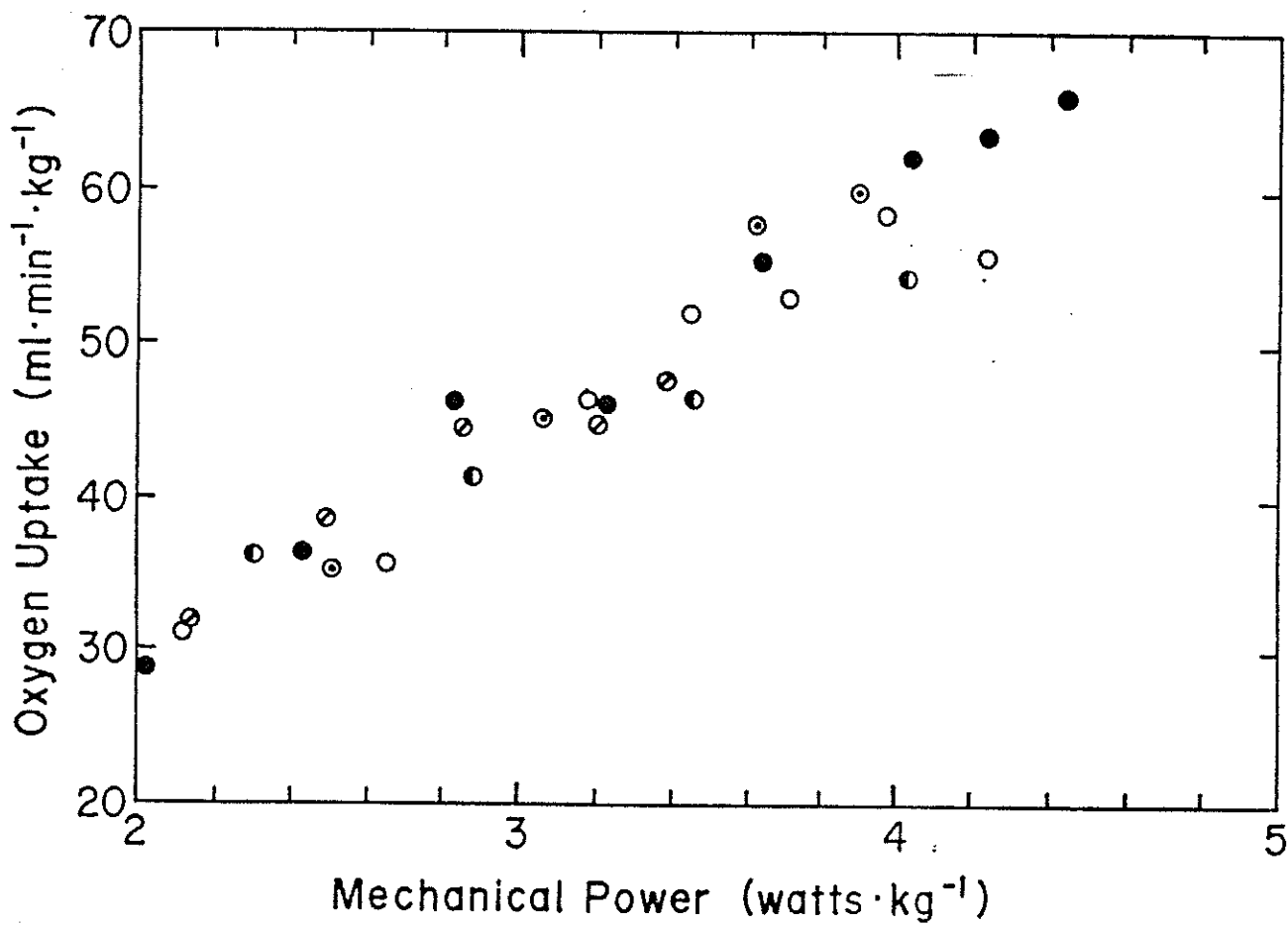


Figure IV-1 Human power output vs time as measured in previous studies (1937 - 1985).



**Figure IV-2** Diagram of coupling between pulmonary, cardiovascular, and muscular systems used in mechanical power productions.



**Figure IV-3** Measured oxygen uptake ( $\text{VO}_2$ ) vs power delivered during  $\text{VO}_{2\text{max}}$  tests. Key to figure: ● - RS, ○ - LM, ● - LG, ⊗ - PW, ⊖ - LB.

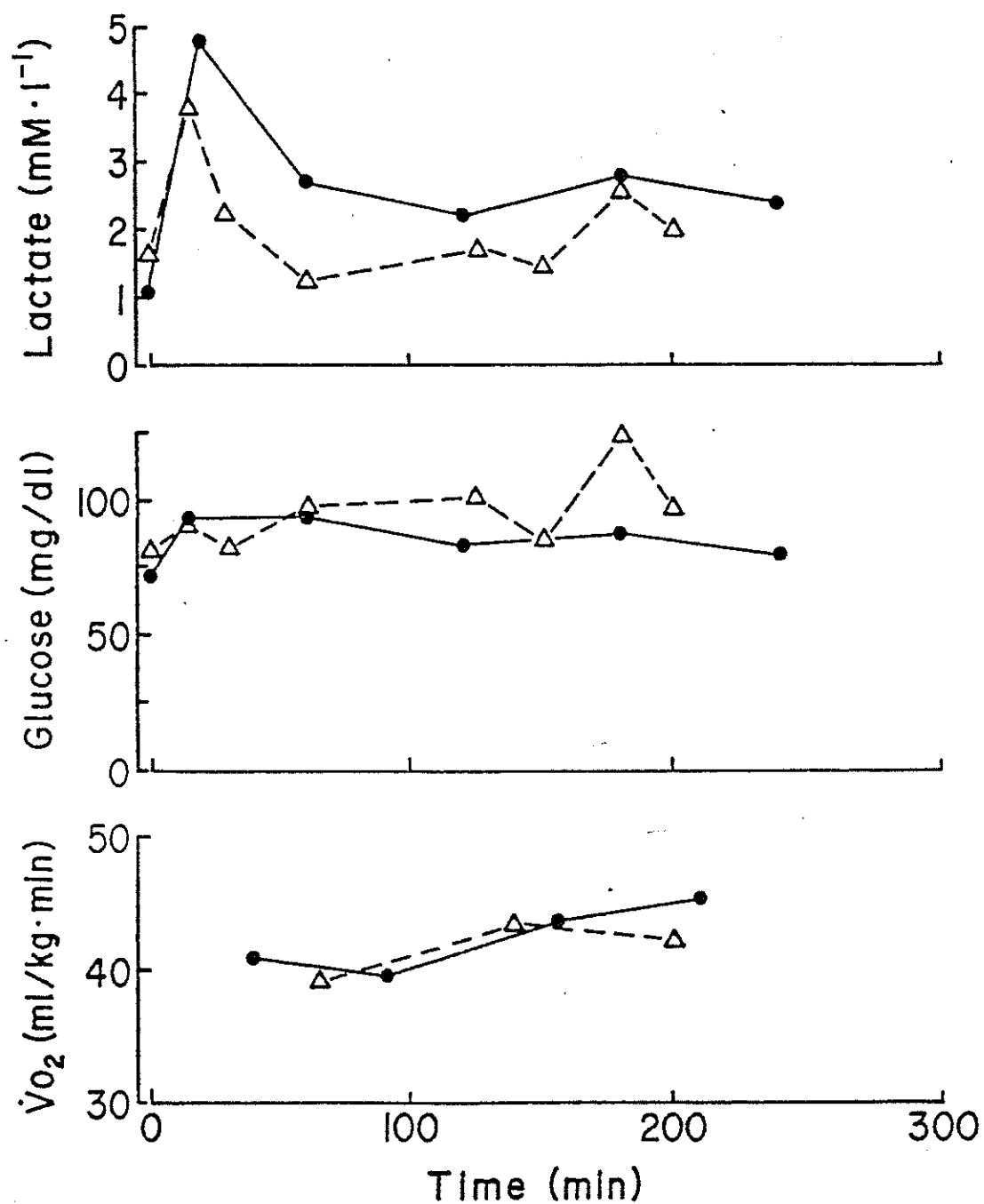


Figure IV-4 Long duration ergometer test measurements: Blood Lactate Concentration, Blood Glucose Concentration, and Oxygen Uptake vs time. Key: ● - LM, Δ - RS.

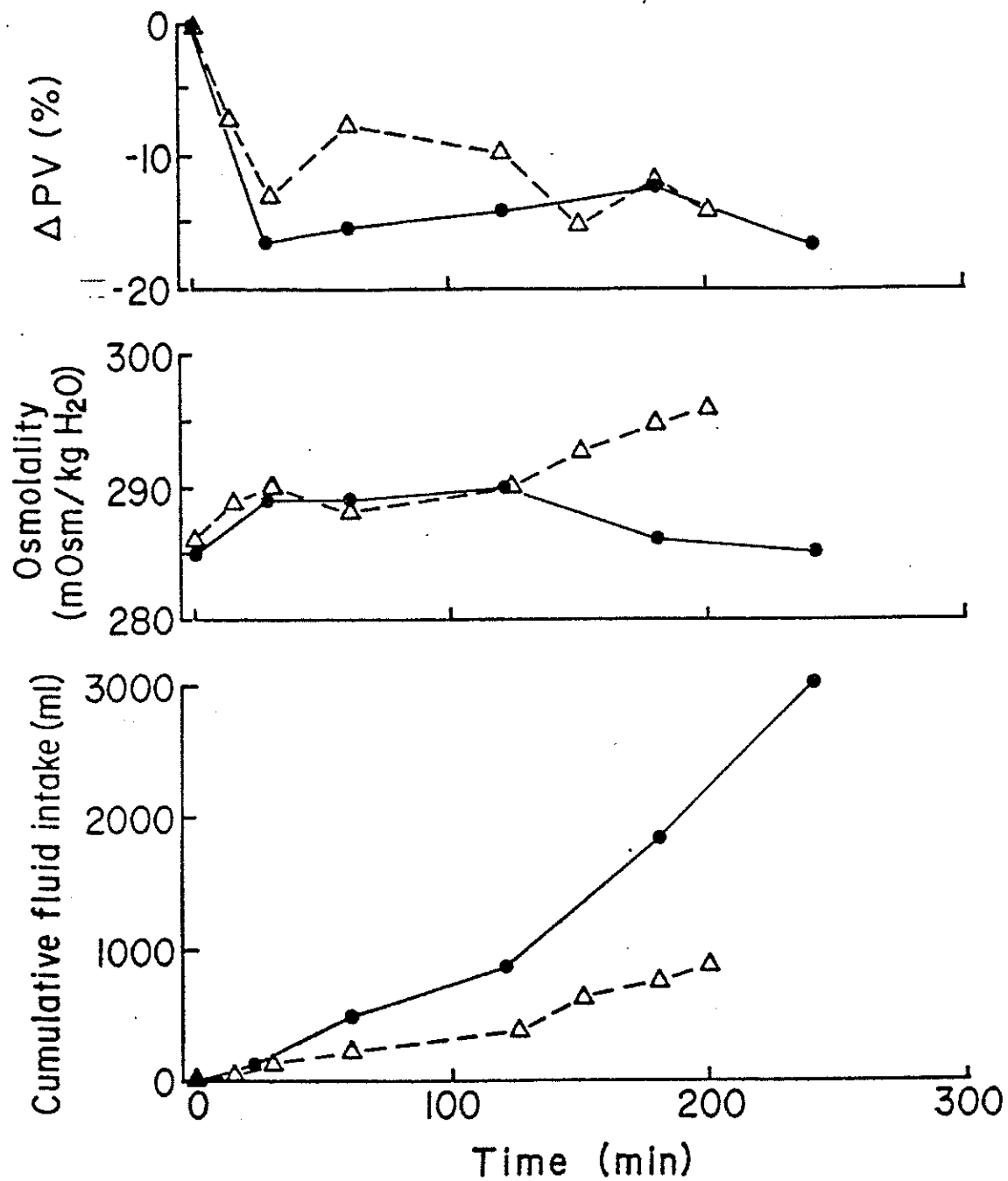


Figure IV-5 Long-duration ergometer test measurements: Plasma Volume, Blood Osmolality, and Cumulative Fluid Intake vs time. Key: ● - LM, ▲ - RS.



## REFERENCES

1. Scientific American article by Langford and Drela
2. American Scientist article by Nadel.
3. - X. References for Figure 1.

# Daedalus Airfoils

## Airfoil Requirements

The aerodynamic performance of a wing and the aircraft as a whole are strongly influenced by the wing airfoil. The *Daedalus* design goal of minimum flight power at a given airspeed dictates the use of an airfoil which has a large lift-to-drag ratio (L/D), implying a large maximum lift coefficient. There is also the additional requirement of a reasonably large L/D at smaller lift coefficients for good penetration capability.

Structural considerations dictate that the airfoil have a pitching moment as small as possible to minimize torsional loads on the wing spar. A small pitching moment also minimizes tail trim loads and hence the trim drag.

The airfoil requirements stated above conflict to some degree. A large L/D and maximum lift coefficient usually result in poor L/D's at lower lift coefficients. The small Reynolds numbers at which the *Daedalus* wing operates favor an airfoil with large pitching moments as will be explained shortly. Thus, good peak airfoil performance is obtained at the cost of degraded high-speed performance and a larger structural weight.

## Design Technique

The airfoils employed in the *Daedalus* wing were designed entirely through numerical design procedures and numerical performance simulations. Preliminary design was performed using a standard inviscid panel method extended to permit calculation of airfoil shape from a specified surface pressure distribution. For viscous performance analysis, the two-dimensional flowfield around the airfoil was calculated using a novel, streamline-based finite volume computational technique. The outer inviscid flow was modeled with an isentropic form of the Euler equations, and the viscous layers adjacent to the airfoil and in the wake were modeled with an integral boundary layer formulation. The effect of the boundary layers on the inviscid flow was represented by adding the displacement thickness distribution to the airfoil contour to determine the effective airfoil shape actually "seen" by the inviscid flow. Transition location on the airfoil surface was determined by a formulation which models the growth of unstable waves in the boundary layers which are known to ultimately lead to turbulence.

The overall viscous prediction algorithm is capable of simulating airfoil flows with limited separation regions, and is thus capable of predicting the onset of stall and the resultant loss of lift and rapid drag rise. Because the physics of separation bubbles are adequately modeled, the drag penalty of separation bubbles can be assessed. In the design of the *Daedalus* airfoils, these predictive capabilities were relied on extensively.

## Design Rationale

A parameter which strongly correlates with airfoil performance at the low Reynolds numbers of the *Daedalus* wing is the pitching moment, with

larger pitching moment implying higher performance. There are two reasons for this. Adding undercamber to the bottom surface, as shown in Figure 2.1, usually adds lift without adding much drag, thus improving both the maximum lift coefficient and the L/D. This added performance naturally results in a larger pitching moment since the additional loading must be added towards the rear of the airfoil if laminar flow is to be maintained on a sizable portion of the pressure surface.

The second reason why high performance at low Reynolds numbers is obtained at the expense of large pitching moment is that a suction surface pressure distribution which minimizes the losses associated with separation bubbles necessarily has a substantial amount of loading towards the rear of the airfoil. To explain this more clearly, it is necessary to examine how the pressure distribution affects bubble losses.

The relation between the loss associated with a laminar separation bubble and the pressure gradient (or equivalently, the velocity gradient), can be obtained from standard boundary layer (BL) theory. The loss accumulation in the BL, which ultimately results in drag, is directly related to the rate of growth of the BL momentum thickness "t" on the airfoil surface. Near the reattachment point which terminates a laminar separation bubble, there exist nearly discontinuous jumps in both the momentum thickness t and the edge velocity u. The fractional jumps  $\Delta t/t$  and  $\Delta u/u$  of these quantities at reattachment are approximately related by

$$\frac{\Delta t}{t} = -(2+H) \frac{\Delta u}{u}$$

Here, H is the shape parameter of the BL velocity profile at the jump, and indicates how close the BL is to separation. A small value of H, typically 2.0 to 2.8, implies the BL is well-attached. A value of H greater than 4 implies the BL is separated.

Figure 2.2 shows typical distributions of u, t, and H which occur in separation bubbles of various sizes. Bubble "size" here refers to the maximum value of H which occurs in the bubble rather to any particular dimension of the bubble. It is clear that large values of H in regions where u is rapidly decreasing result in large increases of t. This can be seen in both the equation above and in Figure 2.2. Clearly, to limit both the overall increase in t across the bubble and the attendant drag penalty, it is desirable to have small bubbles with small values of H. The problem here is that at low Reynolds numbers, large values of H are necessary to produce disturbance growth rates rapid enough to trigger transition within the streamwise extent of the bubble. The value of H in the bubble simply grows downstream until its cumulative effect is sufficient to trigger transition. At first this appears to be a no-win situation: to obtain the transition which prevents a large bubble, it seems it is necessary to have a large bubble in

the first place. It is possible, however, to minimize the peak values of  $H$  which occur in the bubble by sufficiently destabilizing the BL before the bubble, and by avoiding excessively steep adverse pressure gradients at the bubble itself.

One way of destabilizing the BL early is to use a surface roughness strip in front of the bubble. Indeed, if the roughness is substantial enough, transition might occur early enough so that the bubble never forms. The primary disadvantage of using roughness is that ideally the position of the bubble and the transition point should shift with angle of attack so that turbulent flow only occurs in regions of strong adverse pressure gradients. Hence, a roughness strip will produce a drag penalty at lift coefficients below design, and a lower peak lift coefficient due to the jump in  $t$  which the turbulent BL will suffer as it scours across the roughness strip. Of course, even at design lift coefficient, the additional drag of the roughness might be as large as that of a small bubble which achieves the same end.

The most efficient method used to destabilize the BL before the bubble, and the method employed in the *Daedalus* airfoils, is to use a long laminar run (or "rooftop") with a mild adverse pressure gradient in front of the bubble. Such a pressure distribution (labeled A) is shown in Figure 2.3, together with the pressure distribution of a typical front-loaded airfoil (labeled B). In distribution A, strong pressure recovery is applied only after the bubble is firmly reattached. Distribution B does not have the laminar rooftop long enough to permit sufficient destabilization of the BL, which results in a much larger bubble and hence a larger drag. Furthermore, distribution A has lower peak velocities and less turbulent flow than distribution B, which further contributes to smaller drag values.

One feature of pressure distribution A shown in Figure 2.3 is that although it is favorable from the viewpoint of minimizing drag, it also has more pitching moment than distribution B, thus implying a larger structural weight. Since bubble size is influenced by the adverse pressure gradient at the bubble as well as the destabilization before the bubble, the airfoil contour all the way to the bubble is critical and must be carefully maintained with solid surface sheeting; surface undulations due to covering sag are unacceptable. Because distribution A has a longer rooftop, it needs more of the sheeting and hence will again result in a larger structural weight than distribution B. A tradeoff between the aerodynamic and weight considerations of distributions A and B clearly exists.

The final *Daedalus* airfoils are the result of only a minor compromise between these aerodynamic and structural considerations. Analysis indicated that high airfoil performance was more important than the resulting structural consequences in the overall performance of the *Daedalus* aircraft. As a result, the *Daedalus* airfoils have nearly the highest aerodynamic performance possible at their design Reynolds numbers.

One compromise which was made in the *Daedalus* airfoils was the decision not to use a heavily loaded, turbulent pressure surface. The pressure surface loading was made just large enough so that fully laminar flow could still be obtained over the entire lift coefficient range 0.75-1.40.

Although this resulted in a small loss in maximum lift coefficient as compared to a heavily-loaded pressure surface, numerous other advantages appeared. First of all, the loss in lift was compensated by the lower drag of an all-laminar bottom, which is not possible if substantial bottom loading is present. Secondly, the nearly flat bottom of the *Daedalus* airfoils resulted in a reasonable trailing edge angle which is easy to build, and permitted elimination of the cusped, highly cambered trailing edge typical of turbulent-bottom, aft loaded airfoils. Finally, the pressure distribution of an all-laminar bottom produced a 40% pitching moment reduction over that of the turbulent-bottom distribution, permitting a lighter spar design.

Like the airfoil pressure surface, the suction surface is also only slightly compromised with respect to aerodynamic characteristics. In particular, the length of the laminar rooftop actually used in the *Daedalus* airfoils is somewhat shorter than the length which gave the smallest predicted bubble losses. The consequence of this compromise is a 5% drag increase. A compensating factor is that the resulting airfoil has a 15% lower pitching moment than one with an optimum rooftop. Also, the optimum rooftop requires solid sheeting over 75% of the upper surface, whereas the compromised rooftop requires only 55%. Both of these compensating factors result in smaller structural weights.

The aerodynamic design of the *Daedalus* wing is complicated by the fact that the spanwise variation of Reynolds number sweeps across a range (600 000 to 200 000) in which airfoil properties can change drastically. For this reason, using a single airfoil shape across the entire wingspan was deemed inadequate. Three airfoils, optimized for Reynolds numbers of 500000, 375000, and 250000 were therefore developed. They are designated as DA11335, DA11336, and DA11238, respectively, and are shown in Figure 2.4. They differ primarily in shape of the suction surface pressure distribution, with the rooftop length and adverse pressure gradient strength increasing towards the tip to compensate for the lower Reynolds numbers. The predicted polars of these airfoils are shown in Figure 2.5. DA11335 is employed over the entire center panel. DA11336 is used at the break between the outer panels and the tip panels, with the airfoil across the outer panel being linearly interpolated between DA11335 and DA11336. The tip panels employ airfoils which are linearly interpolated between DA11336 and DA11238.

### Summary

The three *Daedalus* airfoils, having entirely laminar bottoms, long rooftops, and moderate pitching moments, have characteristics of both front and rear-loaded airfoil families. The laminar flow on their pressure surfaces persists across the entire useful lift coefficient range (roughly 0.75 to 1.40). In order to achieve this behavior, the airfoils have bottom surfaces with very mild curvatures and reasonable trailing edge angles. These characteristics are desirable from a weight and manufacturing standpoint. The long rooftops give a long laminar run which promotes adequate instability growth and rapid transition at the start of the steep

pressure recovery. This tends to minimize the size and losses of laminar separation bubbles, which almost invariably appear on airfoils operating at low Reynolds numbers.

Feasibility Study on the Implementation of a  
Flight Control System in the Daedalus  
Human Powered Aircraft

by

Stephen L. Finberg

R. Bryan Sullivan

Steve Hall

Submitted to:

National Air and Space Museum  
Massachusetts Institute of Technology

April 9, 1986

Feasibility Study on the Implementation of a  
Flight Control System in the Daedalus  
Human Powered Aircraft

1.0	Introduction .....	2
2.0	Sensors .....	3
3.0	Pilot's Display .....	9
4.0	Autopilot Design .....	10
5.0	Actuators .....	13
6.0	Test Requirements .....	14
7.0	Flight Monitor .....	15
8.0	Communication .....	16
9.0	Power and Weight .....	17
10.0	Conclusion - Summary .....	22



## 1.0 Introduction

Because the ultimate flight of the Daedalus aircraft will require four to five hours to complete, it has been proposed that a flight control system be incorporated into the aircraft to reduce the pilot's mental workload. In addition to doing this, the autopilot will improve the performance of the aircraft by maintaining flight near the aircraft's optimal operating conditions, particularly the velocity that corresponds to the maximum lift to drag ratio. Also, the autopilot will allow the possibility of flight in reduced visibility, specifically at night, as might be necessitated by the short period of calm winds during daylight.

The proposed functions of the autopilot are to hold a desired airspeed, to maintain a wings level attitude, and to hold a desired heading. The airspeed hold system maintains the aircraft's optimum airspeed by commanding the aircraft to gain altitude if the airspeed is higher than optimum. Thus to maintain the desired velocity, the aircraft converts kinetic energy into potential energy. Similarly, if the airspeed is too low, the autopilot causes the aircraft to lose altitude and thus regain velocity. The wing leveler and heading hold system act together to keep the aircraft on the desired course. The wing leveler tries to keep the wings level despite any atmospheric disturbances, thus the perturbations in the aircraft's heading are minimized. The heading hold system observes any drifts in the heading and removes them by commanding a slight roll angle until the correct heading is achieved.

These three autopilot functions appear quite feasible. Based on information collected on potential sensors and based on the performance of an autopilot model operating in a computer simulation, it appears that a control system can be built that will dramatically enhance the flight characteristics of the Daedalus aircraft without adding significant weight.

## 2.0 Sensors

In selecting sensors for an HPA autopilot, several unique considerations apply. First we must minimize overall weight; it is very expensive in terms of pilot energy to fly with any excess baggage! This leads to a further requirement to minimize power consumption. For extended duration flights it is expected that the batteries running the instruments will weigh as much as the instruments themselves.

One factor which helps reduce weight is the low aircraft movement rates expected and the lack of "aerobatic" requirements. Low rates allow the electronics to operate relatively slowly which in turn permits very low power consumption.

### 2.1 Airspeed Sensor

The airspeed sensor will consist of a free wheeling prop with two imbedded magnets coupled to a digital hall effect sensor. Each time the prop rotates, the hall effect switch puts out two pulses. The pulses are coupled to a 555 IC timer operated as a oneshot tachometer that produces an analog output voltage proportional to prop speed and therefore air speed.

The electronics of the sensor is very lightweight, (less than the prop and mounting structure). The connection to the hall effect switch can be made with only two wires, simplifying hook up. This sensor was used throughout the Monarch test flights and demonstrated very high reliability.

The main drawback to this sensor is the relatively high 10 ma bias current of the hall switch. A possible improvement could be to sense prop position capacitively. An investigation will be done to determine if any power saving can be had, and what the weight trade-offs are.

Overspeed and stall warnings can be implemented in the display section by analog voltage comparators on the output voltage or by digital pulse width comparators at the hall switch output.

### 2.2 Altitude Sensors

For low altitude operation, a Polaroid Sonar range finder will be used as an altimeter. With the stock "antenna" its range is limited to less than 50 feet. The effective range

of the sensor can be extended to 100 feet by adding a focusing horn to the antenna at the expense of weight and complexity. The sensed output will be displayed digitally with a resolution of 0.1 foot. To conserve power, readings will be made only once every 3-5 seconds. The display circuit will hold the reading between samples. A second display mode will be available where differentiated altitude is displayed to show sink rate. In this mode a low altitude warning will be provided.

The sonar system is readily available and the readout electronics fairly straightforward. A similar system has demonstrated its reliability on the Gossamer Albatross, and in millions of cameras.

The sonar's main problem is with the high power and current required for each ranging. A short pulse of current of about an amp is required. This will impose some constraints on the power system to avoid interfering with the other sensors. The average current will be held down by limiting the frequency of the rangings; however, this may be a problem if we must operate over choppy seas.

For operation above 50 feet, a sailplane barometric type altimeter/variometer will be adapted to the Daedalus. Operation is required between the expected cliff launch height of 2000 feet and 50 feet, below which the sonar altimeter will take over. As the pilot must monitor sink rate to optimize range, a variometer display is important. Weight will be minimized by removing the altimeter's case and structure, consistent with the low stresses expected.

## 2.3 Pitch and Roll

Electrostatic sensors will provide pitch and roll information necessary for low visibility flight and autopilot operation. Electrostatic sensors measure the earth's electric field. They indicate level when the field is equal at the extremities of the plane. Extensive work has been done by Maynard Hill at APL and model aircrafters demonstrating good reliability in the conditions Daedalus can fly.

The sensors are very light weight and low power. It is anticipated the power consumption will be under 5 mw per axis.

---

Hill, M.L., "Introducing the Electrostatic Autopilot,"  
Astronautics and Aeronautics, Vol. 10, No. 11, Nov. 1972, pp22-31)

Experimental work remains to be done to determine the effects of sensor placement on a mylar and carbon HPA, and the effects on gain and sensitivity at the low speeds Daedalus will fly.

The published work has shown problems operating near thunderstorms and around obstructions, neither of which are conducive to HPA flying!! To demonstrate full confidence in these sensors, test flight data must be taken over typical terrain and in expected (otherwise acceptable) flying conditions.

If electrostatic flight tests demonstrate problems, an alternate pitch - roll sensor is a tuning fork rate gyro. While autopilot simulations have shown angle information superior, acceptable performance can be had from rate data. The rate gyro is not subject to atmospheric disturbance, and it would be easier to demonstrate autopilot performance in a lab environment. Unfortunately existing commercial piezo/tuningfork rate gyros require 2 orders of magnitude higher power than electrostatics (600 mw per axis). Discussions with one manufacturer suggest that the power can be somewhat reduced at the expense of maximum rate response, which would not be a problem for our application.

Due to power, cost and time constraints, the rate gyro alternative will be further explored only if the electrostatic sensors exhibit severe problems.

## 2.4 Direction Sensor

To implement a heading hold autopilot function and to allow low visibility flight, a direction sensor must be provided. Several types of sensors can supply suitable data.

### 2.4.1 Magnetic Compass

A single axis flux gate can be used as a compass. It is a no moving part magnetic flux sensor which can sense field direction by changes in the saturation characteristics of a toroidal ferrite core. For a minimal implementation the core is gimbal mounted to allow the pilot to null its output when flying in the desired direction. The feedback operation of the heading hold autopilot is such to keep the sensor nulled.

A bread board version of this sensor has been constructed which weighs 120 grams and consumes 100 mw. It is

anticipated that with better selection of the magnetic core and optimum electronics, the weight can be reduced to 50 grams and the power to 25 mw.

Full 360 degree "strapdown" heading information can be obtained by building two single axis flux gates and combining their outputs, at the expense of slightly more than 2 times the power and weight. It is expected that the single axis null information will be sufficient for the Daedalus mission.

All magnetic compasses have performance limitations because the earth's magnetic field vector is not parallel to the surface, rather it is steeply inclined (~70 degrees in North America). This can cause the compass to get confused if it is tilted. By tilting the sensor sufficiently it is possible to reverse the apparent north direction. This could occur if the craft banks or pitches excessively. By sensing large pitch or bank angles from the angle sensors, data from the compass can be ignored until the normal attitude is re-established. We can minimize any problems by operating the single axis sensor aligned with the inclined field. While the inclination varies in different areas of the globe, it and the deviation (misalignment from true north) change little over the proposed range of Daedalus.

The main advantage of the fluxgate compass over the other possible direction sensors is that it is self contained and requires no active device outside the airplane.

#### 2.4.2 Radio Direction Finder (RDF)

A radio direction finder is a homing type sensor. By using directional type antenna it is possible to "DF" on a radio beacon signal. Using two antenna, one with a sharp null in its pattern and another as a reference, it is possible to get heading error information. Such a system provides the best heading information when operated with the beacon lined up with the null.

This sensor can be used in two ways, it can home on either a strong broadcast station or a beacon located on the lead boat. Homing on a broadcast station has the advantage of not requiring Daedalus ground support personnel to operate a transmitter with its accompanying licensing, and allows a simple onboard receiver.

While many possible broadcast stations are available, there are problems in picking a suitable one over the necessary 60 mile range. Unless the beacon station is located in line

with the destination, the pilot would be required to frequently adjust the antenna to maintain null. Most broadcast signals are subject to considerable propagation variations (fading, etc.) over long distances, depending on the time of day, season and sunspots. These variations can introduce significant errors in the direction information. Further, we must depend on the broadcast station remaining on the air for the duration of the flight.

#### 2.4.3 Follow the Boat

By operating our own transmitter on a lead vehicle we can remove most of the uncertainties. As it is operated over a very short range, the signal arrives from a low and more or less constant angle, giving good separation between direction changes and pitch and roll effects. The main complication is the requirement to maintain a suitably located lead vehicle; this may be a problem during test flights over land. To optimize transmitter size, antenna size and receiver complexity, operation in the short wave band is necessitated.

#### 2.4.4 Optical Seeker

A system similar to the "radio follow the boat" can be done using light (IR or UV). Instead of a radio system, it would substitute a bright beacon on the boat and a lens with photoelectric detector on Daedalus. To avoid homing on other bright sources, the beacon would be uniquely modulated. This seeker would retain most of the features of the radio system while possibly giving a smaller and lighter receiver. A study of the tradeoffs between RF and Optical will be conducted.

Table 2.1 Sensors

Measurement	Usage	Technique
Airspeed	Pilot Display Airspeed Hold	Magnetic tachometer on anemometer
Altitude	Pilot Display Warning	Polaroid Sonar < 50 feet Barometric altimeter > 50 feet
Pitch Angle	Airspeed Hold	Electrostatic Sensor (tuning fork rate gyro)
Bank Angle	Pilot Display Wing Leveler	Electrostatic Sensor
Direction	Pilot Display Heading Hold	Fluxgate Compass Radio Direction Finder Optical DF (local source) (follow the boat) (distant source)

### 3.0 Pilot's Display

A display of the sensors's outputs will be provided to allow the pilot to manually fly the aircraft and to monitor the performance of the autopilot. The display is necessary to allow operation over water where visually judging altitude and speed is very difficult. In addition, it will permit operation at night and in low visibility (light fog) conditions, greatly extending the expected weather (wind) window.

For greater reliability, the display will be interfaced to the sensors independently of the autopilot.

Airspeed will be displayed as a bar graph type speedometer. A blinking warning will be provided below stall speed and above 25 MPH. The high speed warning is necessary due to structural constraints and will be useful during cliff launch "high altitude" operation.

Altitude will be displayed two ways. Below 50 feet, the Polaroid sonar sensor's output will be displayed digitally. The pilot will be able to select either altitude or sink rate. When rate is shown, the display will rapidly flash if the altitude drops below a pilot set limit. Above 50 feet, the display will be a conventional analog sailplane barometer type altimeter.

Bank angle will be shown as a set of crossed lines simulating a conventional artificial horizon.

Heading error will be shown as arrow and dots simulating an expanded part of a compass rose.

The display must be easily readable at night, through sunrise and into the morning. This requirement imposes some severe constraints on a low power display. For the initial flights, until the final display configuration is determined, a LED type display with polarizer will be used. While the power consumption will be high, it has the advantage of ease of availability, and simple modification. Once the arrangement is finalized a tritium or electroluminescent backlit LCD display will be fitted. The LCD will have an order of magnitude lower power consumption than the LEDs.



#### 4.0 Autopilot Design

To illustrate the feasibility of implementing an autopilot into a human powered aircraft, an airspeed hold system and a heading hold system have been designed for the Monarch, the HPA that won the Kremer speed prize in May, 1984. Although the dynamics of Daedalus will differ from those of Monarch, the control system shown here, with only minor adjustment of the feedback gains, should have sufficient capabilities to control either aircraft.

Because weight is such a crucial factor in human powered aircraft, the autopilot presented here was designed assuming no ailerons are on the aircraft, thereby saving the weight of the ailerons, control lines, actuators, and batteries. Lateral control is achieved solely through the use of the rudder. The longitudinal dynamics are controlled through the elevator.

##### 4.1 Airspeed Hold System

The airspeed hold system maximizes the performance of the aircraft by keeping the airspeed close to the velocity at which the maximum lift to drag ratio is achieved. If the aircraft is flying faster than this speed, the control system corrects by gaining altitude, thus converting the excessive kinetic energy into potential energy. If the aircraft is flying slower than the optimal speed, the aircraft dives to regain the necessary velocity.

To implement this system, both an attitude sensor and an airspeed sensor are required. Due to their light weight and low power consumption, electrostatic sensors have been chosen to measure the pitch attitude of the aircraft. Although these sensors tend to have a bias in the measured pitch angle, this bias is removed by closing the outer loop around airspeed. The bias, therefore, is evident only in the startup transients of the autopilot and should have no significant effect on performance.

A block diagram of the airspeed autopilot is shown in Figure 1. The first step in stabilizing the longitudinal dynamics is achieved by feeding back the signal from the attitude sensor. Next, the airspeed is regulated by feeding back the difference between the aircraft's desired velocity and it's actual velocity. Finally, the steady state error is forced to zero by feeding back the airspeed error through a lightly damped integrator. The three feedback signals are summed to create the position signal for the elevator servo. Due to structural load limits, the position signal is limited

to prevent excessive force generation if the autopilot is switched on at high airspeeds.

To illustrate the performance of the airspeed hold system, the following scenario has been simulated (see Figure 2). The pilot is initially flying near trim conditions (approximately 33 feet per second) but with slightly more thrust than required. At time zero, he activates the flight control system and the autopilot begins to stabilize the velocity even though the pilot is supplying more thrust than required. At five seconds into the simulation, the pilot decides to stop pedalling; however, the autopilot maintains the proper speed by converting altitude into velocity. After ten seconds of rest, the pilot starts pedalling again and the aircraft pulls out of the dive to remain at the optimal velocity.

#### 4.2 Heading Hold System

To maintain a wings level attitude and to maintain the proper heading, a lateral control system has also been designed for the aircraft. This system uses electrostatic sensors mounted on the wings to measure the roll angle and uses a low power radio direction finder or magnetic compass to measure the heading. The block diagram in Figure 3 illustrates the organization of the control system.

A six degree of freedom simulation was run for the aircraft with both the airspeed hold and the heading hold autopilots functioning (see Figure 4). At two seconds into the flight, a five degree heading change is selected by the pilot. The autopilot commands a rudder deflection that causes the aircraft to yaw to the right. This causes the aircraft to roll right and therefore to steer toward the desired heading. As the aircraft approaches the commanded heading, the autopilot banks the aircraft slightly to the left, thus reducing the rate of change of the heading. After a slight overshoot, the heading error and the roll angle eventually damp out to zero.

#### 4.3 Controller Implementation

Because the sensor outputs are analog in nature, the proposed simple autopilot function loops can best be implemented as an analog computer using op amps. We can minimize weight and complexity by using modern low power monolithic op amps. It is estimated the controller will consume less than 50 mW.

The control function can also be implemented using a

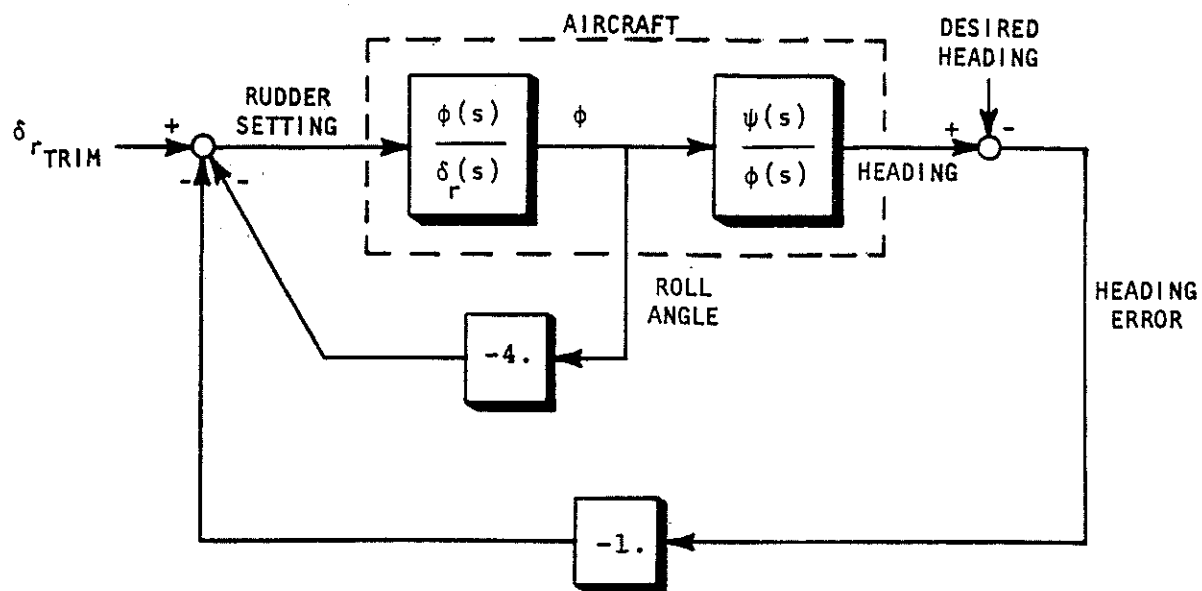


Figure 3. Heading Hold System

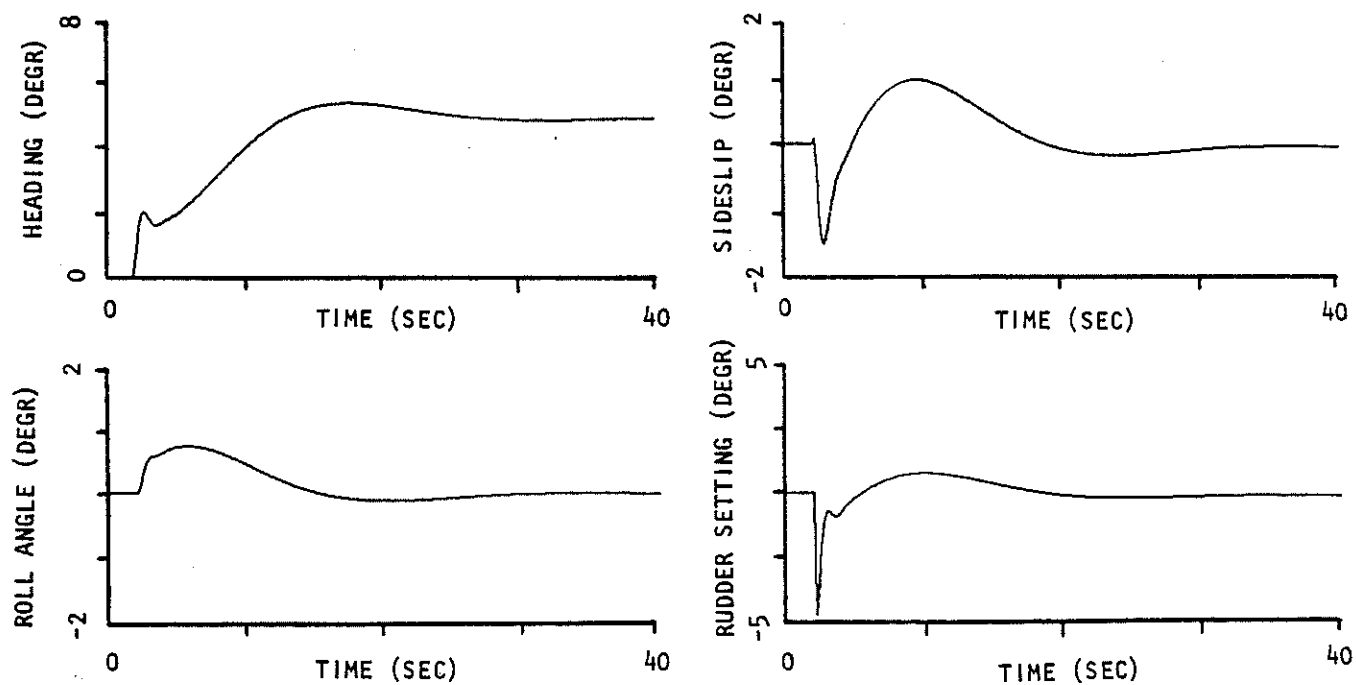


Figure 4. Demonstration of Five Degree Heading Change

single chip microcomputer. Several models are available with the necessary A-D converter built in. Unfortunately the minimum complexity and power requirements are higher. The controller complexity would have to more than double before a digital design would be justified.

#### 4.4 Interface to Actuators

To minimize actuator power consumption, a deadband will be added to each command output. This will allow the actuators to be completely off for a large percentage of the time. It will prevent the system from hunting about the correct operating point, which would consume considerable excess power.

Copper wire or fiber optic connections are being considered to connect the remote actuators to the central computer. The direct wire connection is simplest, but would weigh more and, due to the long lengths needed, may be subject to stray RF fields. While the actual fiber optic cable is very light and immune to disturbance, it requires additional power hungry drivers and receivers.

As an alternative to long interconnections, the entire system (sensors, computer, actuators) could be located in the tail, at the control surfaces. This option becomes particularly attractive if we can assure that autopilot control of the ailerons will not be necessary. The difficulty then becomes getting sensor data to the pilot's display.

## 5.0 Actuators

Because model aircraft servos require little power and are relatively light, they have been selected as the actuators that will drive the aircraft's control surfaces. To reduce the power required by the actuators, the servos will drive trim tabs attached to the trailing edges of the control surfaces. The trim tabs interact with the airflow to produce a moment about the control surface hinge line and thus can be used to control the position of the elevator, rudder, or aileron. This method of control improves the safety of the system since at any time, the pilot, simply by moving the control yoke to the desired position, can overpower the actuators and thus override the autopilot.

A suitable servo is the Ace-Bantam Midget model. It weighs 0.85 oz. (18 grams) and can provide 18 in-oz of torque. At rest it draws 8 mA (at 5V) which increases to 125 mA while torquing against a moderate load. If we assume a 50 percent duty cycle (stopped vs torquing) about 400 mAh of battery capacity is needed per servo for a six hour flight. This can be supplied by four AA (500 mAh) rechargeable NiCad batteries weighing 3.6 oz (85 gr). A better choice would be four 2/3AA size non-rechargeable Mercury batteries to run two servos. They would provide more than 3 times the capacity (1800 mAh) in about the same weight, at the expense of replacement after each flight.

To minimize wiring losses, due to the high current demands of the servo motors, it is necessary to locate the batteries close to each motor. This may create some operational problems with checking and replacing many separate battery packs, especially if aileron servos are required.

## 6.0 Test Requirements

Before the autopilot is used inflight, the individual components of the control system must be tested. The first series of tests will characterize the operation of the sensors in the environment that they will experience in flight. If rate gyros are used, their sensitivity must be tested on a rate table at rotation rates equivalent to those generated by Daedalus. This test is important since the gyros will be operated at a power level less than that for optimum performance. If electrostatic sensors are used, their response must be validated in low air velocities and near large areas of dielectric material, ie.- mylar. The simplest method of achieving this is to mount the sensors on a boom attached to a truck. The boom will be sufficiently high such that the sensors are not affected by the distorted electric field around the truck. Using this technique, the sensors can be tested at various velocities and the effects of atmospheric humidity and temperature can be studied. The performance of the electrostatic sensors must also be characterized near cliffs and near waves. These tests can be performed by mounting the sensors on a radio controlled model aircraft, and flying the aircraft near a cliff and near the surface of the water. The operation of the magnetic sensor must be examined in the highly inclined magnetic field present in Greece. This test can be performed in a lab in Boston where the magnetic field is also highly inclined. Finally, the radio direction sensor must be evaluated to determine its accuracy in a noisy electrical environment.

The second step in the test program is to evaluate the interaction between the aircraft, the sensors, and the control system. Initially this will be done on a radio controlled model aircraft; testing on the actual aircraft will be performed during the middle phase of flight tests. The evaluation of the inflight performance of the flight control system will be greatly simplified by the development of the proposed inflight data recorder.

## 7.0 Flight Monitor

To properly observe the aircraft dynamics and to verify the performance of the autopilot, it will be necessary to record the sensor and autopilot signals. By analyzing the data, it will be possible to optimize the autopilot control law.

A light weight "flight recorder" will be made with an analog multiplexer, a single chip A to D converter, and a "walkman" type recorder. It will record 6 fast channels 8 times a second and 16 slow channels once a second. Due to the limited tape capacity it will only record for 45 minutes.

If real time data is necessary, the same data may be telemetered via a radio similar to the pilot's communication radio.

Table 7.1 lists the parameters to be measured. To gain some additional information, a few extra sensors have been added. They will be used only on early test flights.

Table 7.1

---

Fast Channels 8 readings / sec

1	Internal Auto pilot error 1
2	Internal Auto pilot error 2
3	Internal Auto pilot error 3
4	Prop Rate
5	Prop Torque
6	Pitch Angle / Rate

Slow Channels 1 reading / sec

1	Air speed
2	Altitude (sonar)
3	Altitude (barometric)
4	Bank Angle / Rate
5	Rudder Angle
6	Elevator Angle
7	Aileron Angle
8	Rudder Command
9	Elevator Command
10	Aileron Command
11	Compass error
12	Prop Pitch
13	Slip Angle
14	Pilot Temperature
15	Spare
16	Spare

## 8.0 Communication

Ground to pilot two way communication is necessary for safe and efficient flight operation. A commercial "ham" type VHF FM walkie-talkie will be used. The pilot will have a headband mounted mike and earphone. A push to talk switch will be mounted on the control joystick.

Transmitting with 150 mw of power, a range of greater than three miles over water or level terrain is expected. At this low power level, a full 6 hours of communication can be expected using the radio's normal alkaline battery pack. If higher power is required a larger external battery will be needed.

Total radio weight including battery and antenna will be under 300 grams.



## 9.0 Power and Weight

To be practical, the avionics must not impose a significant weight penalty on the aircraft. To minimize overall weight, both electronics weight and power consumption must be limited. Limiting power is important to minimize the necessary battery weight.

The anticipated flight duration is from 4 to 5 hours. The necessary battery capacity has been calculated based on 6 hours of operation. This allows test time prior to take off and provides some margin to insure reliable operation at the end of the flight when the tired pilot will need the system most.

Table 9.1 summarizes avionics component weight and power consumption goals. It is estimated that the added weight of the control system including batteries and radio will be 850 grams. If ailerons must also be controlled, this will add another 168 grams. The flight test monitor system will add 500 grams.

Consideration was given to wing tip mounted generators to extract power from the tip turbulence, this was dropped due to excess system weight and difficulty in distributing the power to the avionics.

## 9.1 Power Saving Techniques

In addition to using inherently low power devices, several techniques are planned to further reduce power consumption. Data from several sensors is needed only at slow rates. The sonar altimeter is a good example. It takes only 60 ms to take a reading. Altitude readings are needed only every 3 to 5 seconds. To save power it will only be powered for 60 ms out of every 3 seconds. The display will hold the reading between soundings. Provision will be made to further reduce the frequency of readings at high altitude, and to turn it completely off when above it's range, where the barometric altimeter will be used.

## 9.2 Batteries

The sensors, computer, and display will be located in the cockpit area and will be powered from a common battery. The radio will also be in the cockpit, but will be powered from it's own battery due to it's unique voltage requirements. The actuators located at the control surfaces will have their own individual power sources due to long distance wiring limits.

The monitor system is designed as an independent removable subsystem, with it's own battery. As it can only record 45 min of data there is no need for 6 hours of batteries. The weight of the monitor is not a primary design issue since the system will probably be removed during any record duration attempts.

Energy density will be the principal criteria in evaluating candidate battery technologies. Weight is a strong driving factor in HPA design. Next is the ease of testing to assure that full battery capacity is available. It is necessary to be able to perform preflight tests on the batteries, and to have some indication of the health of the batteries in flight.

A prime candidate for the cockpit battery is the Polaroid Pulapulse battery, due to it's demonstrated ability to supply the high peak currents demanded by the sonar altimeter.

Table 9.2 lists several likely battery types and their weights.

While present battery technology appears adequate, new innovations in cell design will be pursued to try to reduce weight further.

Table 9.1 Power and Weight Goals/ Estimates

Load	Weight (gr)	Power (mW)	V	Current mA	6 HR capacity req (mAh)
-----					
SENSORS					
-Airspeed	10		5V	10	60
-Sonar Altimeter	40		6V	2500 peak	55
-Barometric Altimeter	5		6V	1	6 pickoff only
-Roll Electrostat	40	5	+5V		6
-Pitch Electrostat	40	5	+5V		6
-Fluxgate Compass	50	25	5V	5	30
SENSOR	----				-----
SUB TOTAL...	186 gr	.....			163 mAh
DISPLAY					
-Interim LED	100	1400	5V	280	1680 <sup>1</sup>
-Custom LCD	100	15	5V	26	156
COMPUTER	100	50	+5V	5	50
COCKPIT	-----				----- 1
TOTAL.....	386 gr	.....			369 mAh

NOTE 1. The interim LED is planned only for relatively short test flights until a LCD display can be fabricated. LED battery drain capacity not included in totals.

Table 9.1 Power and Weight Goals/ Estimates (Continued)

Load	Weight (gr)	Power (mW)	V	Current mA	6 HR capacity req (mAh)
-----					
ACTUATORS					
-Rudder and Elevator (data line)	36 100		6V		800
-Aileron (data line)	18 100		6V		400
AUTOPILOT -----					
TOTAL.....	640 gr	.....			
RADIO	200		8.4V		500
MONITOR (connections)	300 100		6V		500

Table 9.2 Proposed batteries

---

Cockpit	6V	2x P80 Pulapulse	520 mAh	40 gr	
Radio	8.4V	6x AAA Alkaline	750 mAh	68 gr	
Actuators					
Tail	6V	4x 2/3 AA Mercury	1800 mAh	120 gr	
Aileron	6V	4x N Mercury	800 mAh	50 gr	
Monitor	6V	4x AA NiCad	500 mAh	85 gr	45 min capacity

## 10.0 Conclusions - Summary

To simplify the pilot's task of flying the Daedalus aircraft for over four hours, it has been proposed that an autopilot be included in the aircraft. This system will ease flight during low visibility conditions and will improve the performance of the aircraft by keeping it flying at near optimal conditions. After studying the requirements for the autopilot, the implementation of this system appears quite feasible. Numerous low power sensors and actuators have been identified and procedures for testing them have been investigated. Simulations of a human powered aircraft flying under the control of an airspeed hold and a heading hold autopilot have been performed and look quite promising. For these reasons it is suggested that an airspeed hold and a heading hold control system be included in the final Daedalus design.

ESTIMATE OF THE DIAMETER REQUIRED  
FOR THE FRESH-AIR INTAKE OF THE DAEDALUS FUSELAGE

THEODOSIOS P. KORAKIANITIS,      February 10th, 1936

SUMMARY

I estimated that the diameter required for the fresh-air intake of the Daedalus fuselage is between 80 mm (about 3 inches) in the most-favorable-weather conditions and 130 mm (about 5 inches) in the worst-weather conditions anticipated.

The above numbers correspond to the diameter derived from mass-continuity considerations. The actual diameter of the air inlet should be a little larger (about 20% larger) to allow for entrance effects and loss of total pressure due to friction in the intake duct. If we want to narrow this estimate we should do some experiments.

BACKGROUND

The air admitted to the fuselage serves many purposes. It is used for the respiration system of the engine (pilot). It scrubs the fuselage environment of the carbon dioxide exhaled by the pilot. It serves as a cooling medium to transfer rejected energy out of the fuselage. This energy is the sum of the energy rejected by the pilot, the net energy that radiates into the fuselage and others.

The carbon-dioxide content in the fuselage will be equal to the ambient content at the beginning of the flight. As the fuselage is enclosed, after a few minutes of flight the carbon-dioxide content inside the fuselage will gradually increase (slightly), and with the scrubbing action of the fresh-air intake the constituents of the air in the fuselage will approach a steady state. We assumed here that this change in the constituents of the environment will not alter the psychrometric chart significantly, and that it will not alter the comfort window of the pilot on the psychrometric chart. (The air duct will be pointed so that the pilot will breathe ambient air).

All the results shown here were produced assuming that the speed of the air entering the fuselage is 7.72 m/s (15 knots). The efficiency of the pilot is about 25%. Since the pilot produces about 0.2 kW, the first law of thermodynamics dictates that he or she must reject to the environment (fuselage) about 0.6 kW of energy (heat). Allowing for radiation of energy into the fuselage we produced results for the air flow carrying out of the fuselage 0.7 kW, 1.0 kW and 1.5 kW of energy.

## METHOD

From meteorological data we expect that during the flight the environmental temperature is between 14°C and 18°C (57°F and 64°F), and the relative humidity (rh) is about 70%. These are the conditions of the air admitted to the fuselage. At the exit duct of the fuselage the conditions are those inside the fuselage. Thus in the simplest approach (illustrated in figure 1), we can assume that the mass flow entering the fuselage is the same as that exiting and then the energy balance for the fuselage is:

$$\dot{m} h_{out} = \dot{m} h_{in} + \dot{Q} \quad (1)$$

where  $\dot{m}$  is the mass-flow rate through the fuselage [kg/s]  
 $h_{in}$  is the specific enthalpy of the incoming air [kJ/kg]  
 $h_{out}$  is the specific enthalpy of the exiting air [kJ/kg]  
 $\dot{Q}$  is the amount of energy (heat) that the fuselage rejects to the environment [kJ]

This expression governs the thermodynamic analysis of the fuselage regardless of the various mechanisms that occur to generate the total amount of  $\dot{Q}$ . However, we may be able to design the intake in a way that makes the pilot feel more comfortable than the inside conditions, for example by having the incoming air blow over his or her face and body (and thus gain some additional advantages by evaporation and convection of sweat).

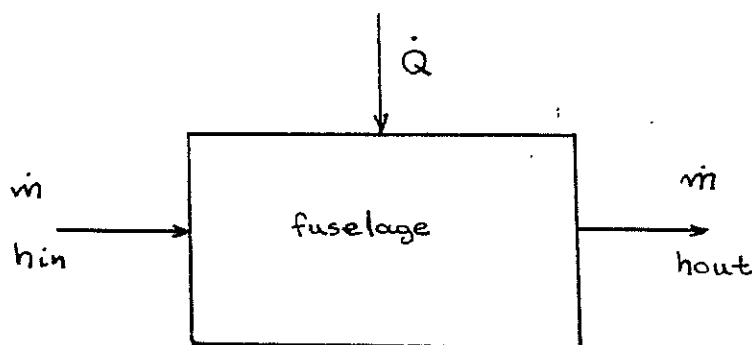


Figure 1: Diagram for the simple thermodynamic analysis of the fuselage

The equations that govern the properties of various atmospheric conditions are derived in most thermodynamic textbooks and are based on the assumption that the constituents form a Gibbs-Dalton mixture. From these equations various psychrometric charts have been published. In this study we used the one published by CIBS, London, 1978, shown in figure 2.



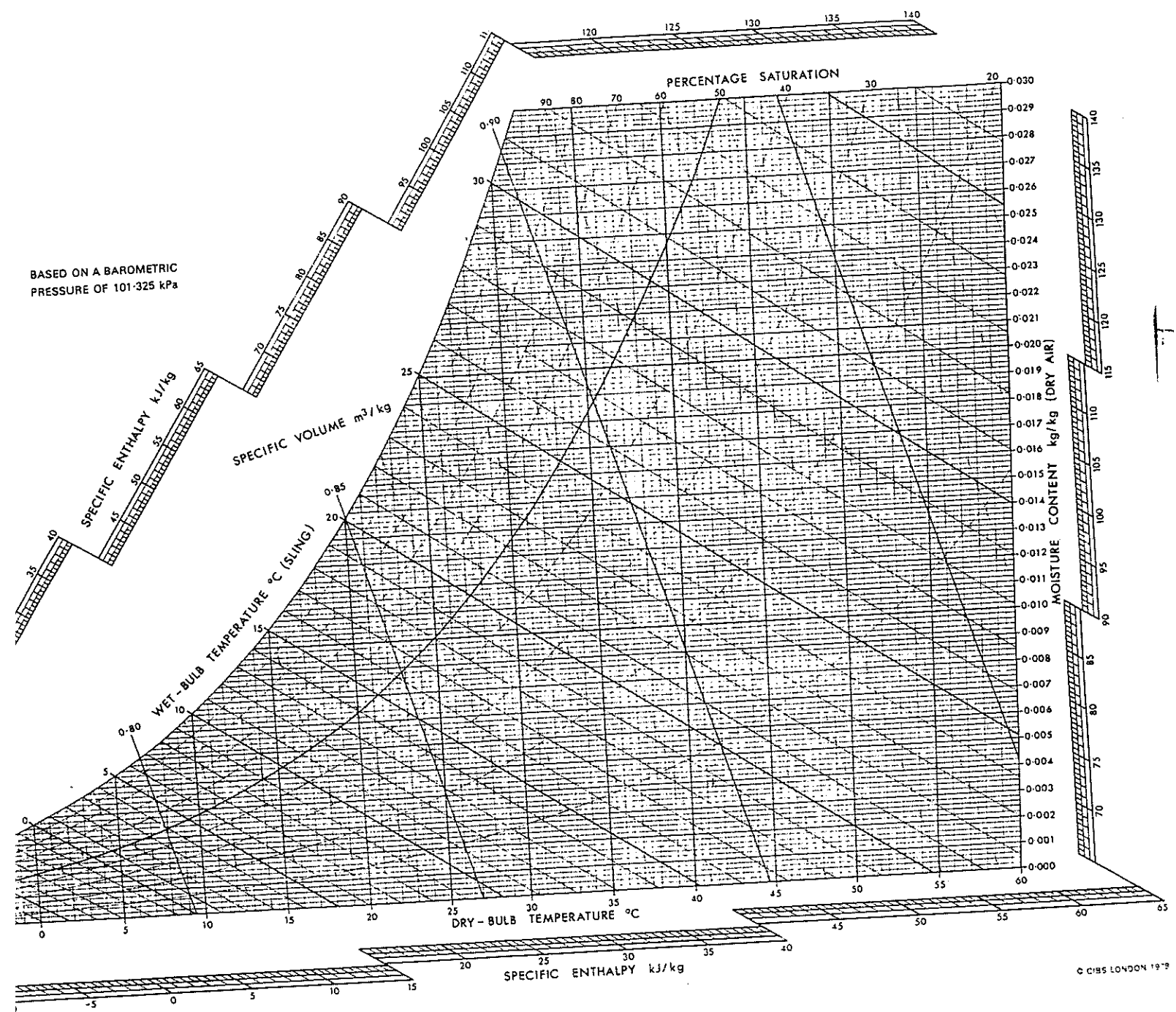


Figure 2: The psychrometric chart  
From CIBS, London, 1978

The equation of continuity through the inlet opening is:

$$\dot{m} = d \frac{\pi D^2}{4} c \quad (2)$$

where  $d$  is the density of the incoming air [ $\text{kg/m}^3$ ]

$D$  is the diameter of the inlet duct

$c$  is the velocity of the incoming air [ $\text{m/s}$ ] (here assumed equal to the velocity of the aircraft)

In the following we also use specific humidity ( $sh$ ) and temperature  $T$ . Using values from figure 2 and specifying temperature and relative humidity for the inlet and outlet conditions we constructed the following table.

Inlet conditions					Outlet conditions				Diameter for $Q$ in kW		
$T$ $^{\circ}\text{C}$	$rh$	$sh$	$d$ $\text{kg.m}$	$h_{in}$ $\text{kJ/kg}$	$T$ $^{\circ}\text{C}$	$rh$	$sh$	$h_{out}$ $\text{kJ/kg}$		$D$ $\text{mm}$	
14	0.70	0.0070	1.2158	32.0	14	1.00	0.0100	39.5	112.5	134.5	164.7
14	0.70	0.0070	1.2158	32.0	21	1.00	0.0157	61.0	57.2	63.4	83.9
18	0.70	0.0091	1.1953	41.0	18	1.00	0.0130	51.3	97.1	116.0	142.1
18	0.70	0.0091	1.1953	41.0	21	1.00	0.0157	61.0	69.5	83.0	101.7
14	0.7	0.0070	1.2158	32.0	21	0.45	0.0070	39.0	116.5	139.2	170.5
18	0.7	0.0091	1.1953	41.0	21	0.58	0.0091	44.3	172.3	206.0	252.3
14	0.70	0.0070	1.2158	32.0	21	0.90	0.0142	57.3	61.3	73.3	89.8
14	0.70	0.0070	1.2158	32.0	21	0.80	0.0126	53.5	66.4	79.4	97.3
18	0.70	0.0091	1.1953	41.0	21	0.90	0.0142	57.3	77.1	92.1	112.8
18	0.70	0.0091	1.1953	41.0	21	0.80	0.0126	53.5	87.9	105.0	128.7

From the above numbers the last four lines seem the most appropriate. They indicate that the diameter required for the fresh-air intake of the Daedalus fuselage is between 80 mm (about 3 inches) in the most-favorable-weather conditions and 130 mm (about 5 inches) in the worst-weather conditions anticipated. The mass-flow rate required in each case can be derived from the equation of continuity (equation 2).

## FURTHER ANALYSIS

Further analysis of the thermodynamics of the fuselage is hampered by the discontinuity and unsteadiness of the processes. Specifically, the pilot uses energy resources from his or her body, may eat food and drink water. All these processes are unsteady and discontinuous. Although the pilot breathes air from the intake duct (at outside ambient conditions), he or she exhales various constituents at the temperature of the body. This temperature is higher than the temperature of the fuselage, and the constituents are different than the constituents in the fuselage. The body of the pilot is cooled through the breathing process and by sweat evaporating (and possibly dripping) from the body. Convection will occur in the parts of the body that are in the stream of the intake duct. Under these circumstances there are too many unknown variables in the problem. Although we can predict that the pilot will feel at least more comfortable than the outlet conditions of table 1 indicate, to be more specific than that we need to resort to experiments.

The experiment we propose is sketched in figure 3. The pilot is working on the ergometer, which is enclosed in a container of volume equal to that of the fuselage. The whole container is inside a room, where the temperature and humidity are controlled and are kept equal to the outside ambient conditions anticipated during the flight. A fan blows air through a hole of variable diameter inside the container. Heat lamps are used to radiate inside the container the amount of solar power we expect that the fuselage will absorb during the flight. These experiments would enable us to optimize the design of the intake duct.

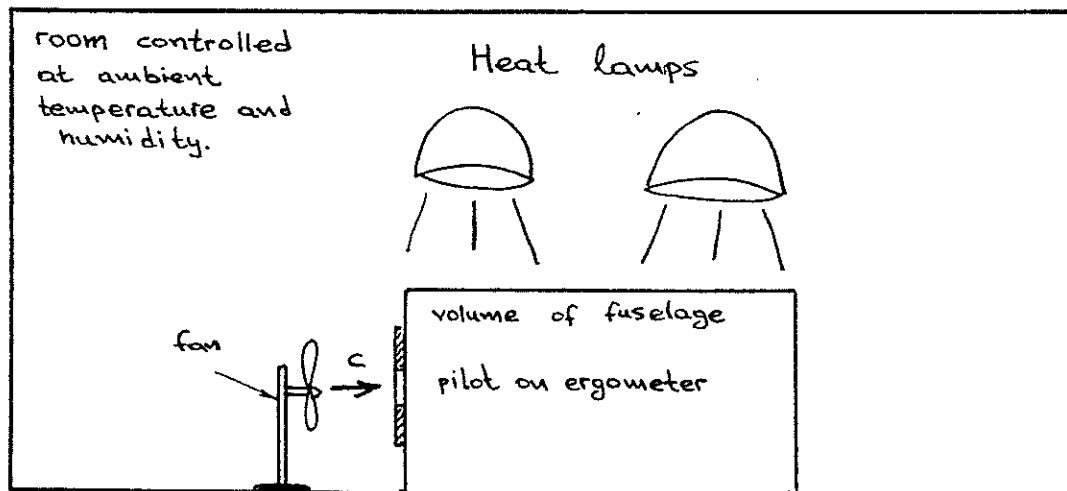


Figure 3: Schematic of proposed experiments

John -  
I don't think  
we should include  
this exp't in  
report as it has  
not been reviewed.  
Perhaps as an  
attachment to  
Vol 2?  
-SB

CLIMATOLOGICAL STUDY  
OF THE KITHIRA STRAITS  
FOR PROJECT DAEDALUS

Jonathan Wyss  
Center for Meteorology and Physical Oceanography  
Massachusetts Institute of Technology

## Introduction

The climate of Crete and southern Greece is, as is that of the Mediterranean region as a whole, generally benevolent: summers are characteristically hot and dry; winters are mild and rainy. The precipitation of the winter months is linked to relatively warm sea surface temperatures (frequently 2 degC warmer than the overlying air). Cyclogenesis, with concomitant stormy winds and rain, results from this interaction of cold polar air from the European land mass with the sea over which it passes. In the summer, intruding air masses from higher latitudes are warmed during their passage over the continent, the instabilities producing cyclogenesis are suppressed, and weak but stable anticyclonic conditions of sunny, warm weather tend to persist over the entire Mediterranean region.

The transitions between these two regimes are often abrupt, and no seasons which correspond to our spring and fall can be accurately defined. Spring is an indecisive period extending from late March to early May, with several attempts by Summer at gaining supremacy. Autumn weather is similarly variable, with rainy periods in September-November appearing with increasing frequency after the isolated thunderstorms of August.

Yet, with respect to human-powered flight - where the aircraft is inoperable in winds greater than a few knots, and the efficiency of the pilot decreases dramatically in hot weather -

it is clear that we must consider spring and autumn most carefully, as it is during these transitional periods that we can expect the greatest percentage of calm, relatively cool days on which a flight would be feasible.

### Data

Data for this study were generously provided by the Hellenic National Meteorological Service, for the localities of Kithira (located on the southern edge of the island by the same name), and Souda (situated on the northern coast of Crete). Each data-set consists of observations made during the five year period from 1979 to 1983 of the following quantities: pressure (mb); dry-bulb temperature (degC); wet-bulb temperature (degC); wind speed and direction (knots); cloud cover (eighths). These quantities were reported at three hour intervals beginning at 00Z (2AM local time).

Not having visited either of the stations, it is difficult to determine what biases the data may have because of the influence of topography or other local features.

There are relatively few reports missing from the data-set; the majority of those missing are during the winter months at Kithira.

### Inter-annual variability

Because there are only five years of data on which to base this climatological study, it was desirable to determine to what extent a time-series for a given year would resemble that

of any other year. To this effect, plots were made of the variation of daily-averaged reports of wind speed, pressure, temperature, and relative humidity. Examples of such time-series of minima, maxima, and averages of these quantities (over a period of a week), are presented in Fig.1 for Kithira, 1979 (Fig. 1a), and 1983 (Fig.1b).

Several features of the regional climate are evident in these graphs. The variance of the time-averaged pressure tends to be greatest in the winter months when intense migrant low and high pressure systems influence the region. Maxima in the wind speed are correlated with, or more usually lag slightly behind, the passage of lows, at which times the region experiences strong northerly flow. The predominance of calm winds during the summer months, the result of small horizontal pressure gradients, is indicated by the lower amplitude fluctuations of the pressure trace from May to August. The temperature is seen to vary sinusoidally with the seasons, reaching a broad maximum over July ( $>25$  degC), and a minimum ( $<10$  degC) in mid February.

Composites of the pressure and temperature time series for successive years (smoothed using a 1-2-1 running average) are presented in Fig.2(a,b) and Fig3(a,b). The lack of significant phase shifts between the annual curves would seem to indicate that a climatology based on periods of a week or longer should be useful in constructing probabilities of the occurrence, or non-occurrence, of a given condition, such as calm winds or moderate temperatures. Most of the data presented here are based on intervals of two weeks, such that for each three-hourly obser-

vation period, there are on the order of  $14 \times 15 = 70$  data points.

### Temperature

Absolute maxima in temperature over the five year period occur 15-30 June (40 degC at Souda, 38.6 degC at Kithira) while the absolute minima occur 15-30 February (-0.6 degC at Kithira, 0.6 degC at Souda).

In general, the diurnal variations in temperature are small compared with seasonal variations. This is illustrated in Figs.4(a,b), where the arrays of climatological average temperatures have been contoured at 5 degC intervals. It does in fact appear from the figures that Souda experiences a significantly larger diurnal variation in temperature than Kithira, a finding which can probably be explained in terms of the topography of Souda Bay.

Figs.5(a,b) explore the seasonal variation of the probability of encountering "moderate" temperatures in the region. In addition to calm winds, moderate temperatures are fundamental to the success of the Daedalus flight. In order to overcome the thermal stresses to which the pilot would potentially be subjected, the air temperature and humidity must be sufficiently depressed to allow for efficient cooling of the cockpit space without requiring too large a volume of ventilation air. This restriction excludes from the outset the period from June to mid-September when the temperature is always above 20 degC, as illustrated in Fig.5a. One should bear in mind that the temperatures quoted in this study were measured in a shaded enclosure, and as such do not represent the additional effects of radiation.



Introducing more stringent requirements on the air temperature (less than 15 degC and greater than 10 degC), Fig.5b indicates that the conditions are met for a three hour period, with 60-80% frequency, in the pre-dawn hours of mid-March - early-April, and again in late November. The bias towards the spring months in terms of desirable temperatures for flight, results from the moderating effect of the sea: the lag in sea surface temperatures relative to the air produces cooling of the overlying air during the spring, but warming in the Fall.

#### Relative Humidity

Values of the relative humidity were calculated from individual observations of the dry-bulb and wet-bulb temperatures. Contoured arrays of the average relative humidity expressed as a percentage, for Kithira and Souda, are presented in Figs.6(a,b). These figures have essentially the same structure as their temperature counterparts, since as the air temperature increases, the relative humidity decreases, if there is no net transport of moisture into the region.

The springtime condition of warm air overlying a colder sea surface, discussed previously in the context of the moderating effect of the sea, is also responsible for the formation of sea fogs. Although no sky-condition or visibility reports were included in the data analysed here (observations of sky cover did not include a code for obstruction by surface phenomena), it is perhaps possible to consider reports of extreme values of relative humidity (greater than 95%) as being indicative of fog formation. Figs.7(a,b) probably accurately resolve the

majority of such events as occurring nocturnally from October to late May. Since the frequencies of occurrence (expressed as tenths of 1%) are relatively low, it would be difficult to determine the climatology of fog formation with any greater accuracy by this method.

### Wind

Wind roses were constructed for each hour and two week period for Kithira and Souda. From this analysis it is apparent that the dominant wind directions are northerly and westerly; otherwise it is, as often as not, calm in the region. The wind rose data is summarized in Figs.8(a,b), where the curves A and B represent climatological averages at 00Z and 12Z respectively. Winds from the southern sector are seen to be almost nonexistent; they occur with near zero probability at Souda (perhaps due to the protection of the surrounding topography), and at 12Z, but not at 00Z, at Kithira (possibly a manifestation of a sea-breeze circulation). The discrepancy between 00Z and 12Z is also reflected in the Westerlies, and in the frequency of reported calms (winds less than 1 knot). Calm winds are typically 30% more frequent during the early morning than in the early afternoon.

The dominant wind direction, both in terms of frequency and strength, is the Northeast. Strong winds blow from this direction in both the winter - called Gregale (similar to the Mistral of the western Mediterranean) - and in the late summer - the Meltemi or Etesian wind, which is produced by the development of a thermal low over Asia Minor.

Ultimately, it is not the winds and their directions which

concern us here, but rather the lack of them: the frequency of extended calm periods of sufficient duration to permit a flight of four and a half hours.

The need for daylight for navigational purposes prompts one to examine the margins of the reportedly calm nights i.e. dawn and dusk. Pre-dawn is traditionally the choice of light-aircraft pilots, since nocturnal cooling at the surface tends to produce stable stratification of the lower troposphere, inhibiting turbulence. Figs.9(a,b,c), depicting averaged wind speeds and frequency of calm or southerly winds less than five knots for 1983, were selected as being indicative of the seasonal variation of the early morning winds.

Because the flight will last several hours, and the period during which the aircraft will be exposed may actually extend up to six hours, it is not sufficient to look only at the occurrence of calm winds at a given time, but also at their persistence. Figs.10(a,b,c) examine conditionally the frequency of occurrence of a calm period lasting three hours or more. In the case of Fig.10c, the criterion for the definition of a calm period is the occurrence of calm conditions at Souda for the hour indicated, followed by a report of calm at Kithira three hours later. Figs. 11(a,b,c) are similar, but refer to six hour calm periods. For Fig.11c, the criterion is defined such that in addition to the above, the wind speed does not exceed five knots at the intermediate observation time for either Souda or Kithira.

Disregarding the hot summer months, figures 10 and 11 collectively suggest that the most promising periods for a pre-dawn take-off are late-March through April, and again in

early September. In both cases, the frequencies are approximately 20%, or one day in five.

### Conditional Analysis

Contoured frequency plots, similar to those presented for temperatures and wind, were generated to determine the correlation between periods of "moderate temperature" and calm conditions. Four examples are presented here, for three hour intervals Figs. 12(a,b,c,d); and six hour intervals, Figs. 13(a, b,c,d). The criterion for an event of three hour duration is that the conditions be satisfied at Souda at the hour indicated, and satisfied at Kithira again three hours later. For the six hour period, in addition to this requirement at the beginning and end of the interval, it is required that the conditions be satisfied at the intermediate hour, at both Souda and Kithira, to within 20%.

In all four plots, "calm" is defined as reported winds less than 1 knot. Figs. 12a and 13a, which place no restrictions on the temperature or humidity, clearly indicate a maximum probability of 30-40% for the night time in April and early May, with secondary maxima in June and September.

When the temperature is constrained to be between 5 and 20 degC, and the humidity is below that required for saturation (relative humidity <95%), Figs. 12b and 13b, only the February and early September maxima appear, with a potential preference for the latter when considering 3Z departure times.

Figures 12c and 13c indicate that the features of the

contour plot are preserved as the constraints are increased, while the frequencies predictably decrease.

In conclusion, figures 12d and 13d represent a relaxation in the temperature criterion ( $T < 25^{\circ}\text{C}$ ). Taken together, these analyses tend to argue for a pre-dawn flight in late March, early April.

### Further Study

The deployment of three portable observation stations in the region this March should provide data of sufficient detail to resolve local phenomena, such as sea breeze circulations, which could be used to the pilots advantage. Although some attempts were made at considering the diurnal variation of the wind velocity in this study, the period of three hours used is probably not adequate to warrant a thorough discussion of these matters. While the climatological study has uncovered the "window regions" in the seasonal cycle, the analysis of the data from the remote stations will answer questions such as the relative merits of dawn and dusk flights, the feasibility of a cliff-top take-off, and the relationship of measurements in the open channel to values obtained at Souda or Kithira.

Also, this climatological study does not consider the dynamical aspects of the regional weather. To this effect - and also as preparation for the operational forecasts that will eventually be required - I intend to follow the synoptic situation of the region over the course of the year. This observation of the day to day motions of the atmosphere will help in answering some of the questions raised by this study.

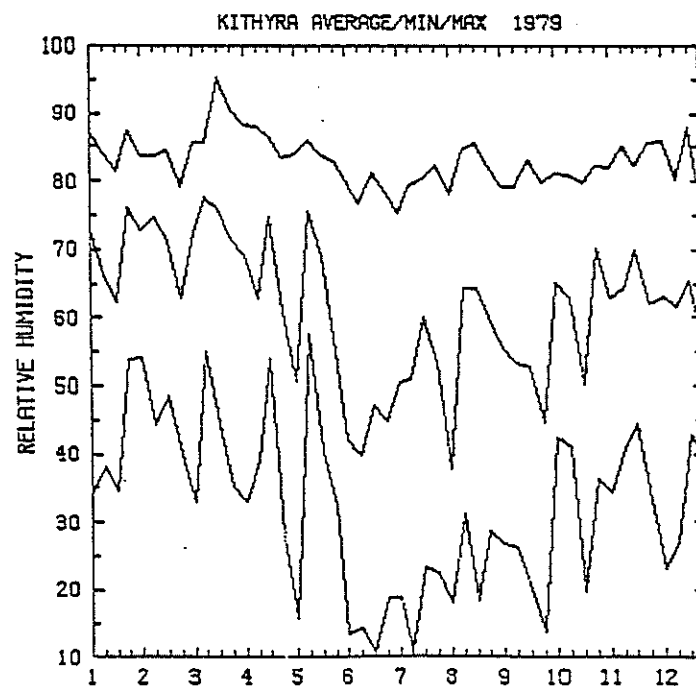
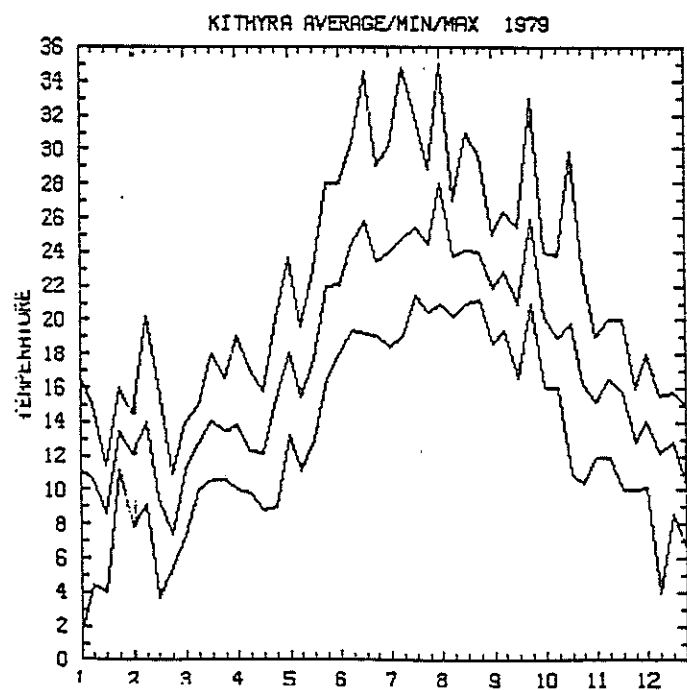
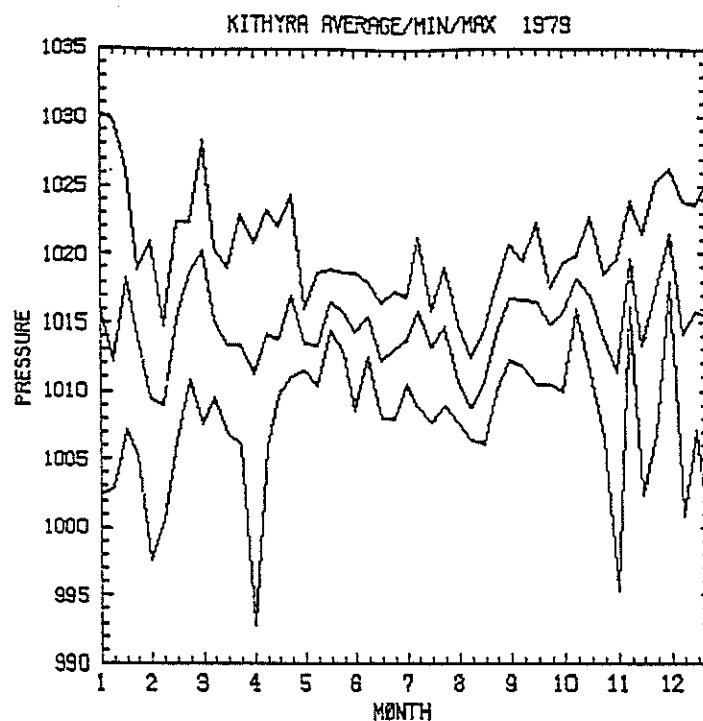
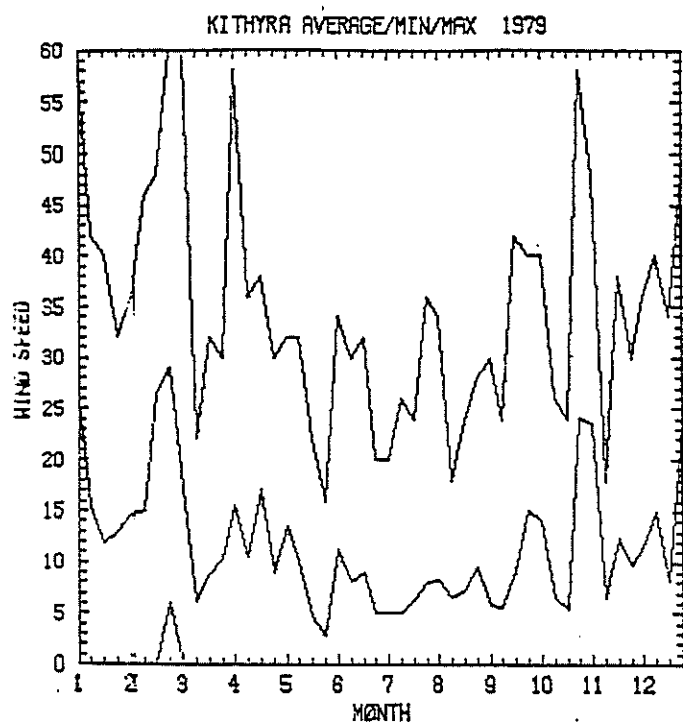


Fig. 1 Time-averaged seasonal variations of wind speed, pressure, temperature, and relative humidity. Minima, maxima and averages are plotted. a) Kithira 1979; b) Kithira 1983. [knots,mb,degC,%]

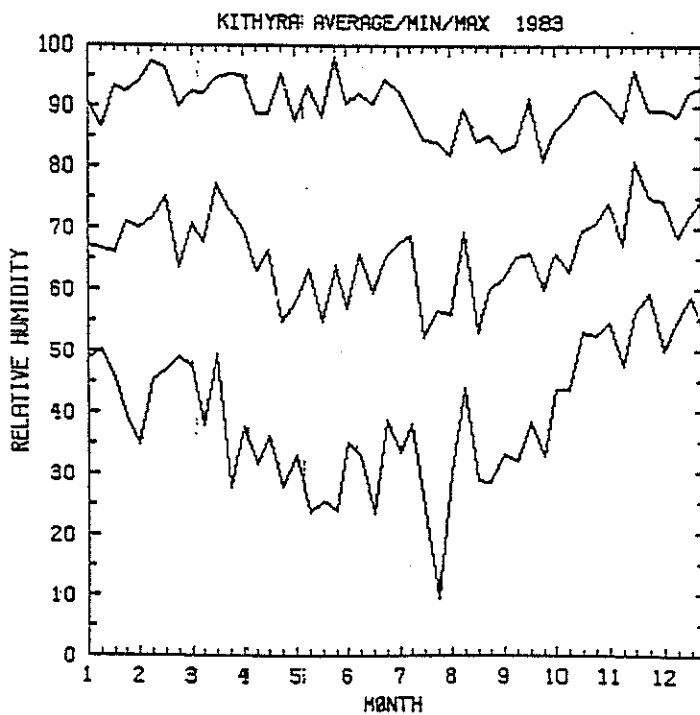
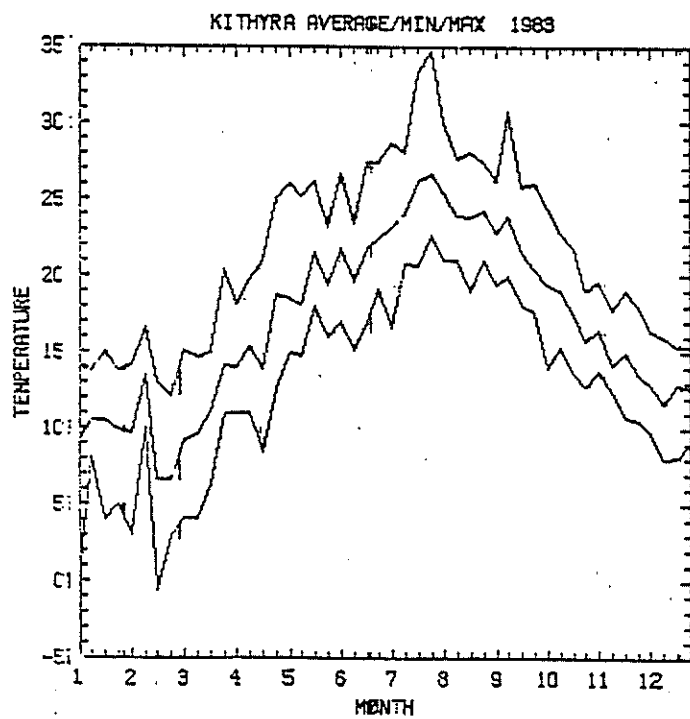
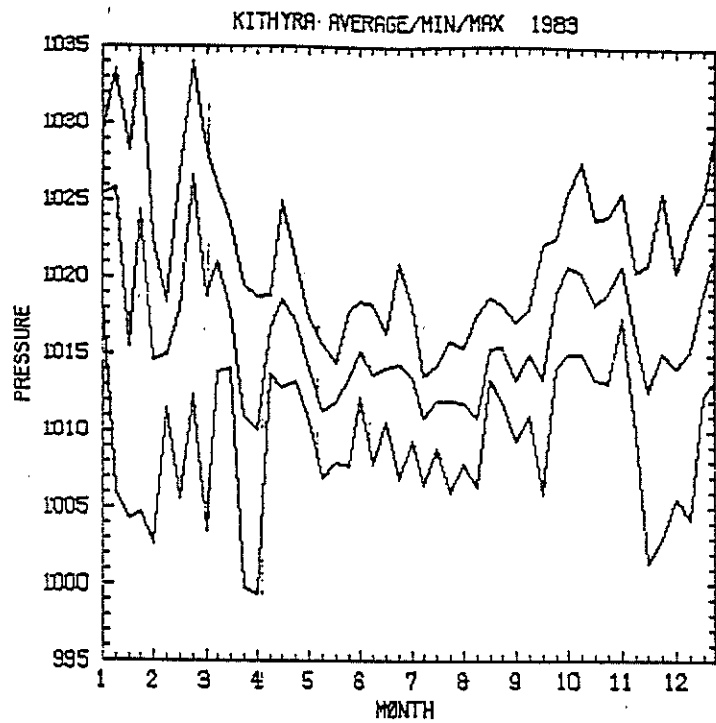
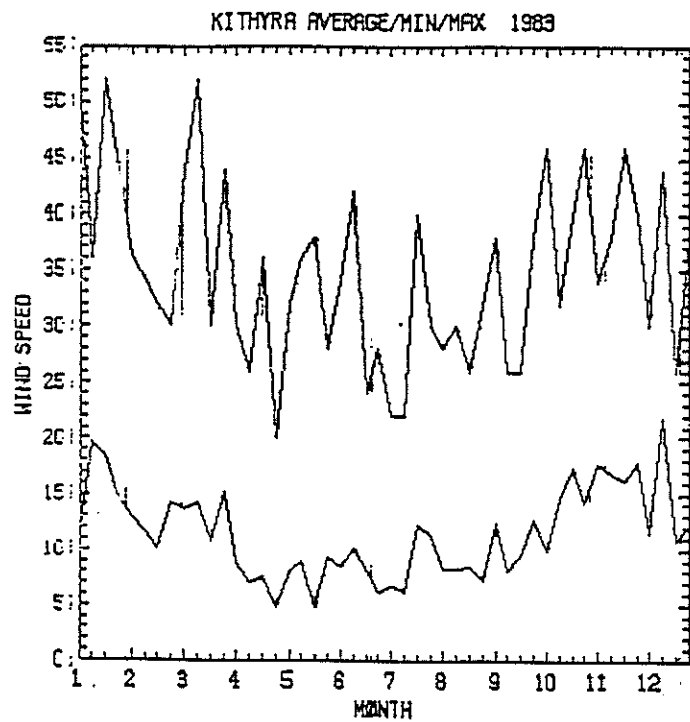


Fig. 1b

# KITHIRA PRESSURE

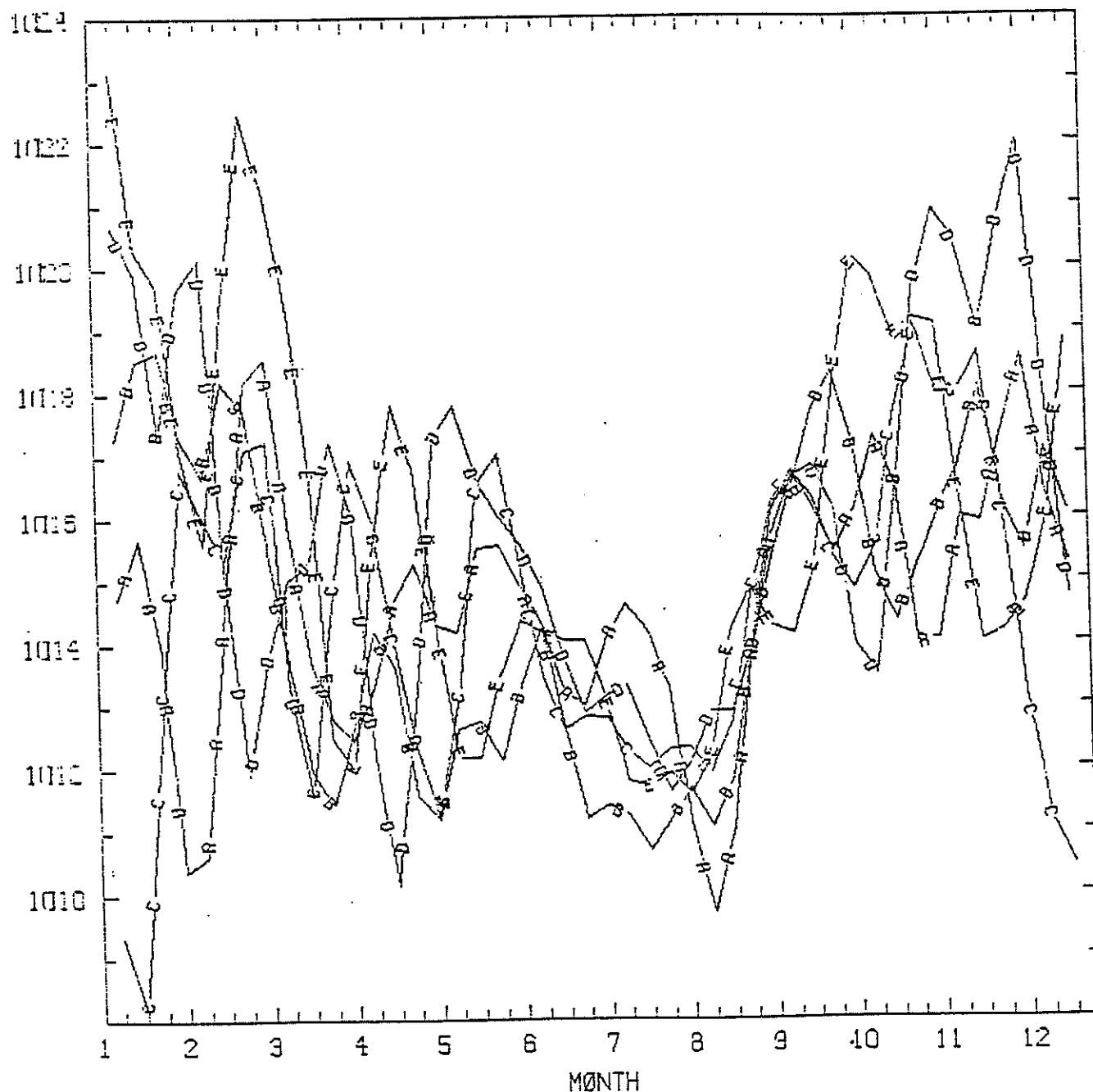


Fig. 2 Time-averaged seasonal variations of pressure, smoothed using a 1-2-1 running mean. Curves for successive years (1979-83) are superimposed (A-E). a) Kithira; b) Souda. [mb].



# SQUA PRESSURE

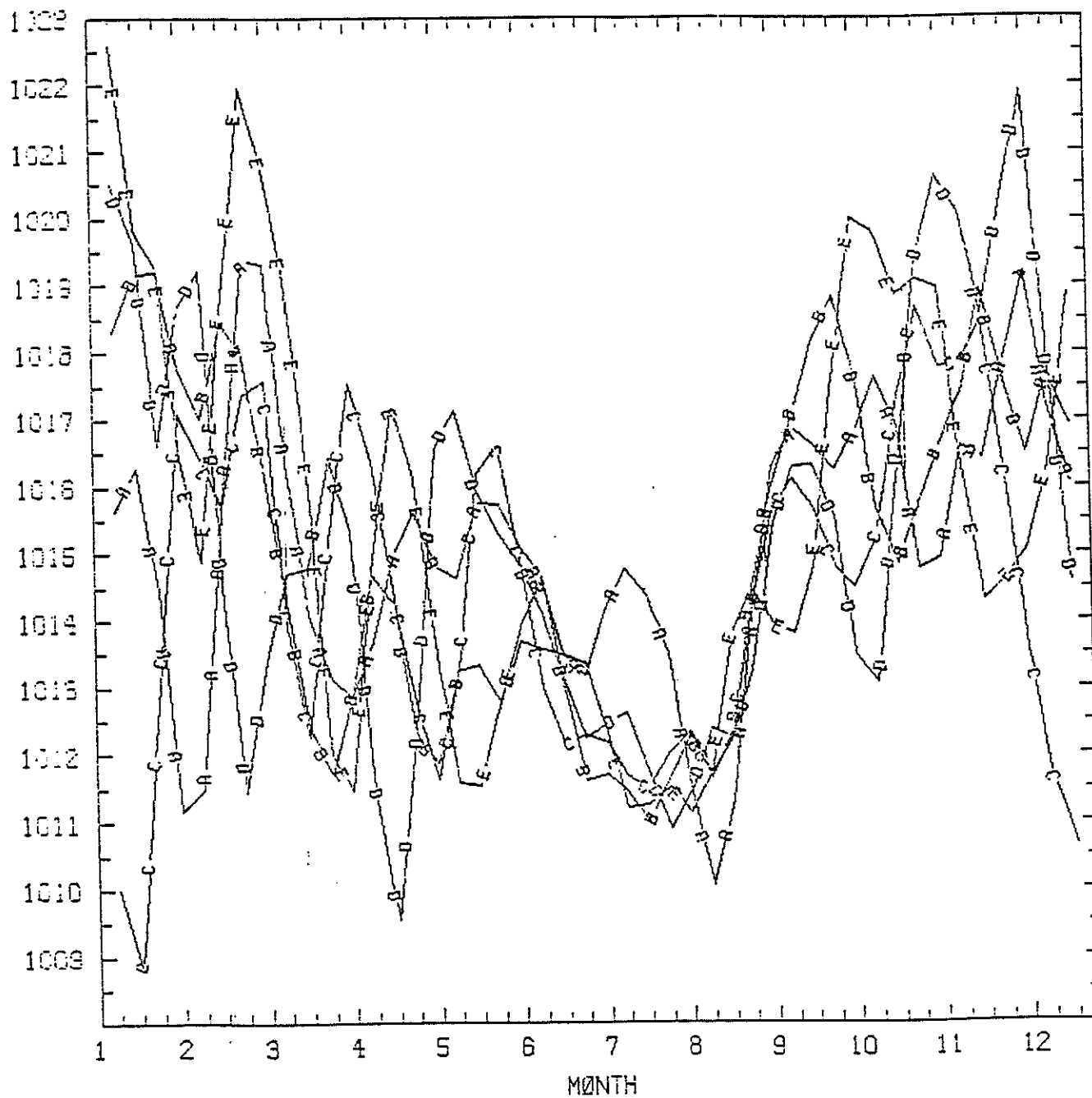


Fig. 2b

# KITHIRA TEMPERATURE

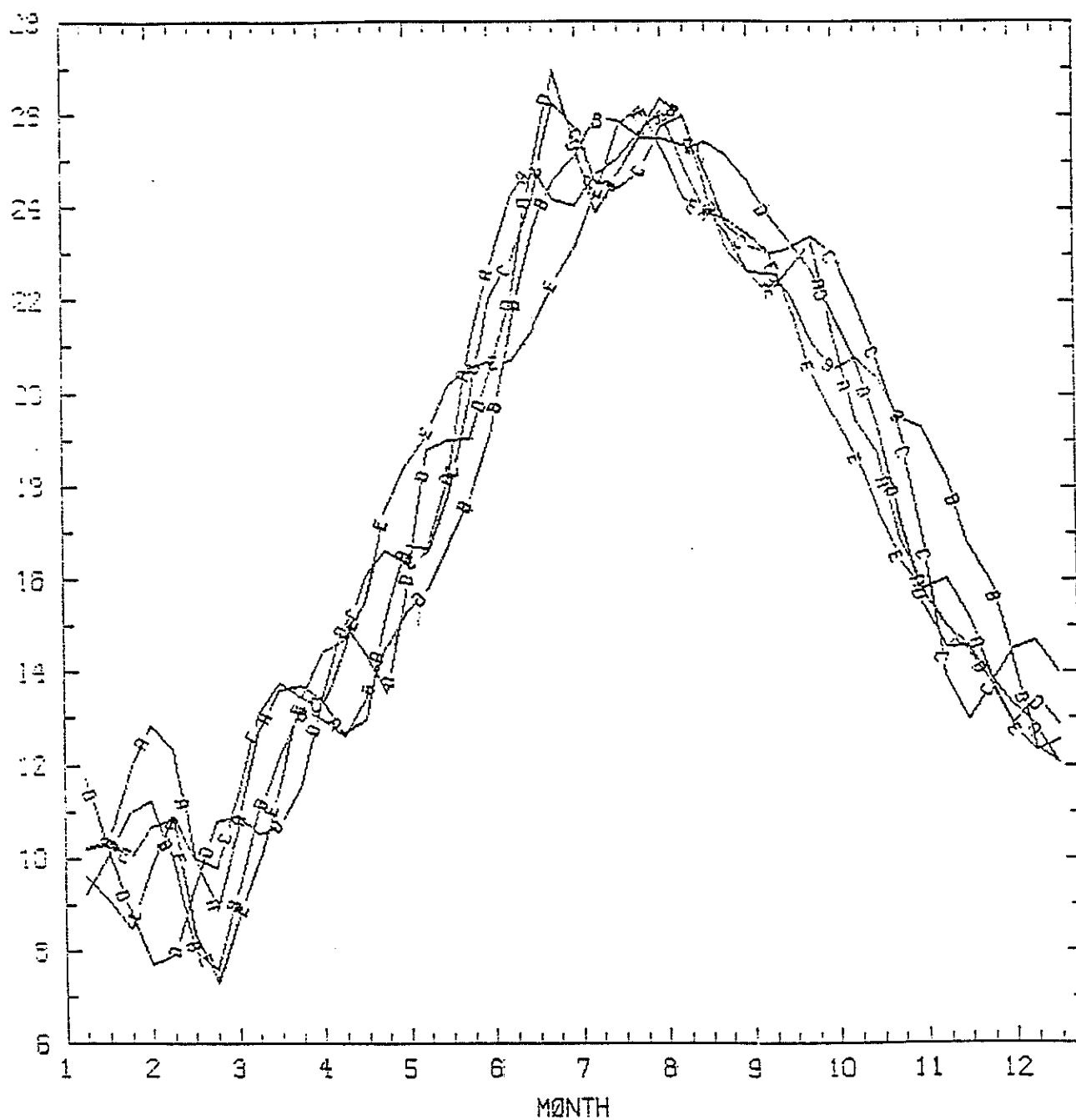


Fig. 3 As in Fig. 2, but air temperature. [degC]

# SOUDA TEMPERATURE

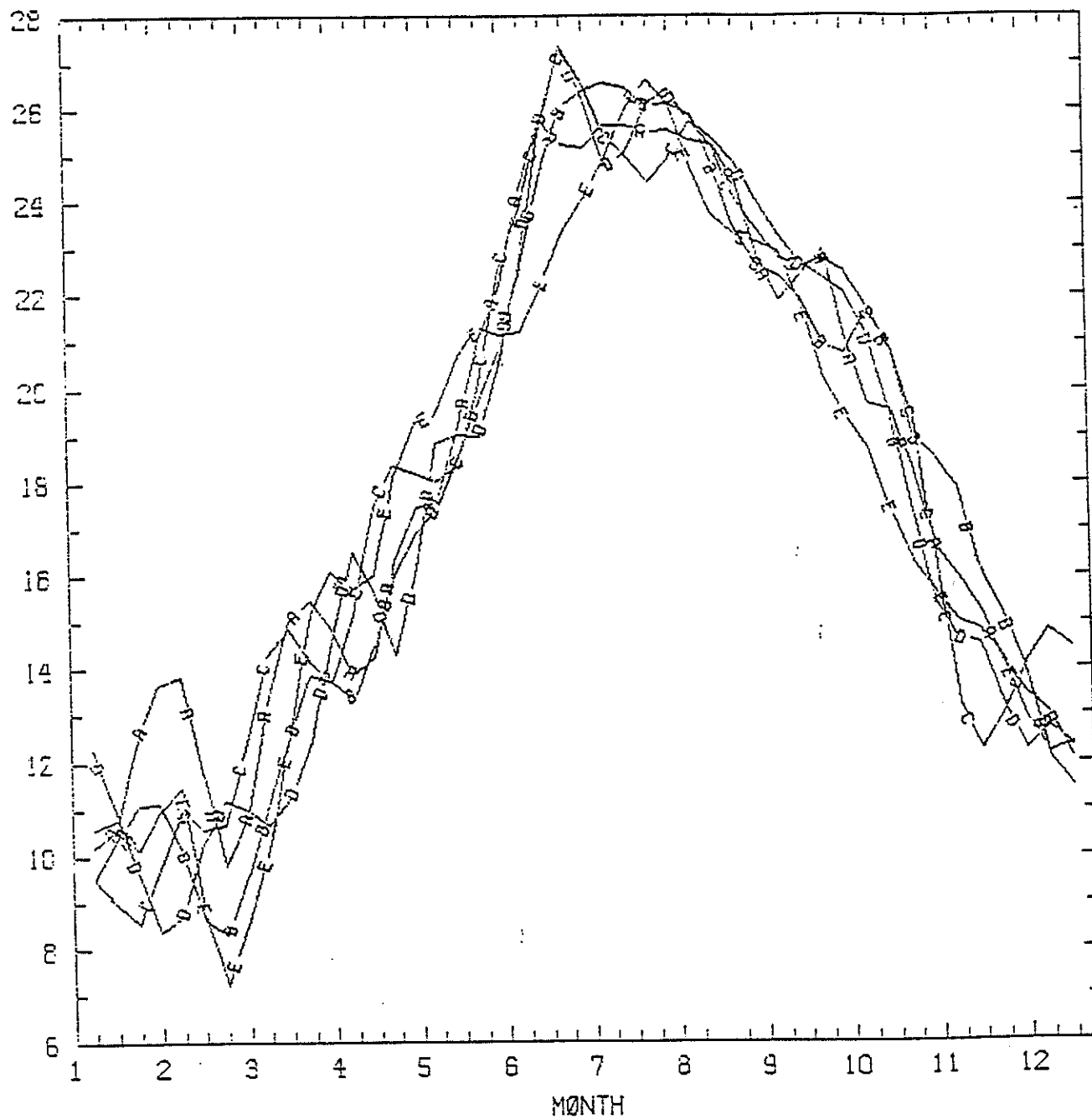


Fig. 3b

# KITHIRA AVERAGE TEMPERATURE

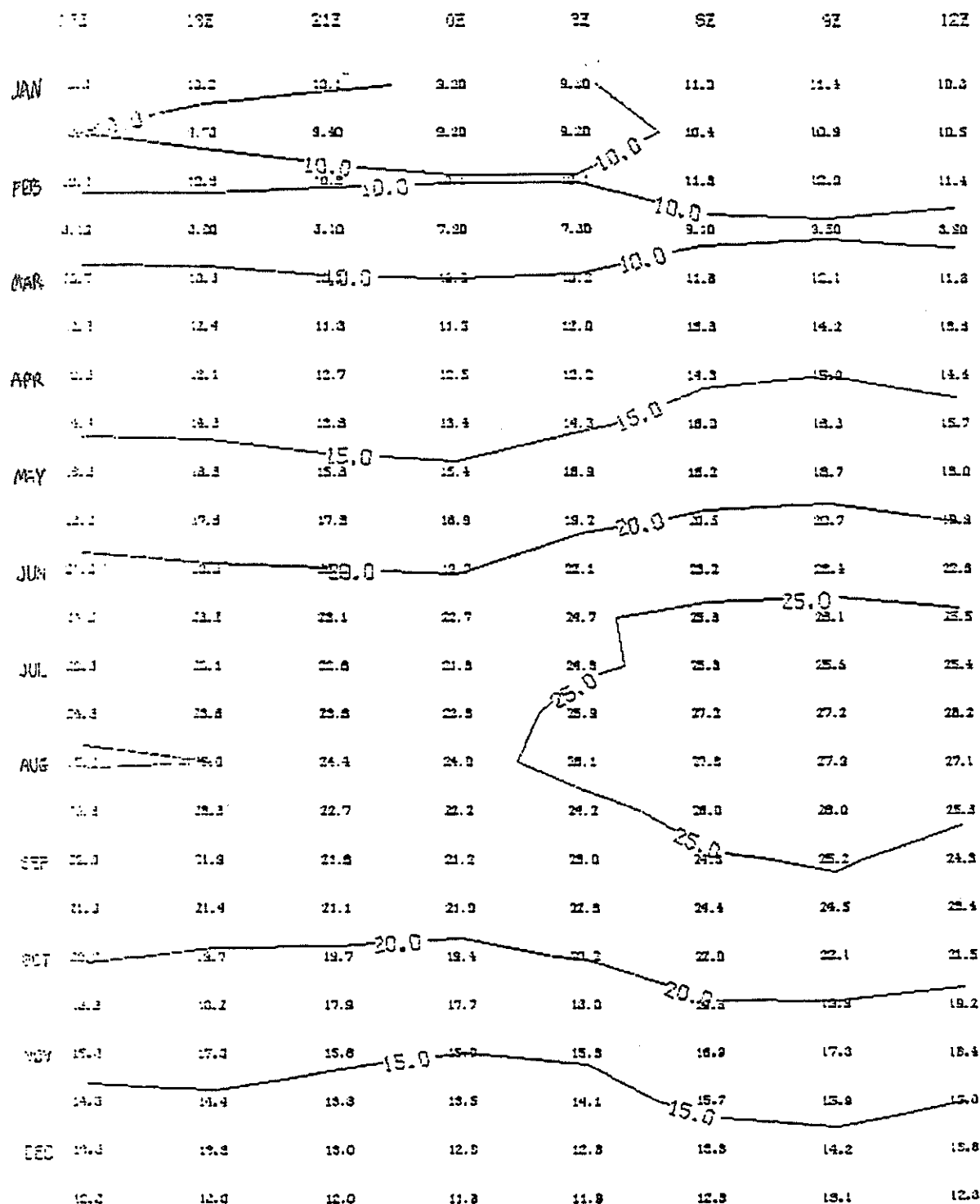


Fig. 4 Contoured array of time-averaged temperature for 8 observation times (GMT), and bi-monthly periods. Values contoured at intervals of 5 degC. a) Kithira; b) Souda. [degC].

# SAUDA AVERAGE TEMPERATURE

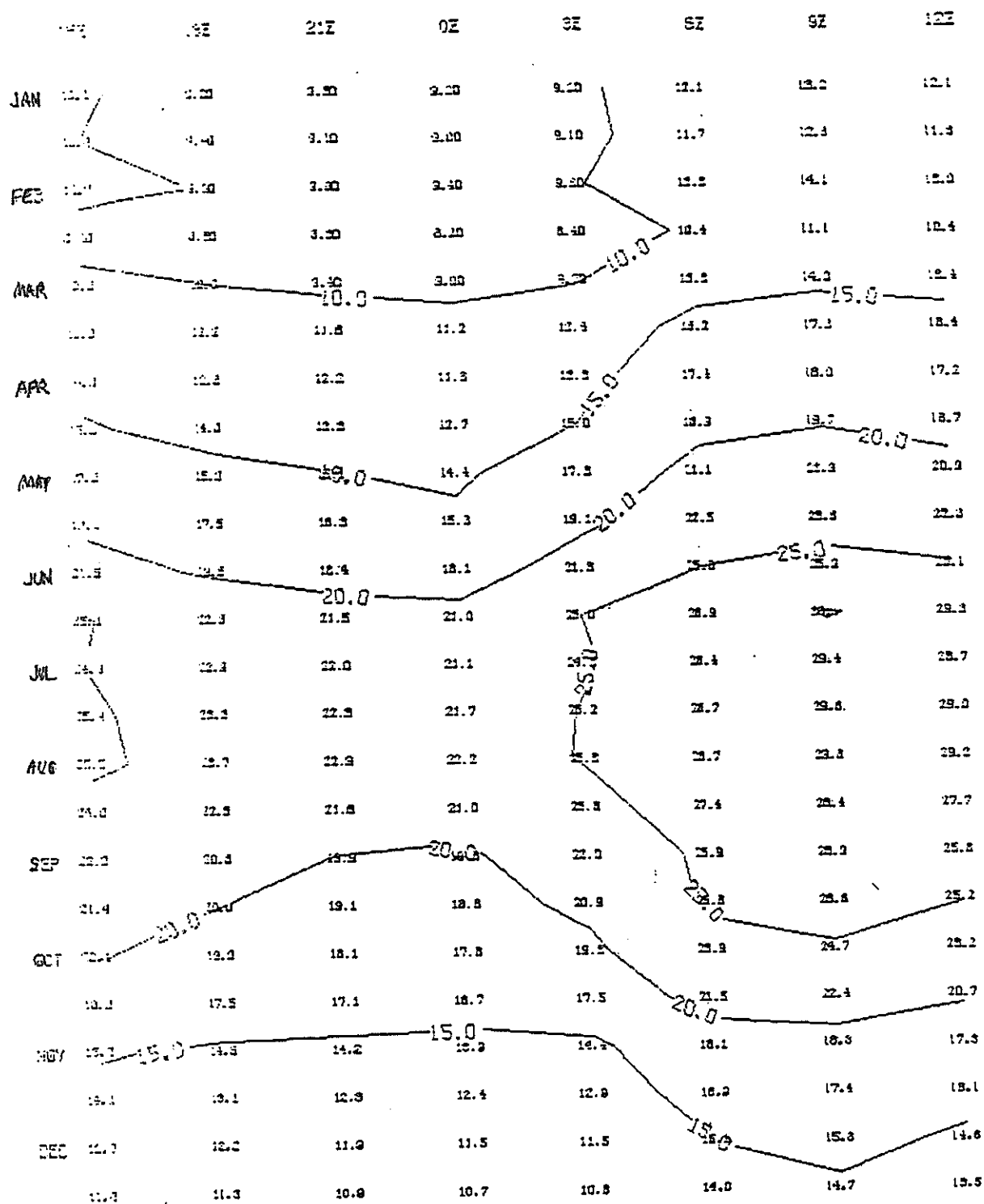


Fig. 4b

# KITHIRA TEMPERATURE LESS THAN 20C FOR 3 HOURS

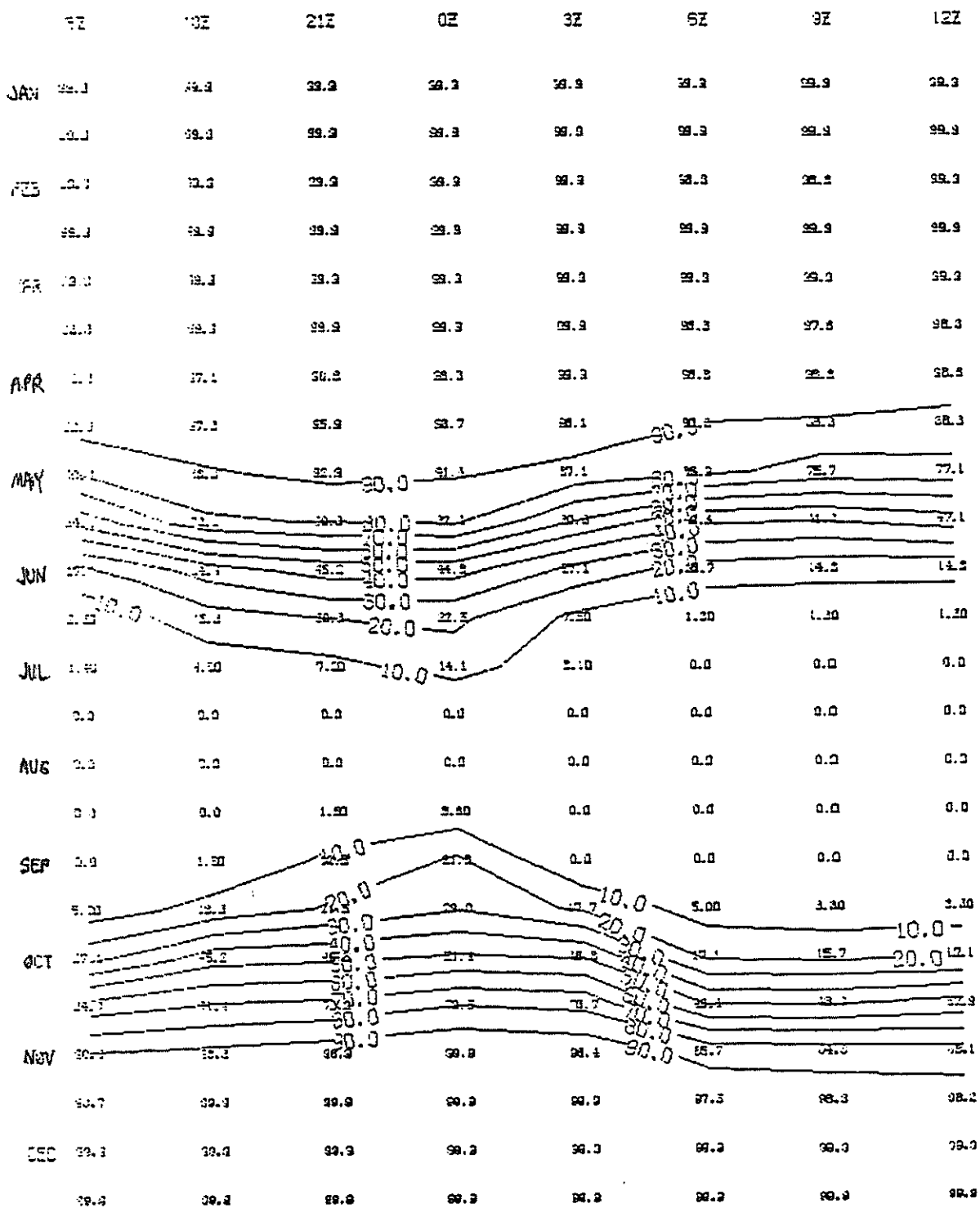


Fig. 5 Contoured array of conditional frequency of occurrence of air temperatures within a certain range degC. In this and subsequent frequency plots, the period begins at the time indicated, and intervals of 10% are contoured. a) Kithira,  $T < 20 \text{ degC}$  for three hours; b) Kithira,  $10 < T < 15 \text{ degC}$  for three hours.

# KITHIRA TEMPERATURE LT 15C GT 10C FOR 3 HOURS

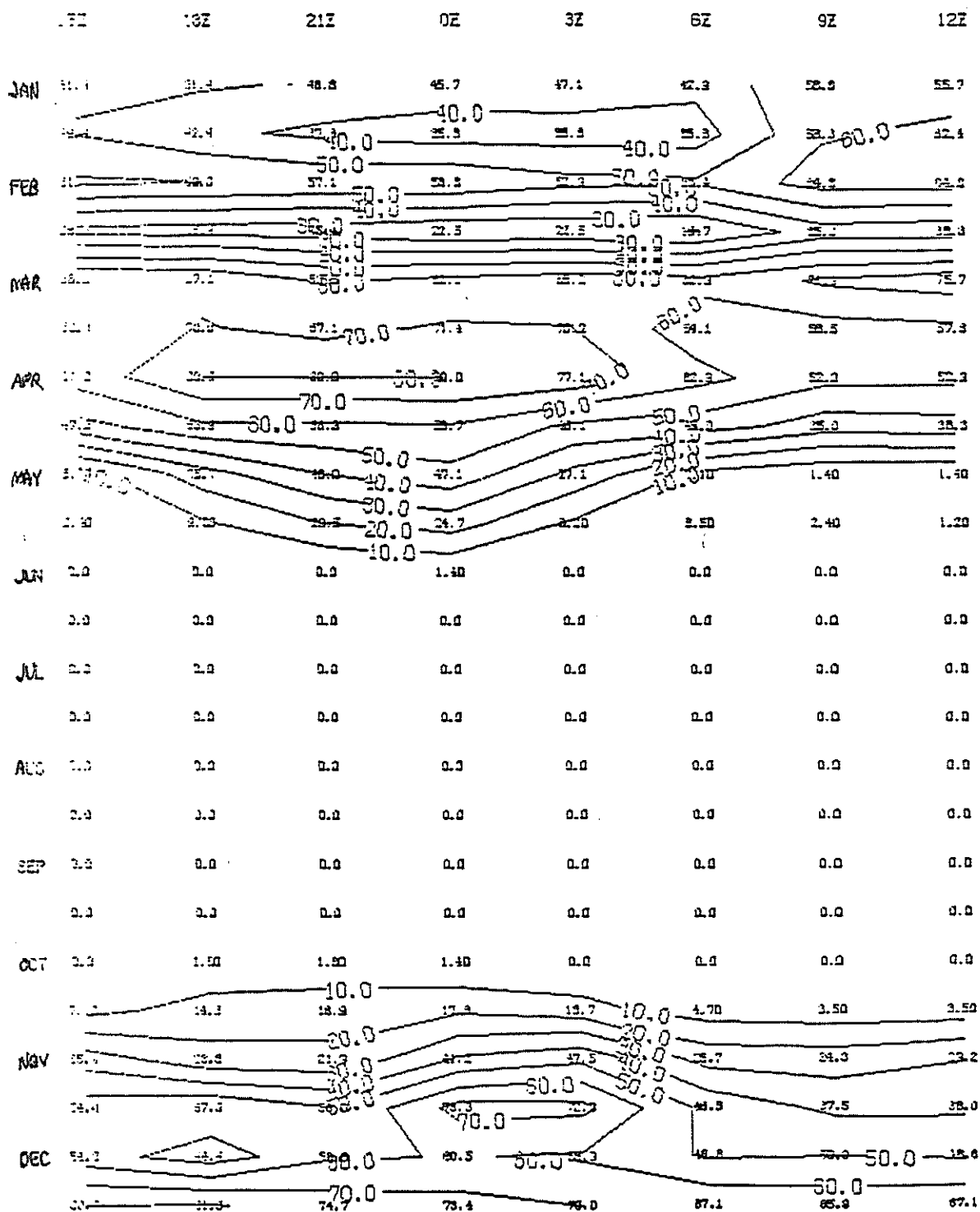


Fig. 5b

# KITHIRA AVERAGE RELATIVE HUMIDITY

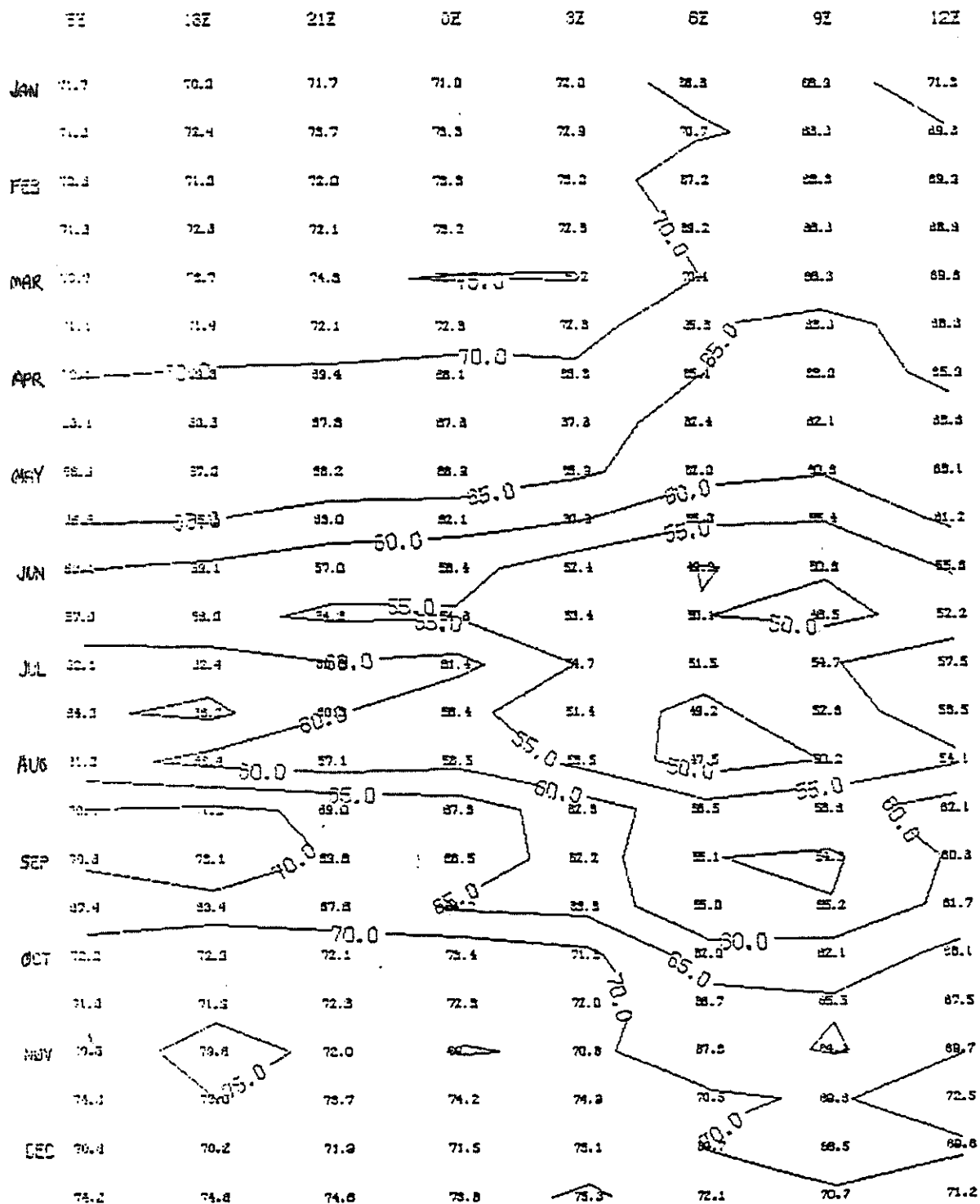


Fig 6 As in Fig. 4, for relative humidity. [%].



# SOUDA AVERAGE RELATIVE HUMIDITY

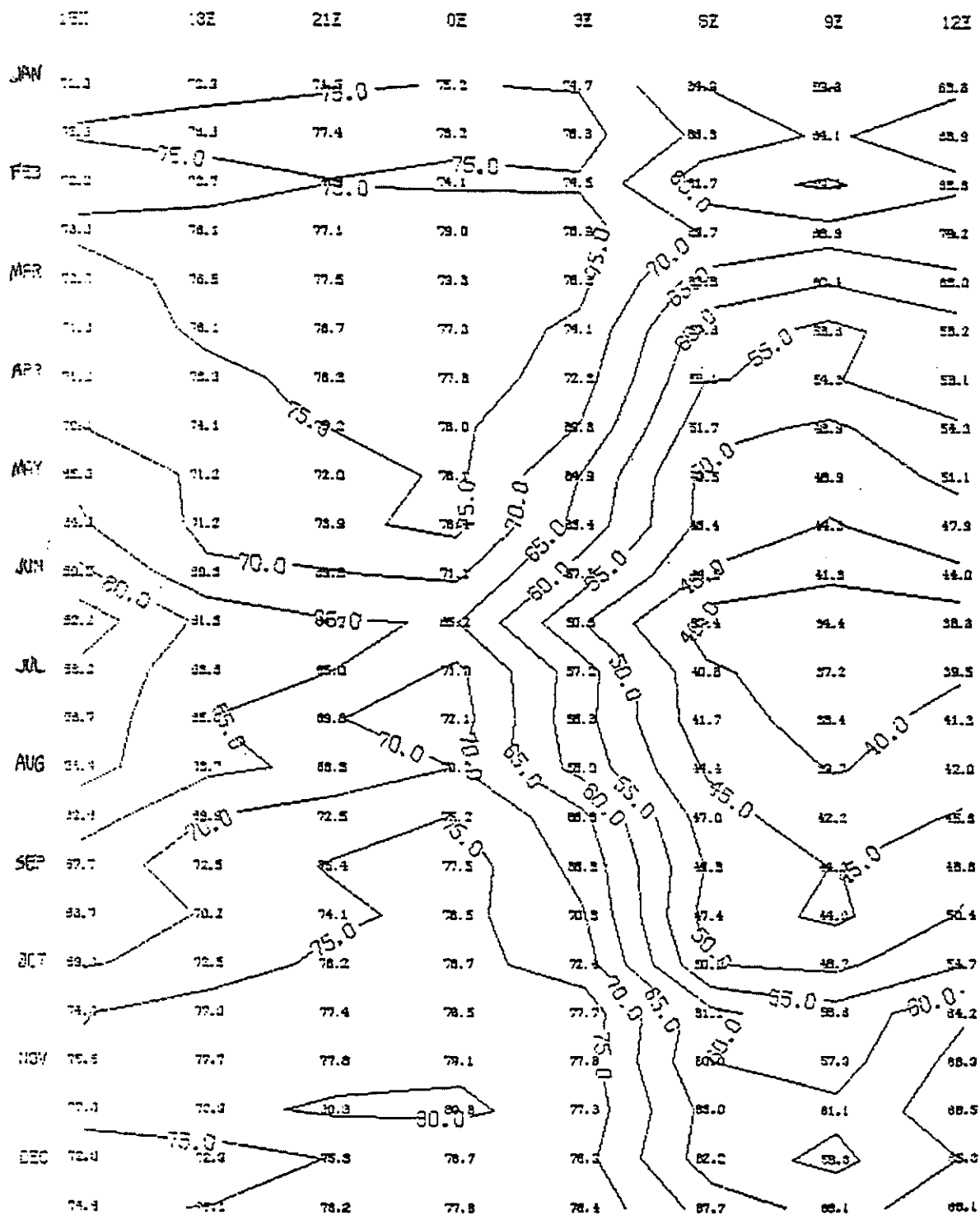


Fig. 6b.

KITHIRA RELATIVE HUMIDITY GT. 95 (1/1000)

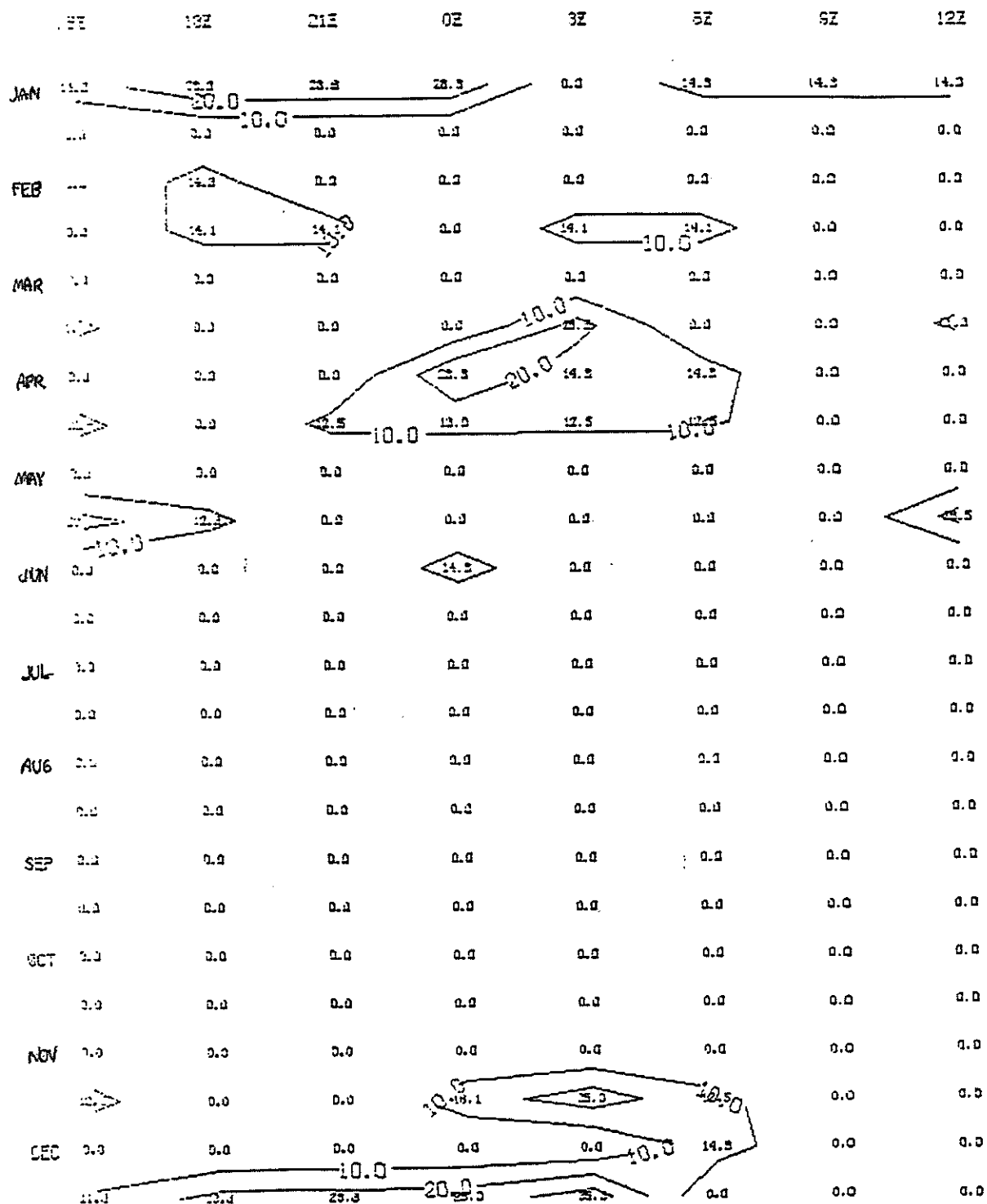


Fig. 7 Frequency plot of the occurrence of relative humidity greater than 95%, expressed as tenths of 1%. a) Kithira; b) Souda.

SAUDA RELATIVE HUMIDITY GT. 95 (1/1000)

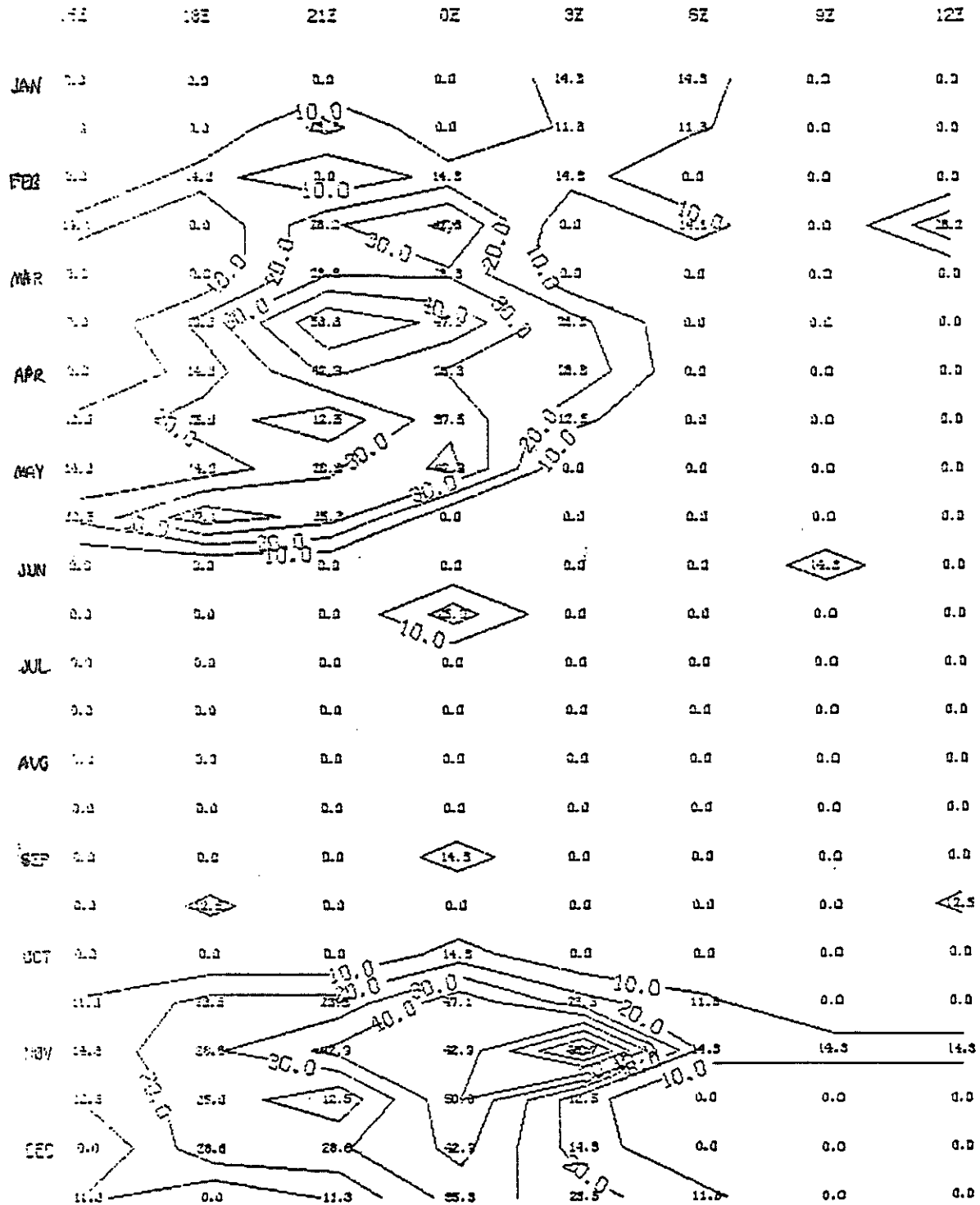


Fig. 7b

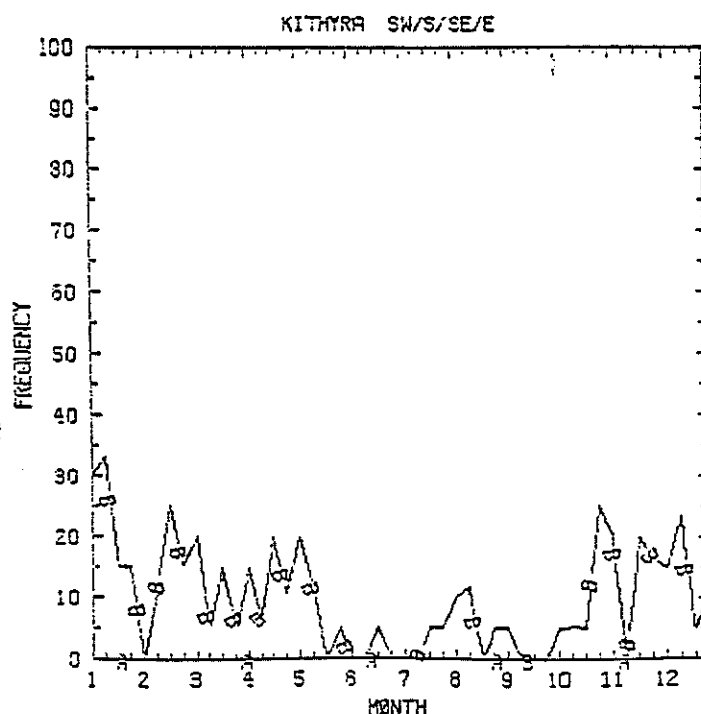
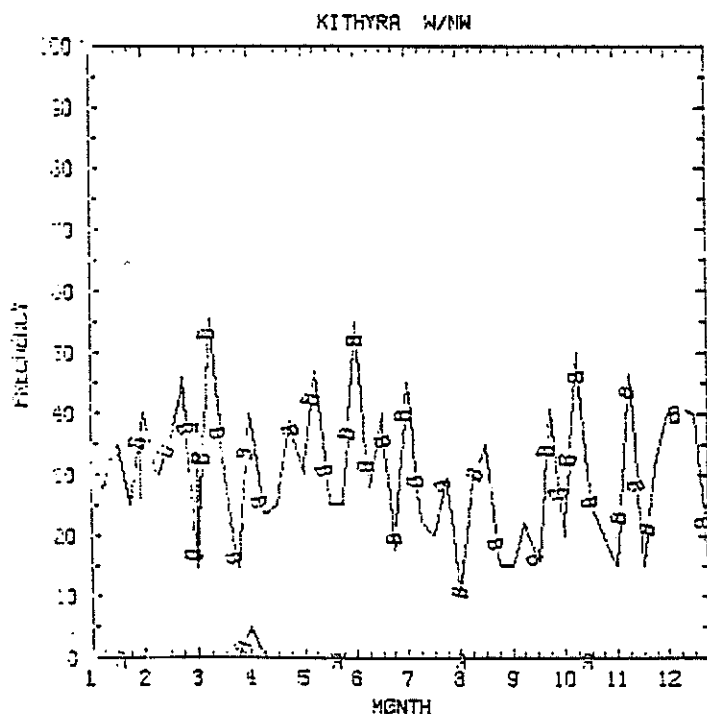
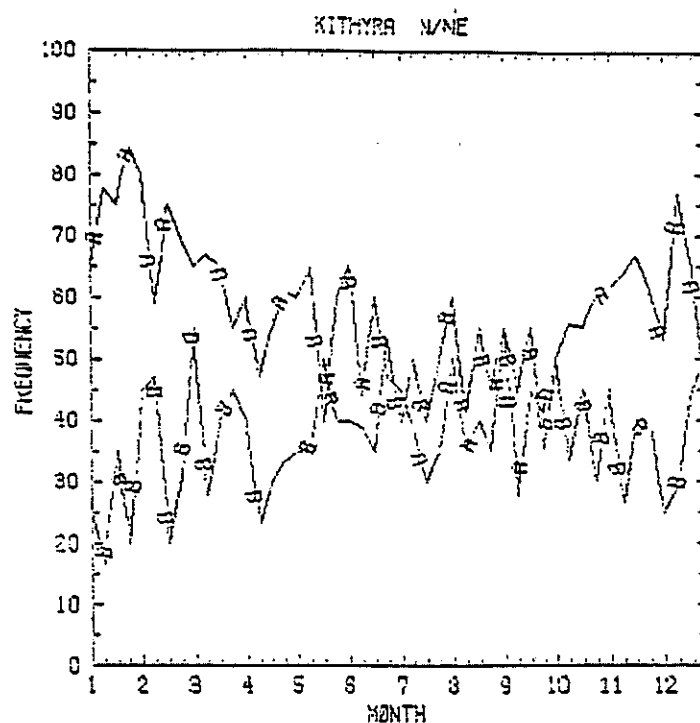
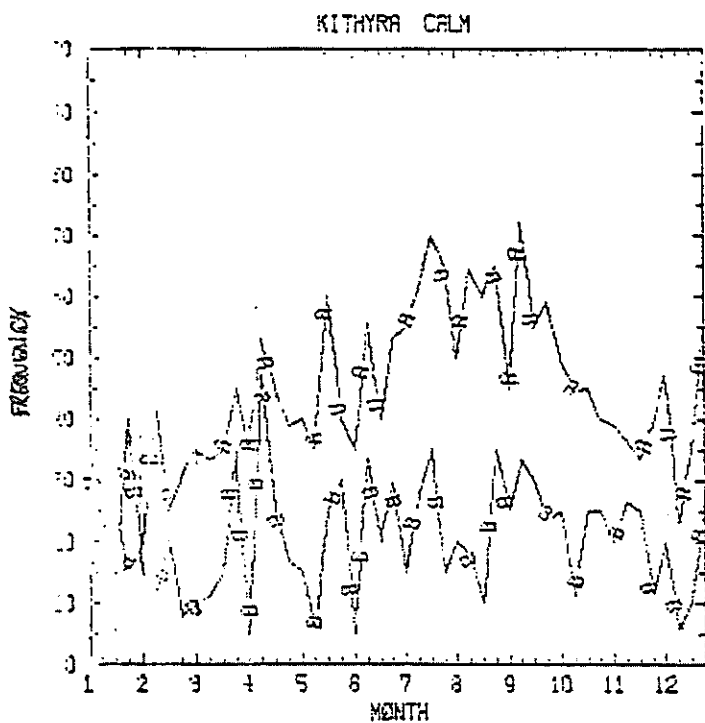


Fig. 8 Relative frequencies of calm winds (<1 knot), North/Northeasterly winds, West/Northwesterly winds, and winds from East - Southwest. The curve labeled "A" represents observations at 00Z; the curve labeled "B" represents observations at 12Z. a) Kithira; b) Souda.

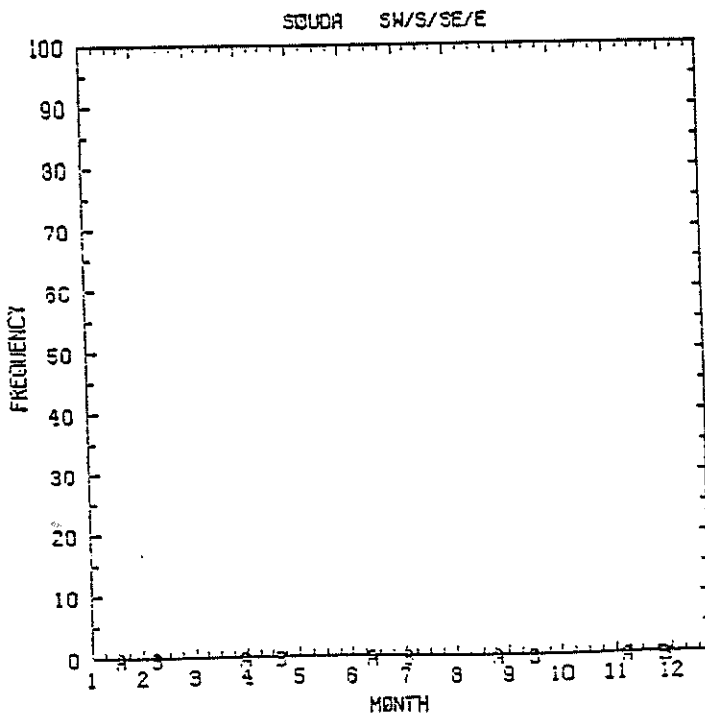
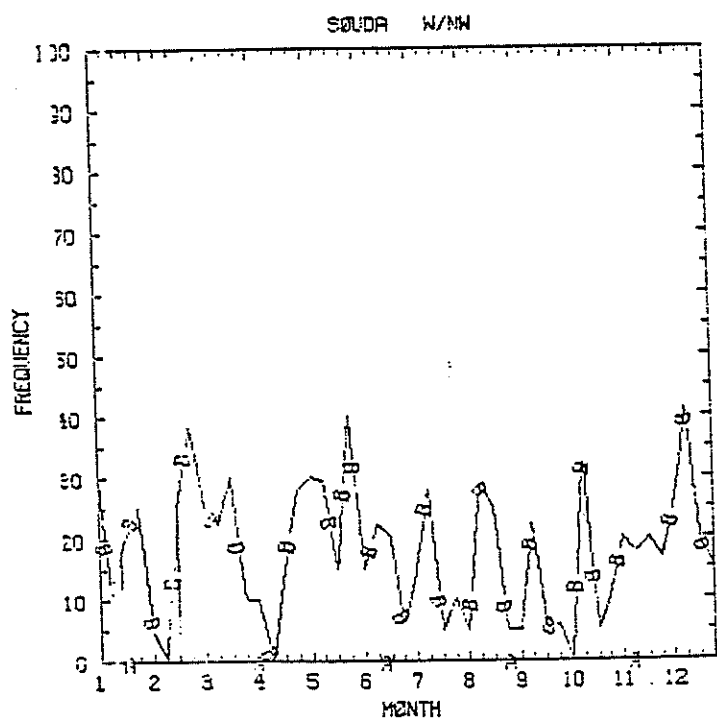
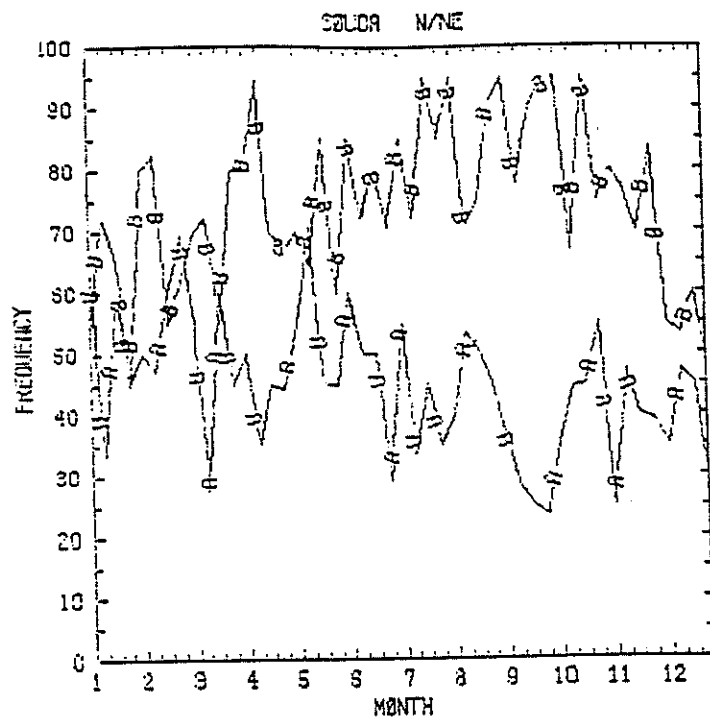
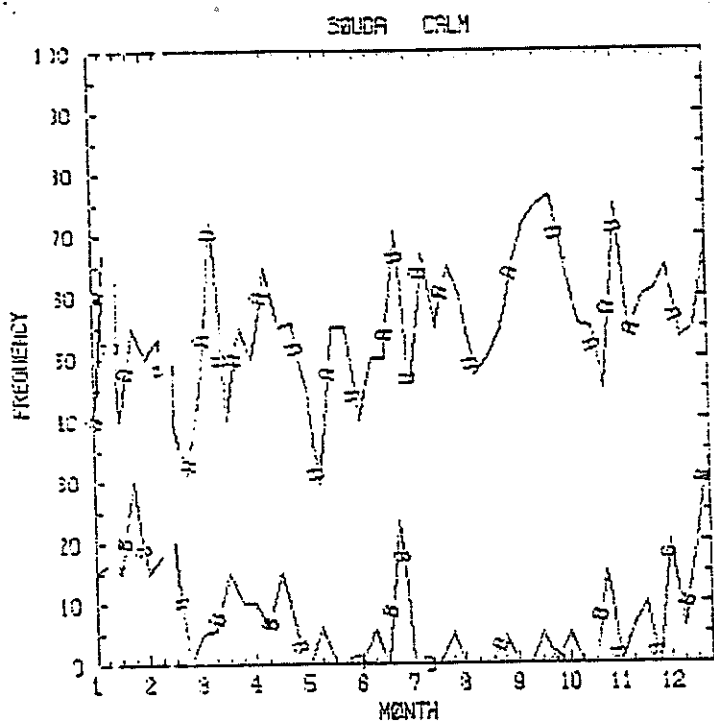


Fig. 8b

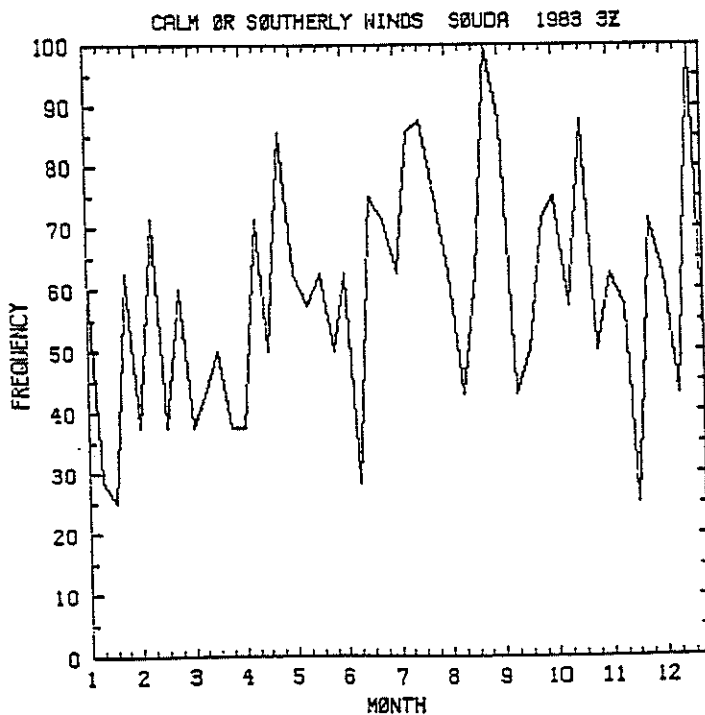
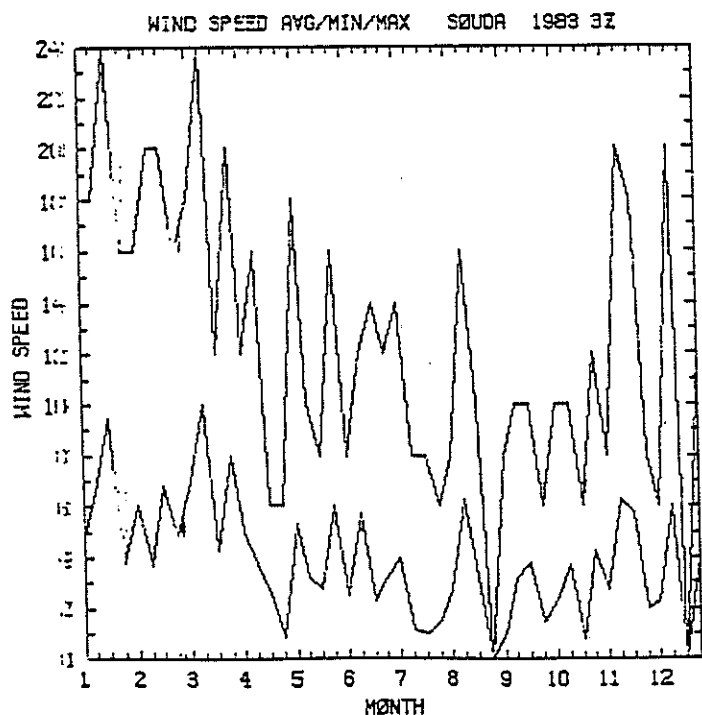
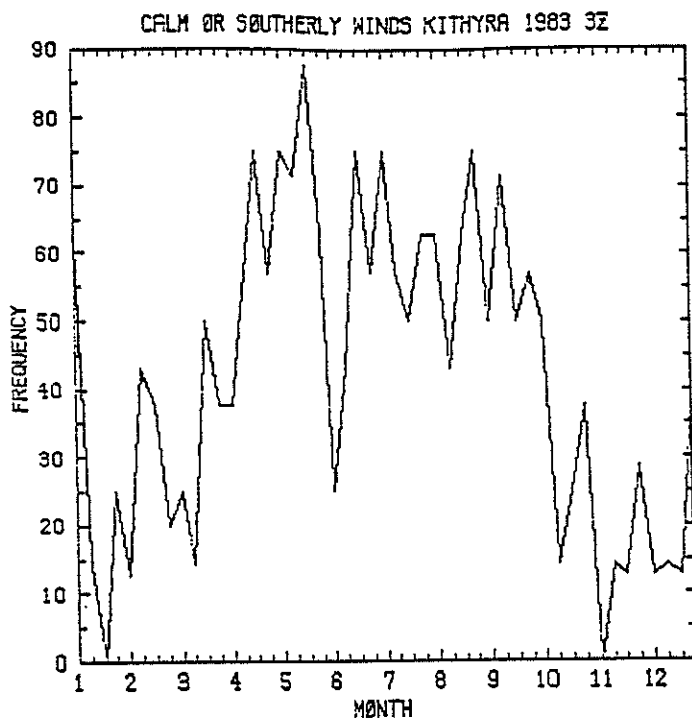
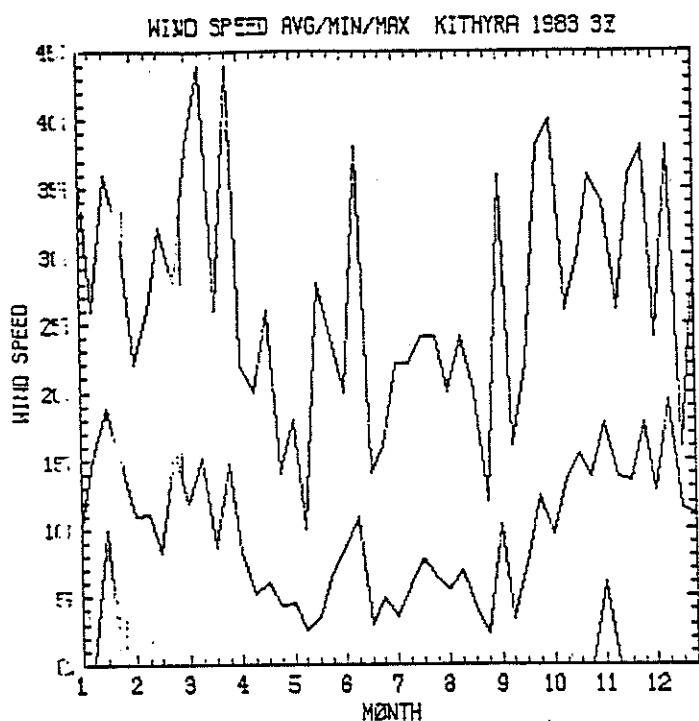


Fig. 9 Maxima, minima, and averages of wind speed, and the frequency of occurrence of calm or southerly winds less than 5 knots, for Kithira and Souda in 1983. a) 03Z; b) 06Z; c) 09Z.

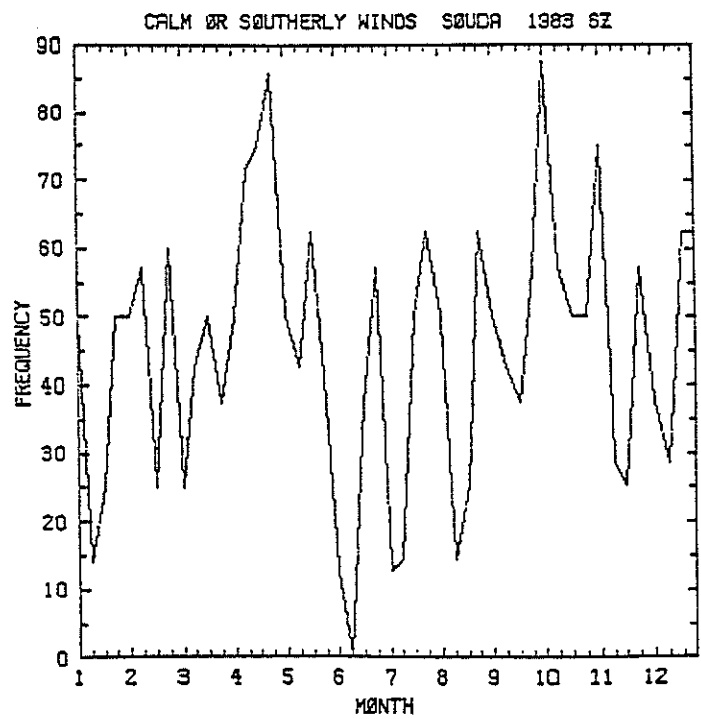
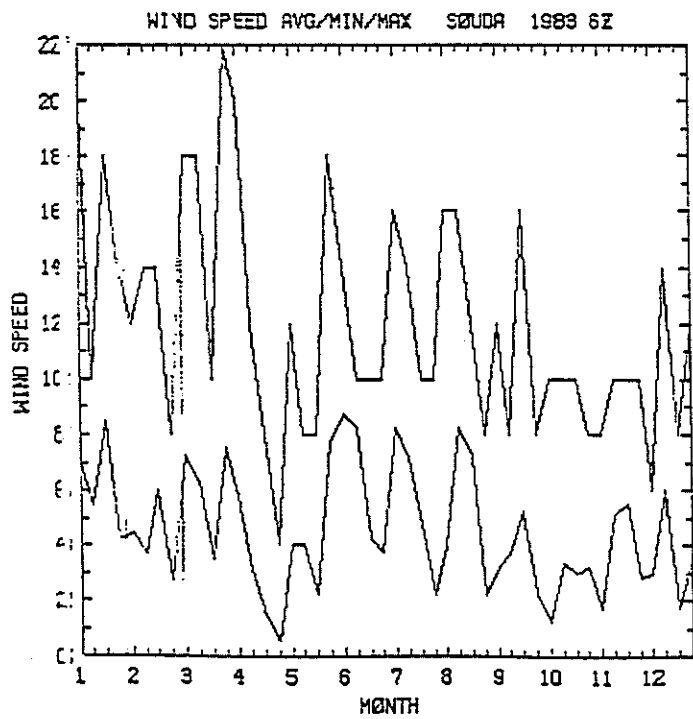
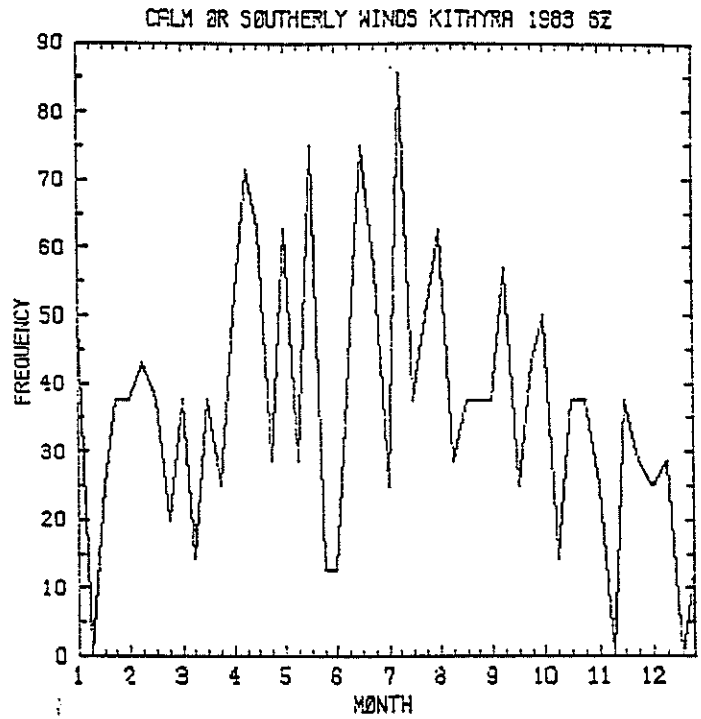
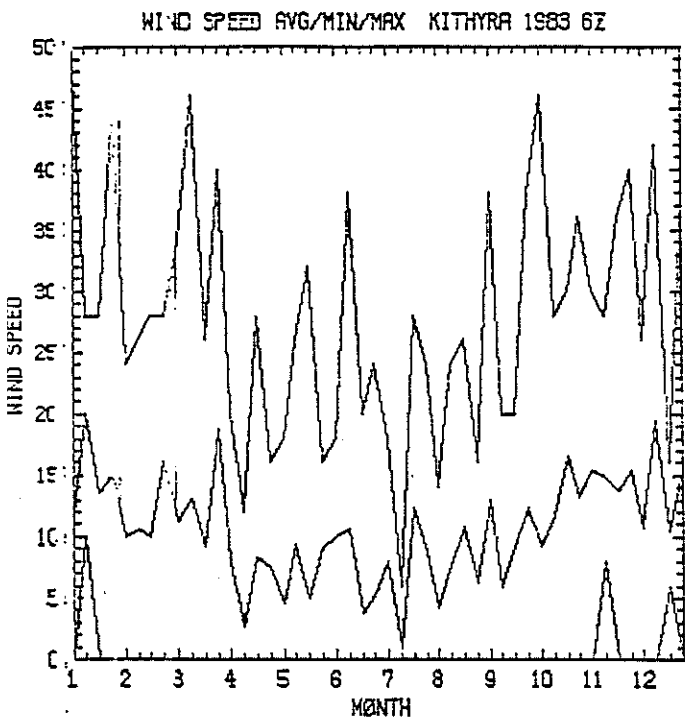


Fig. 9b

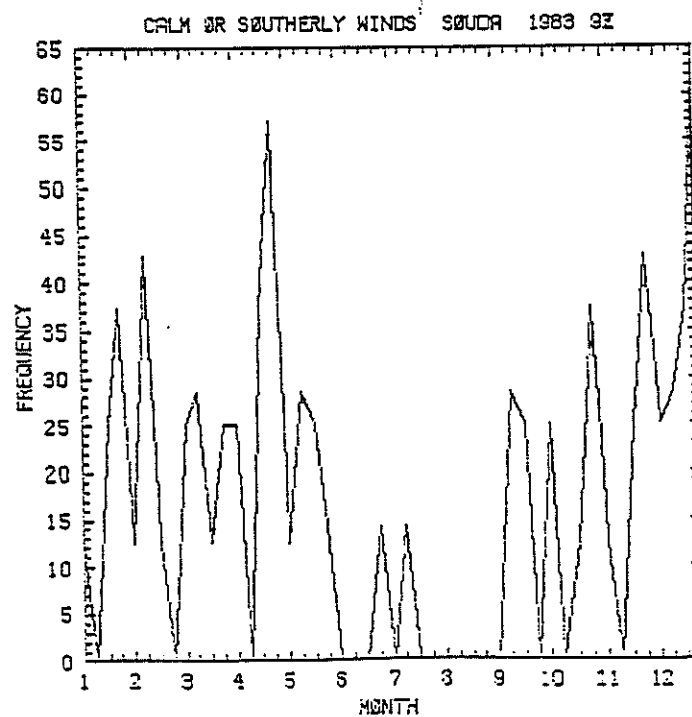
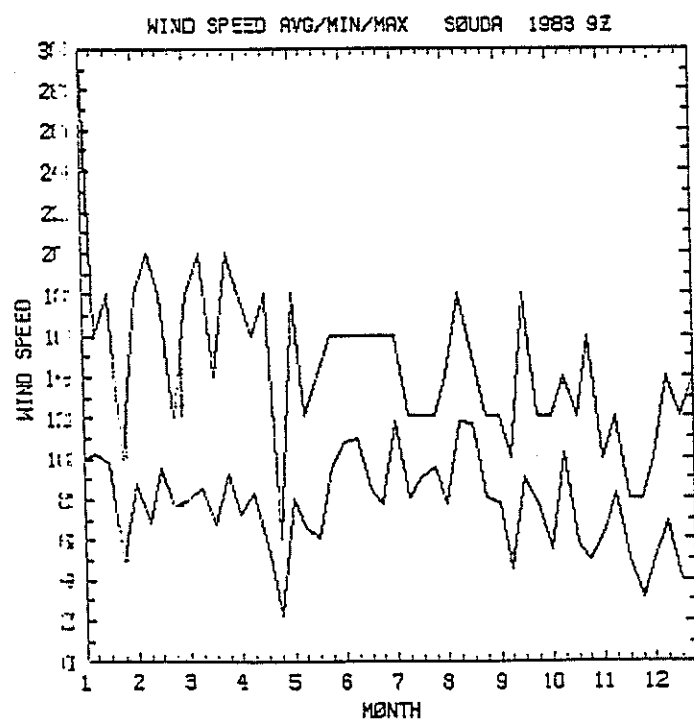
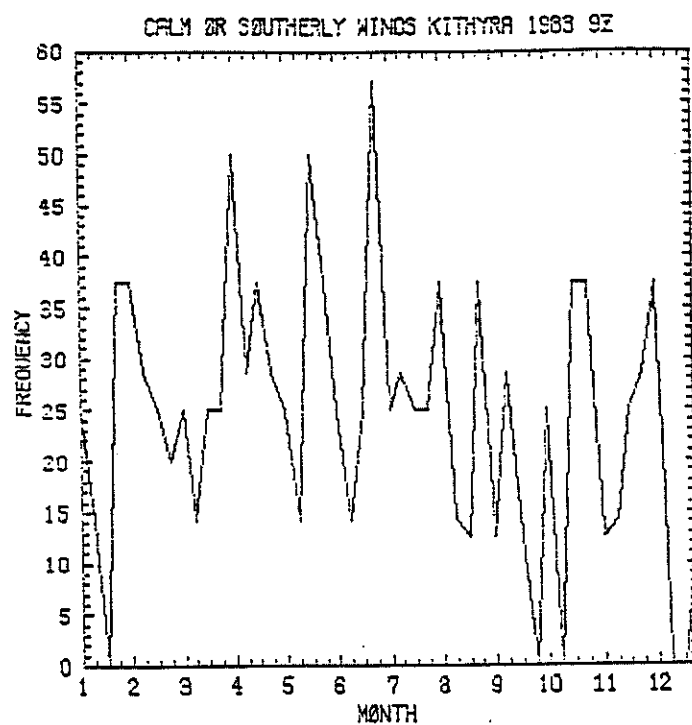
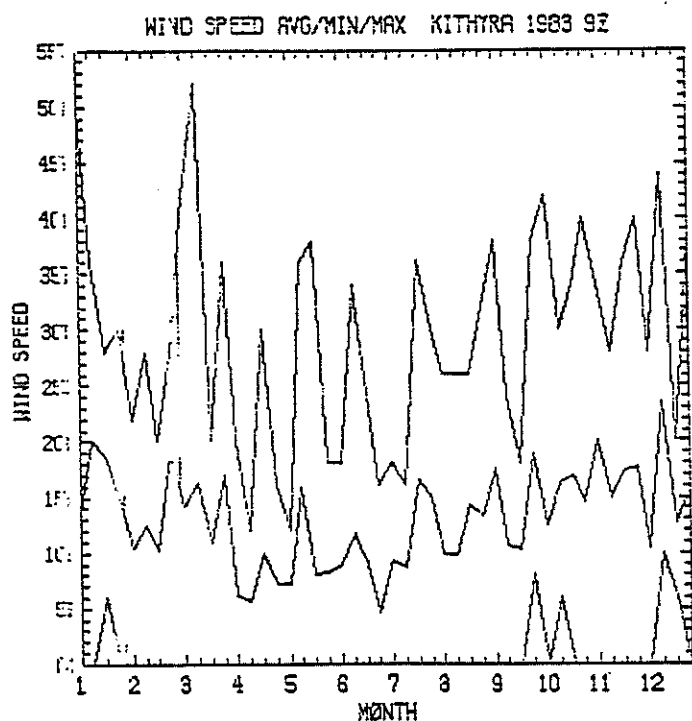


Fig. 9c



# KITHIRA FREQUENCY OF 3 HOUR CALM

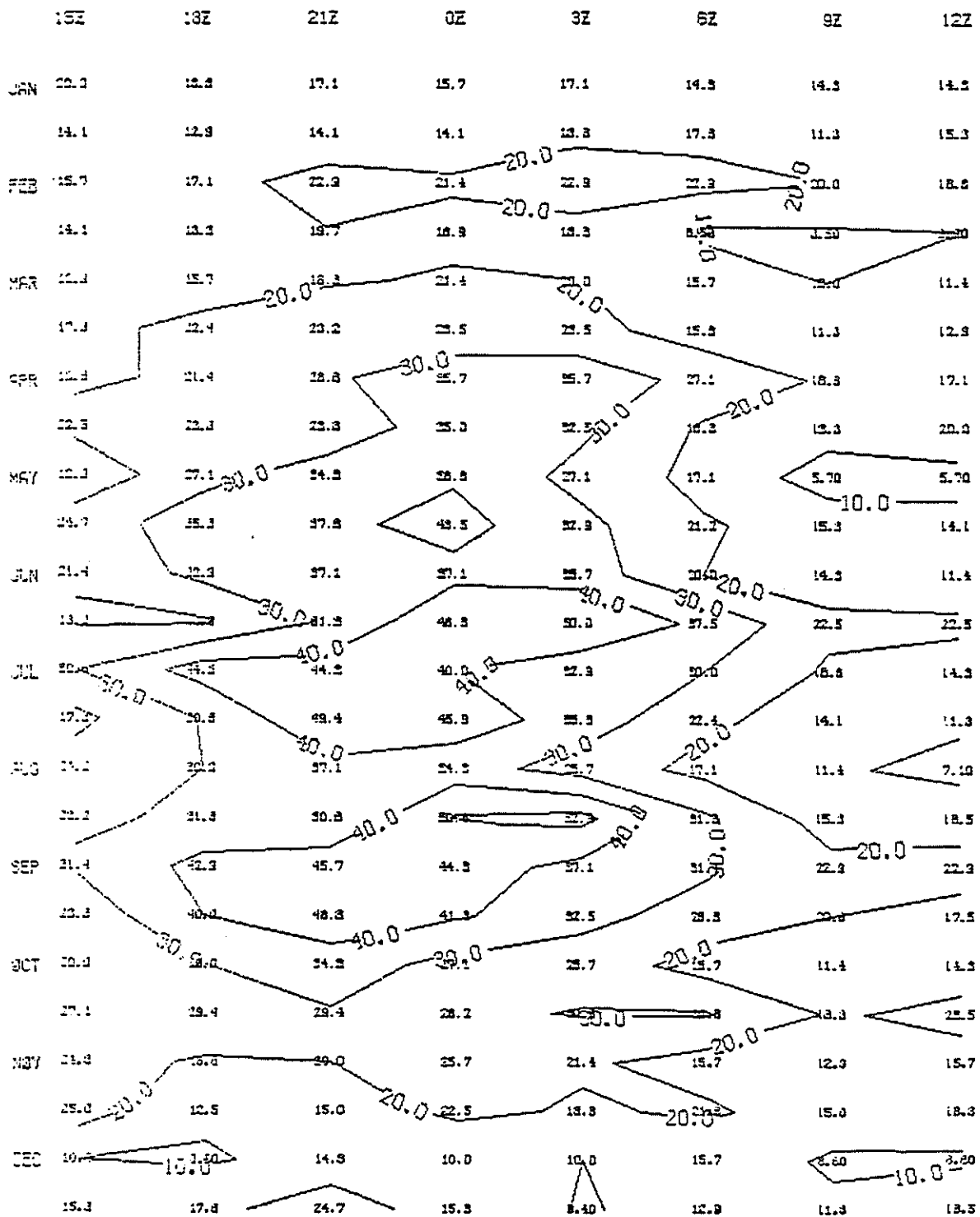


Fig. 10 Frequency plot of the occurrence of a three hour calm period (0 knots of wind reported). a) Kithira; b) Souda; c) Souda then Kithira.

# SOLAR FREQUENCY OF 3 HOUR CALM

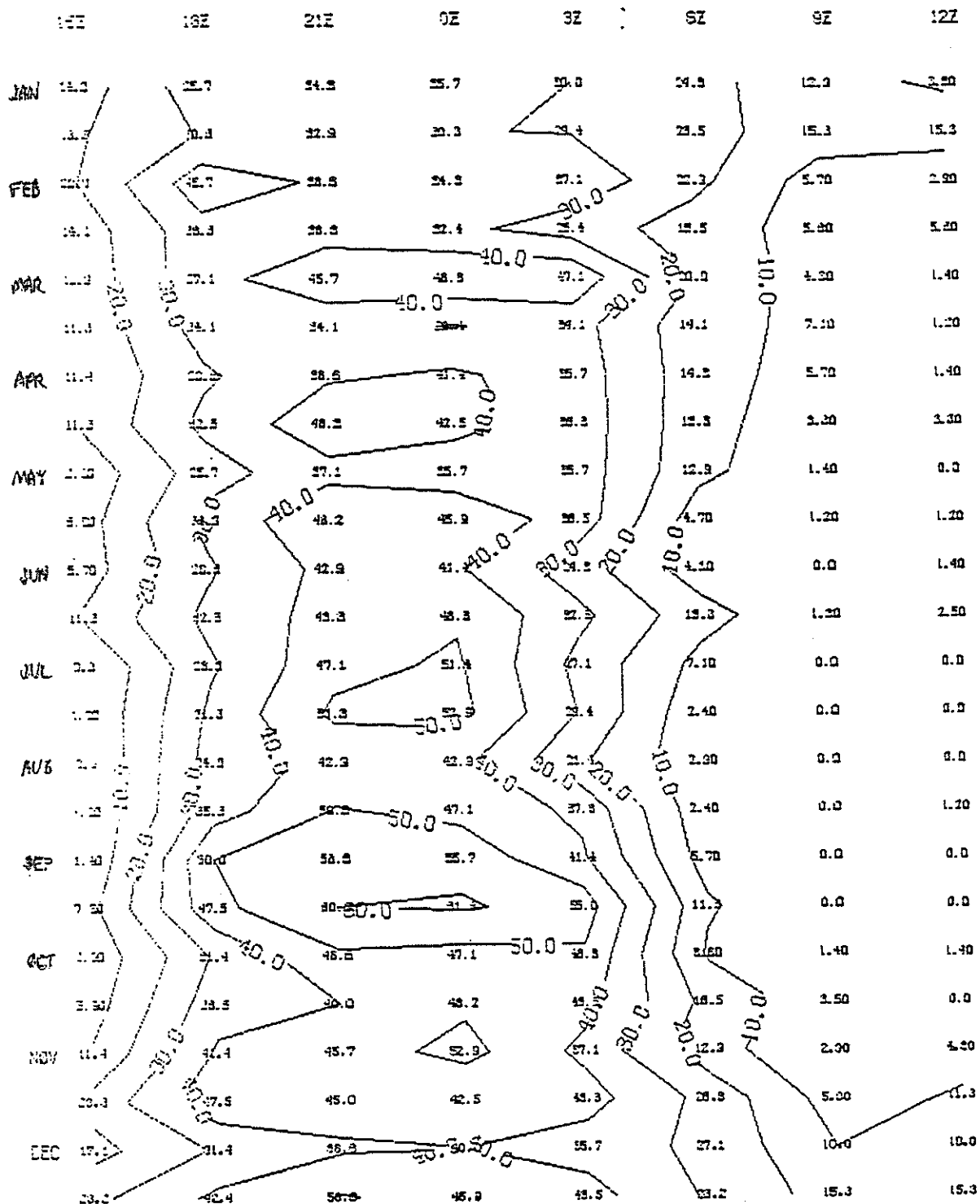


Fig. 10b

# FREQUENCY OF THREE HOUR CALM (SQUA/KITHERA)

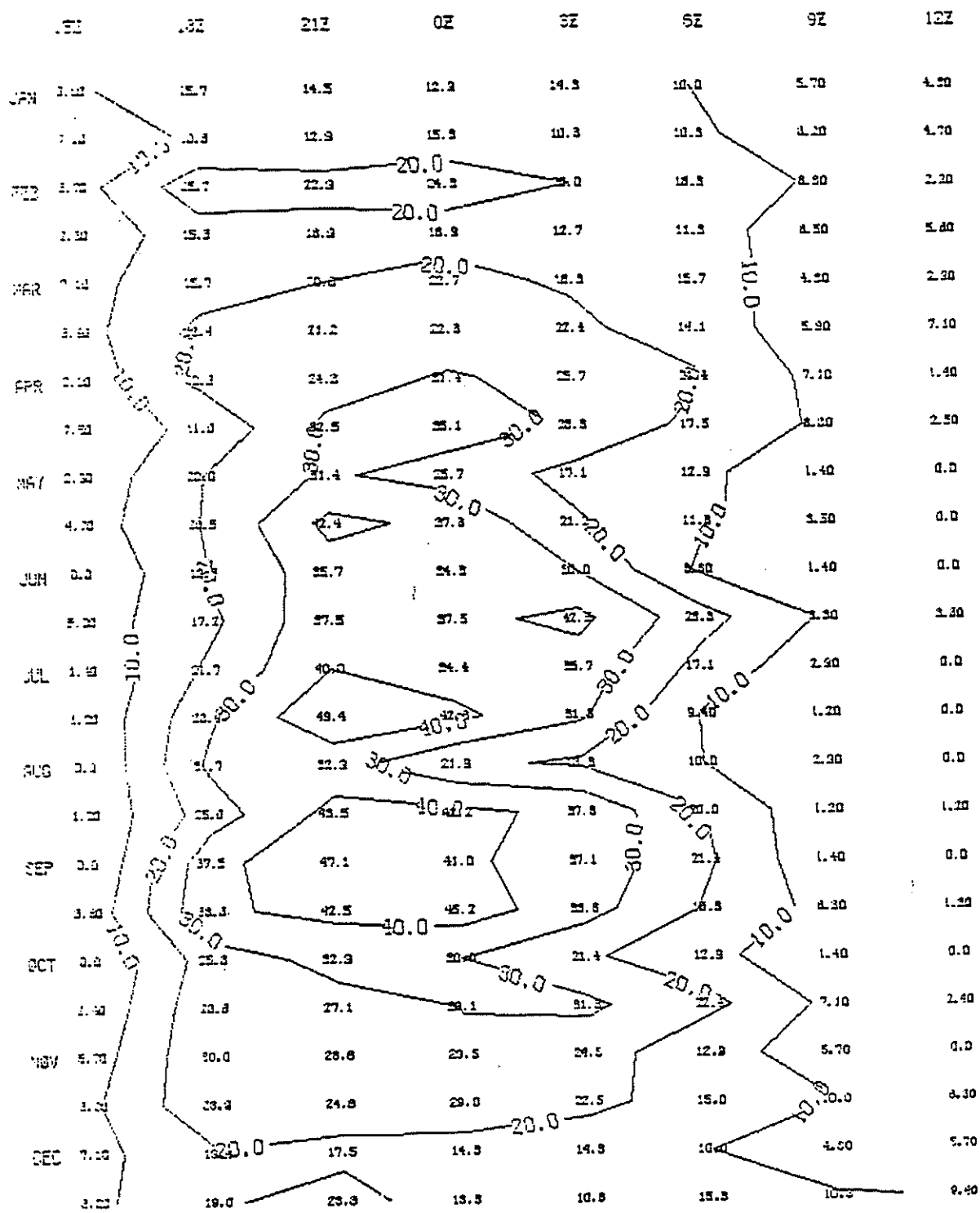


Fig. 10c

# KITHIRA FREQUENCY OF SIX HOUR CALM

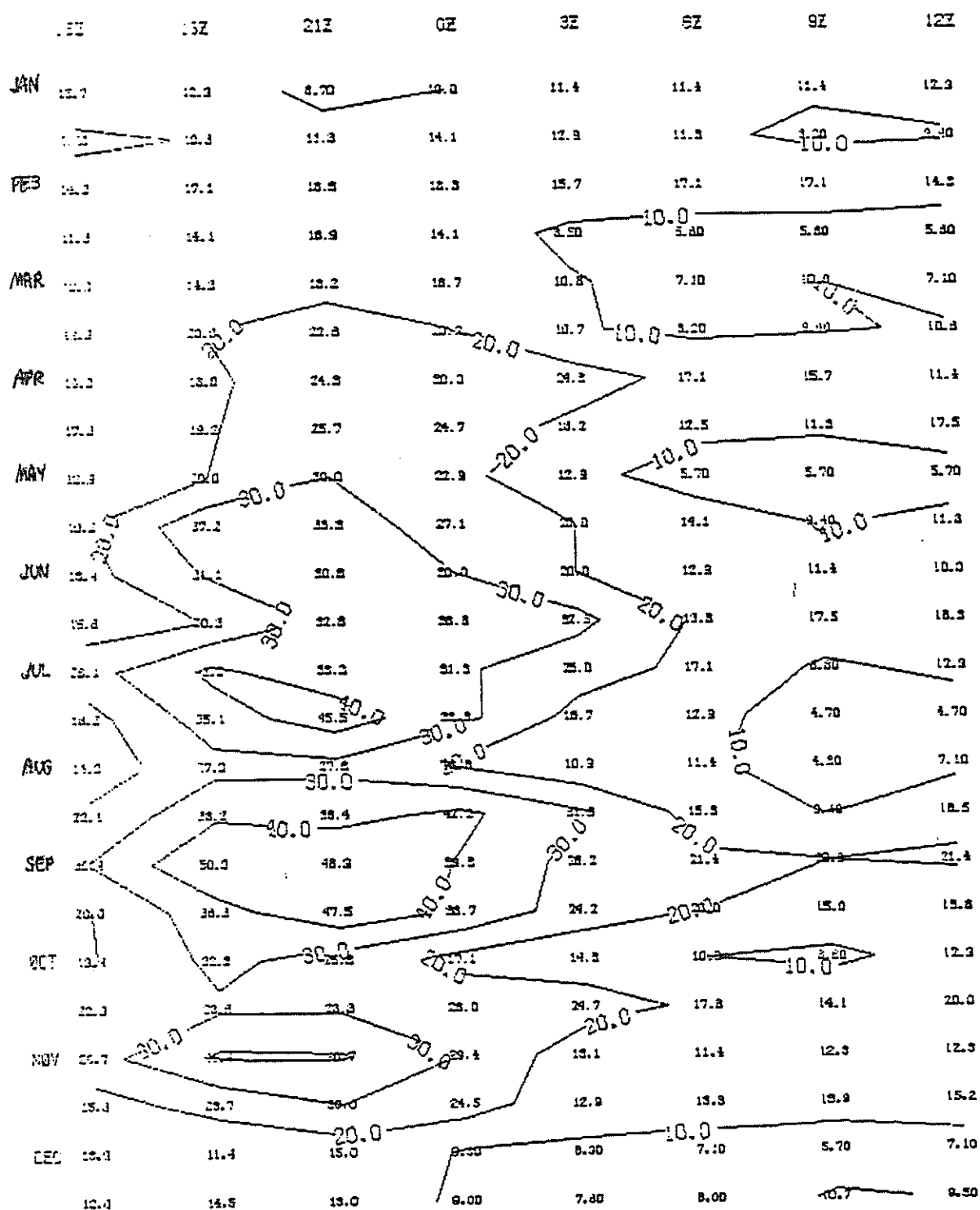


Fig. 11 Frequency plot of the occurrence of a six hour calm period (0 knots of wind reported for the initial and final hours, less than five knots reported in the intervening period). a) Kithira; b) Souda; c) Souda then Kithira.

# SOUDA: FREQUENCY OF SIX HOUR CALM

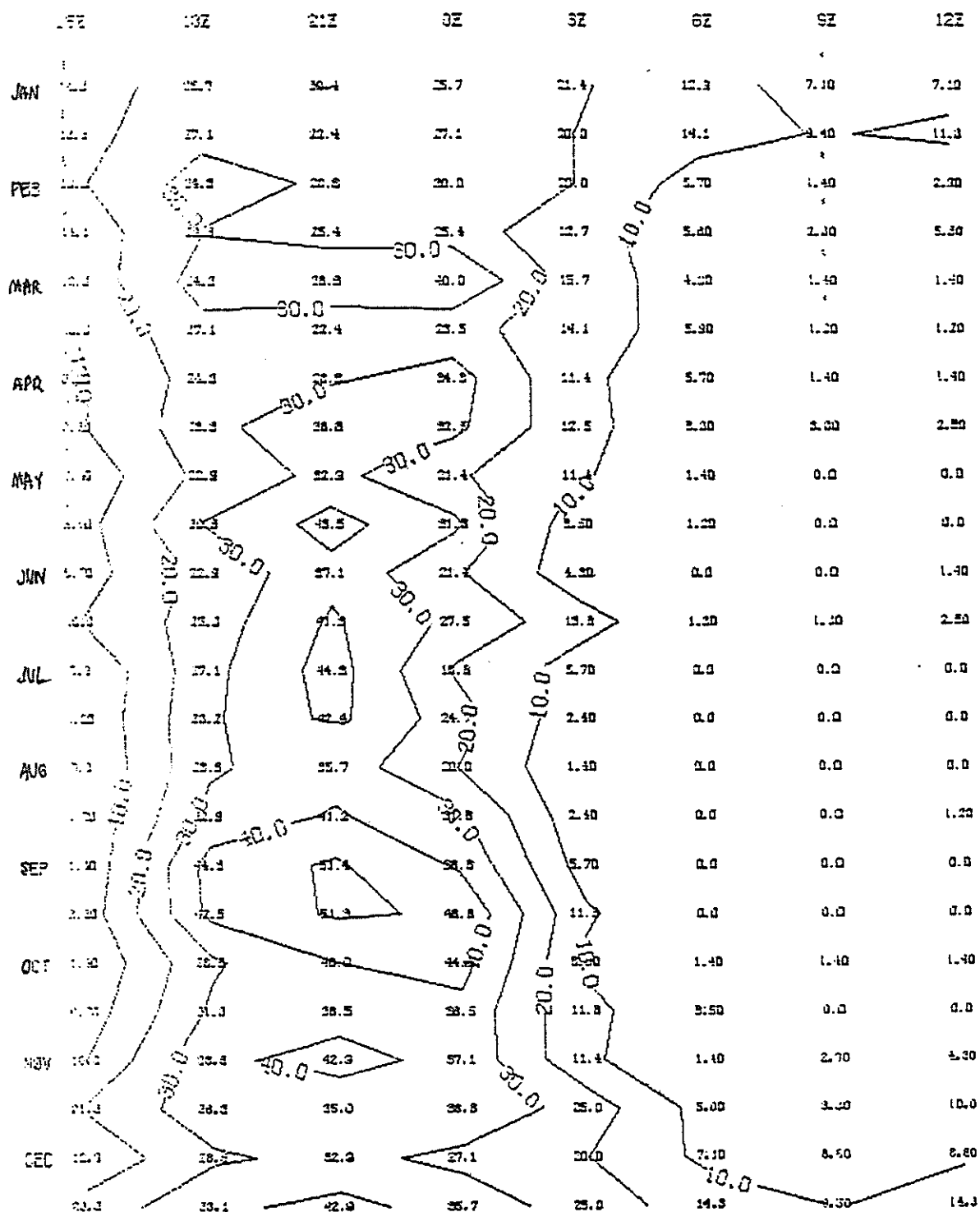


Fig. 11b

# FREQUENCY OF SIX HOUR CALM (SEUDA/KITHIRA)

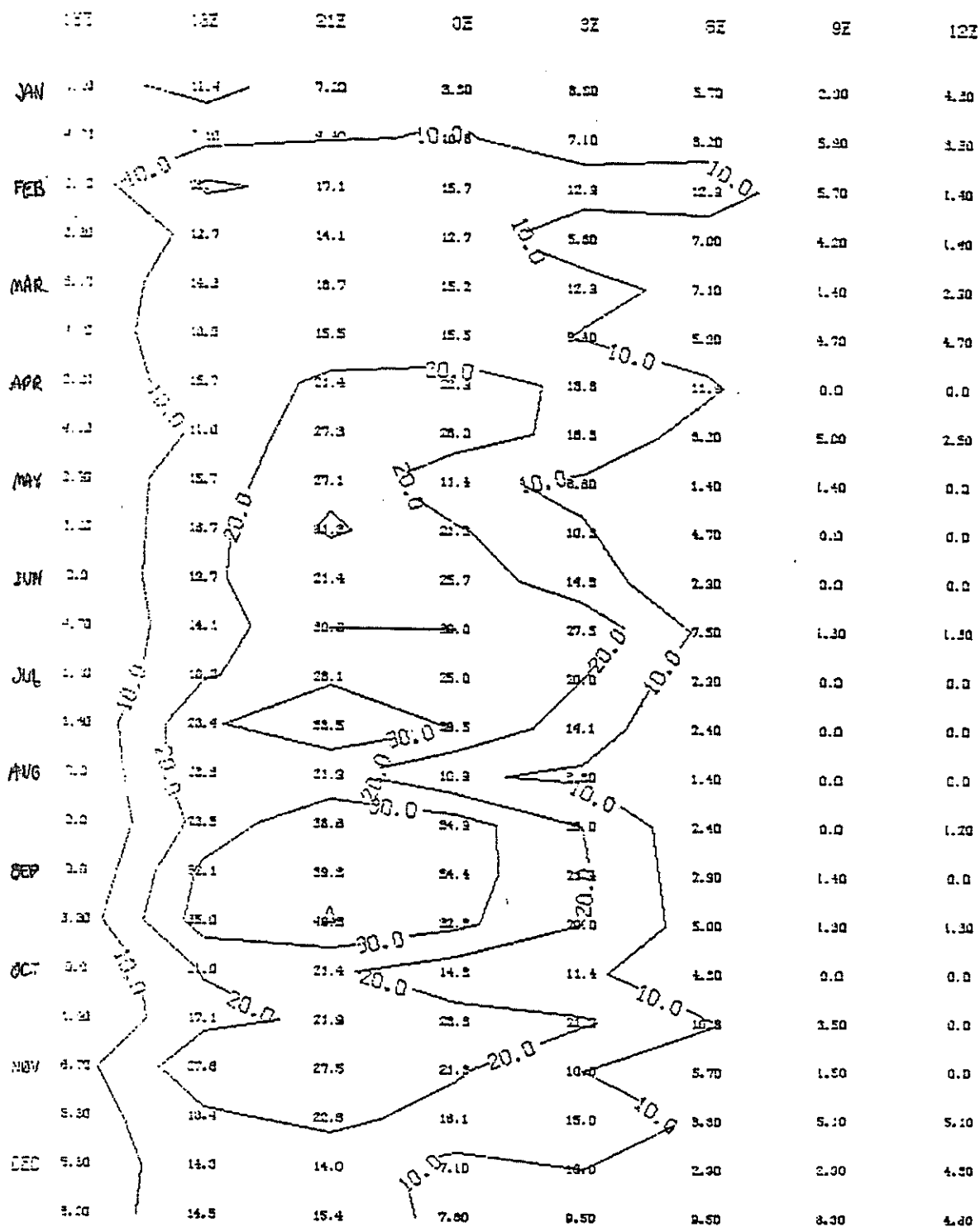


Fig. 11c

3HR MAXWIND = 1

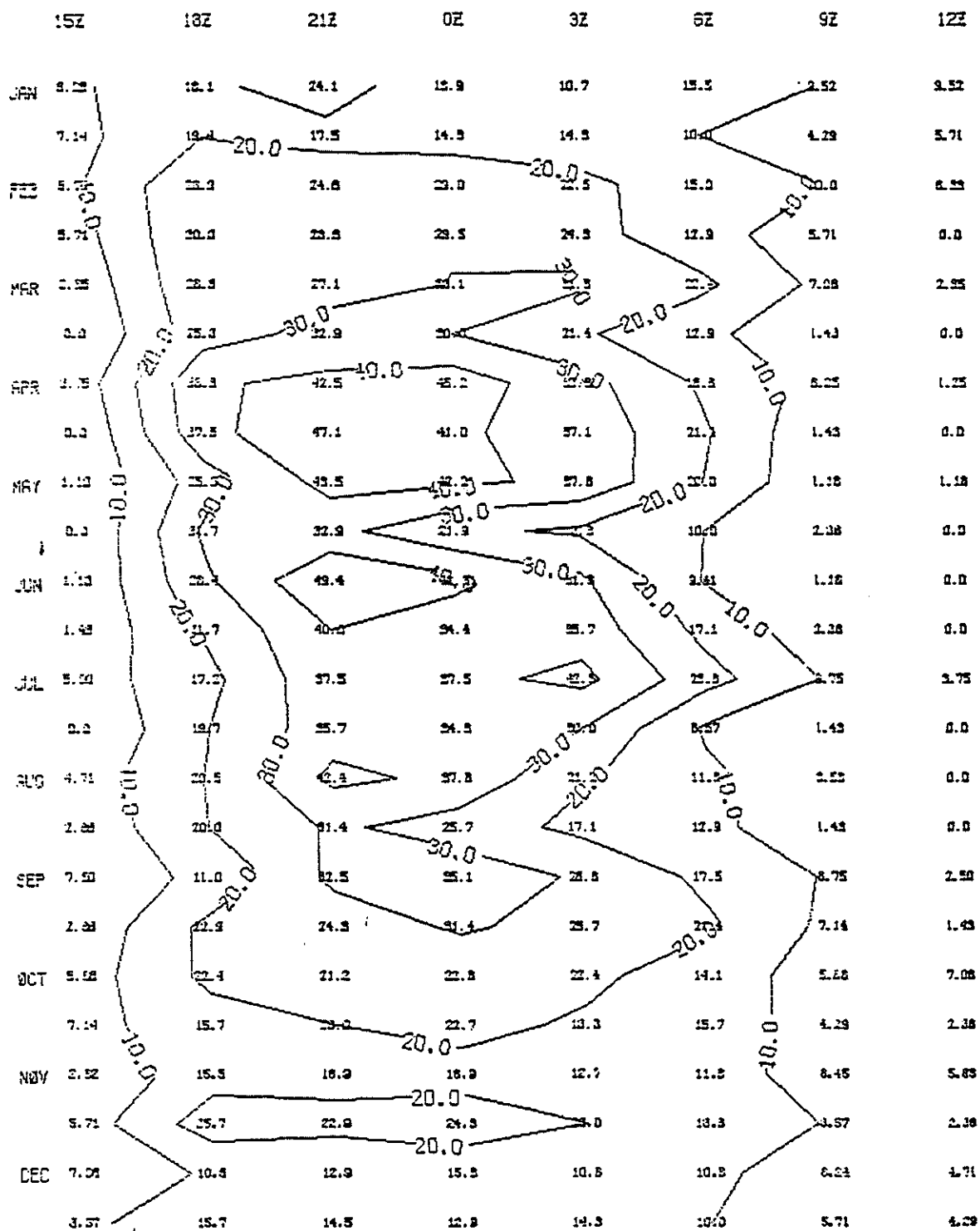


Fig. 12 Contoured frequency plot for the satisfaction of wind and temperature criteria over a three hour period. See text. a) calm; b) calm,  $5 < \text{Temp} < 20^{\circ}\text{C}$ ,  $\text{RH} < 95\%$ ; c) calm,  $8 < \text{Temp} < 18^{\circ}\text{C}$ ,  $\text{RH} < 90\%$ ; d) calm,  $8 < \text{Temp} < 25^{\circ}\text{C}$ ,  $\text{RH} < 95\%$ .

3 HR MAXWIND = 1 MAXT = 20 MINT = 5 MAXHUM = 95

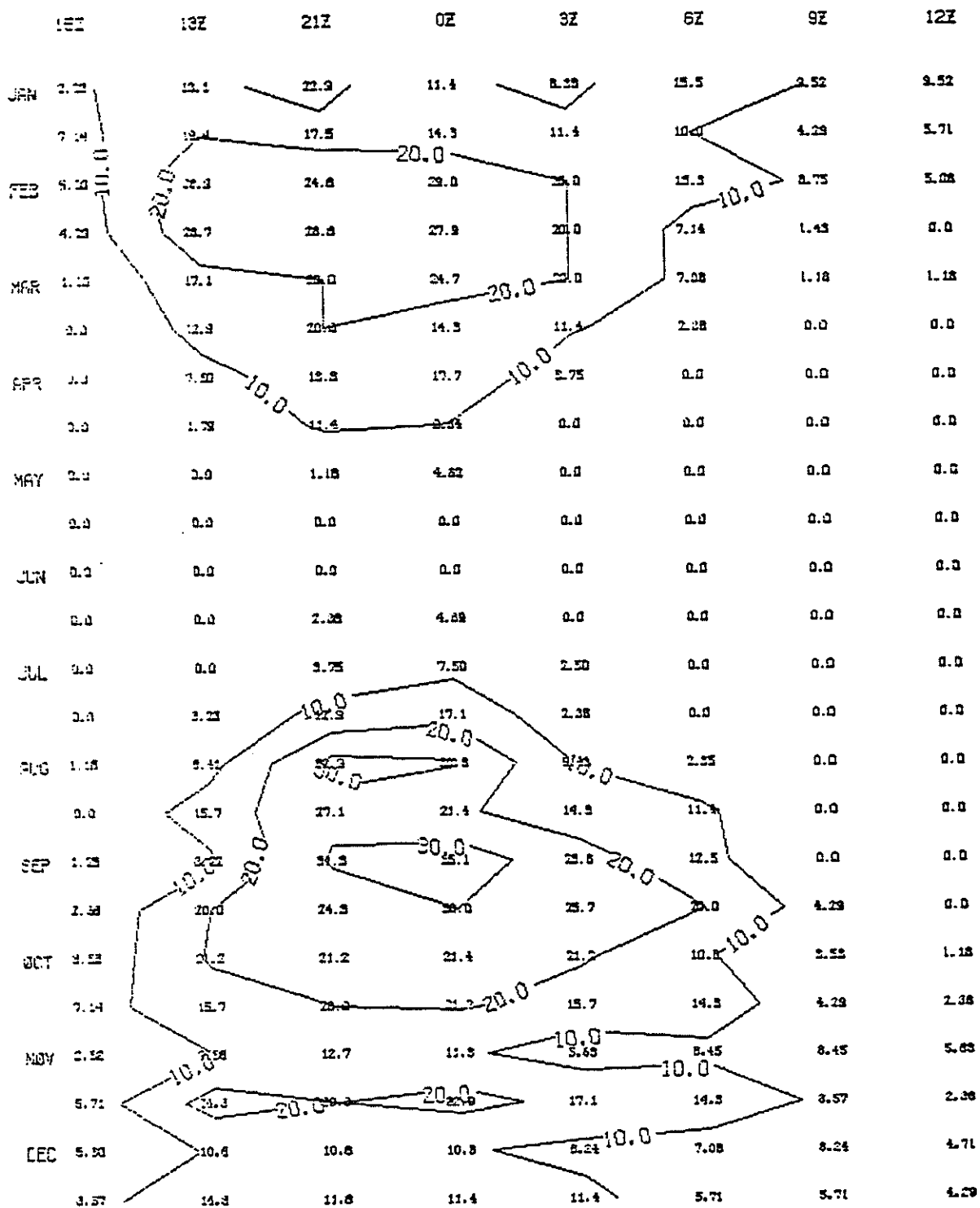


Fig. 12b



3 HR MAXWIND = 1 MAXT = 18 MINT = 8 MAXHUM = 90

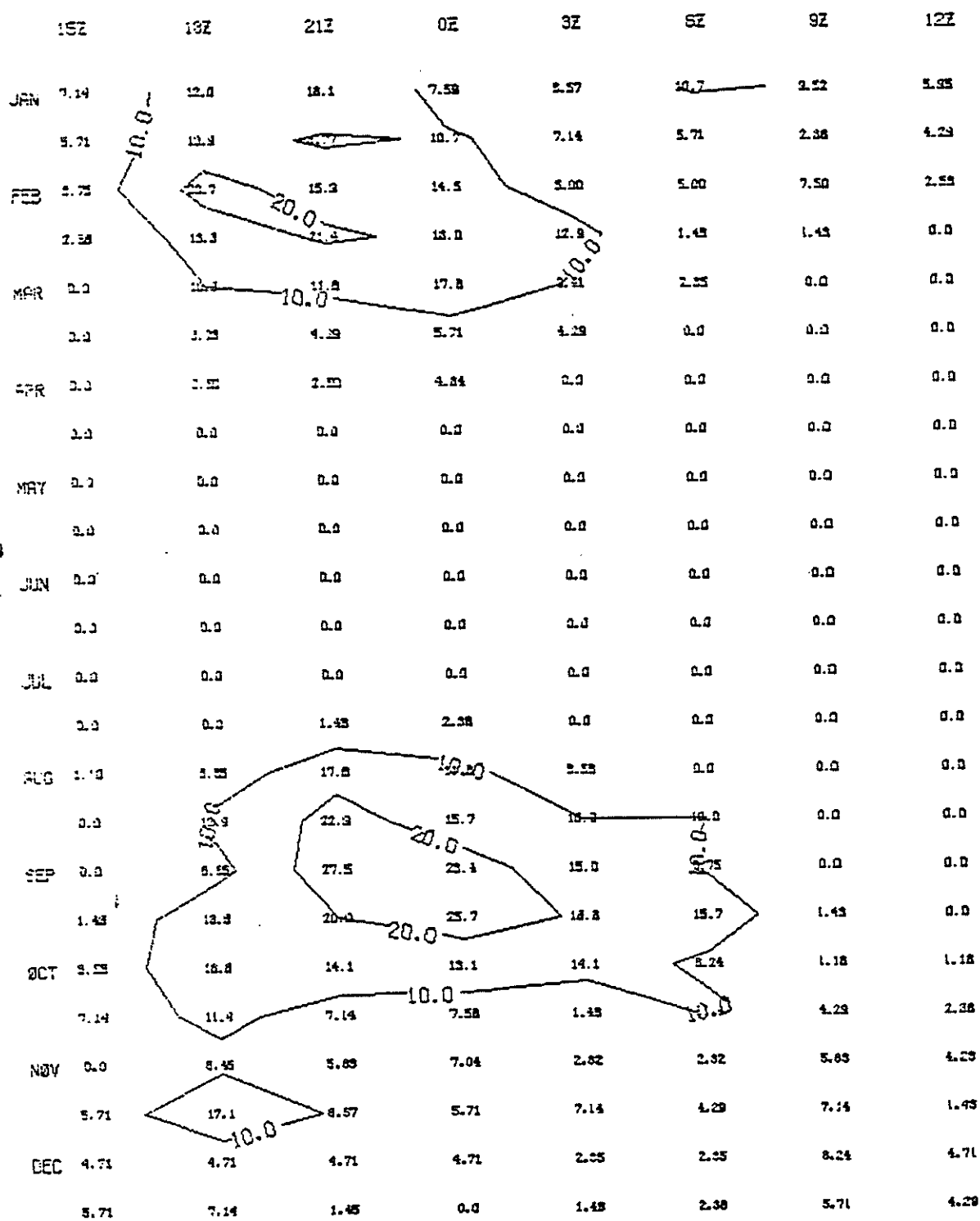


Fig. 12c

3HR MAXWIND = 1 MAXT = 25 MINT = 8 MAXHUM = 95

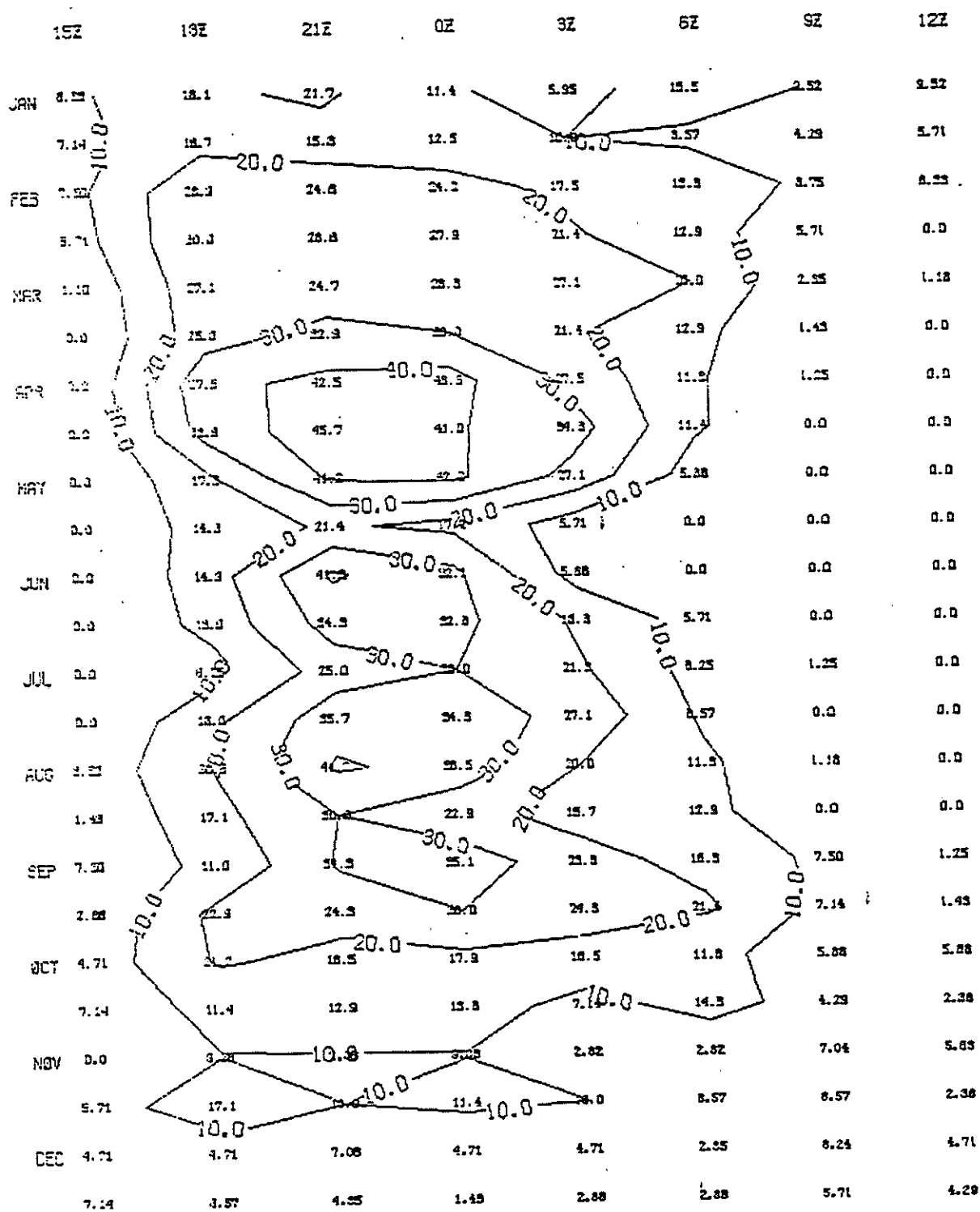


Fig. 12d

MAXWIND = 1

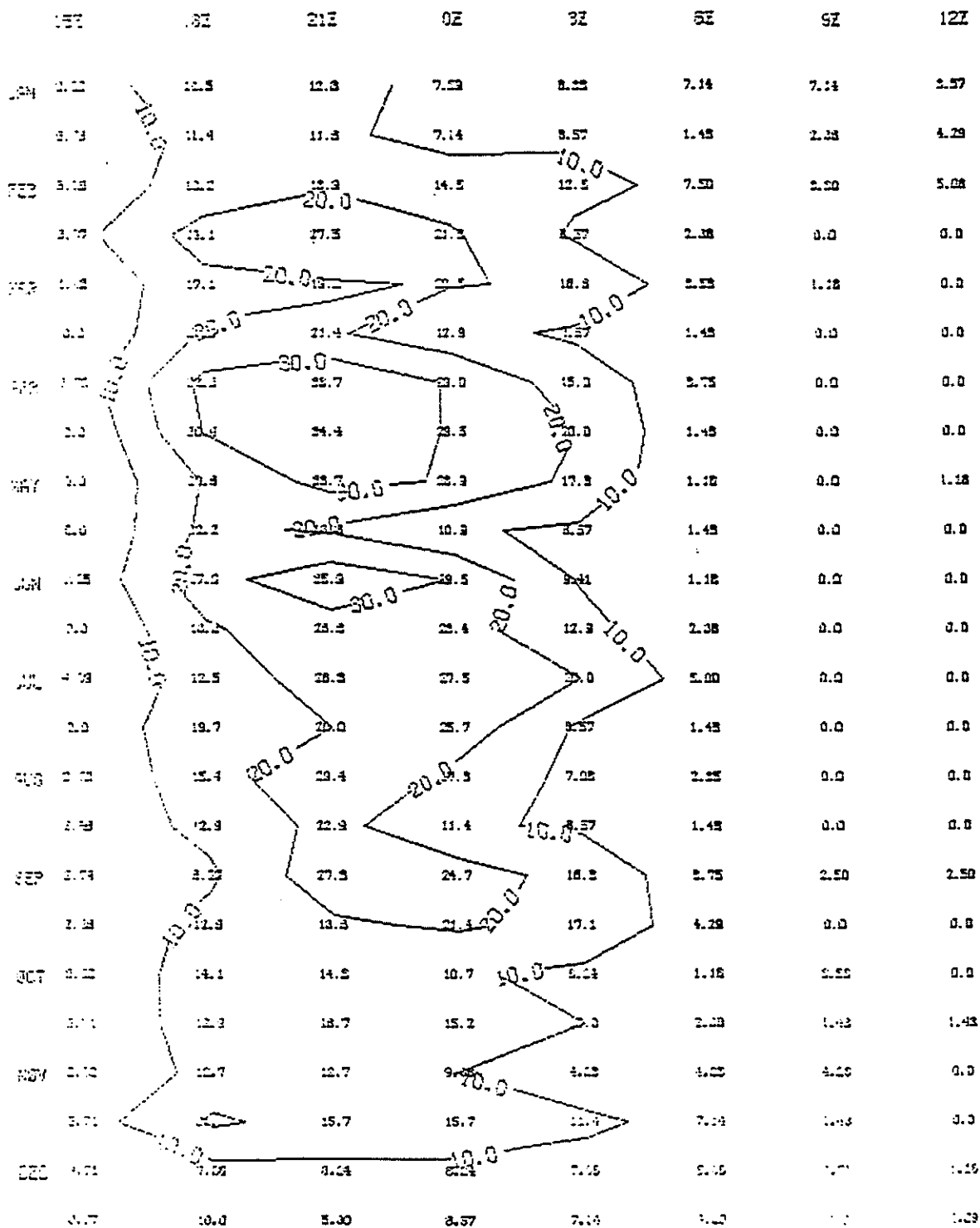


Fig. 13 As in figure 12, for six hour period

MAXWIND = 1 MAXT = 20 MINT = 5 MAXHUM = 95

65 F

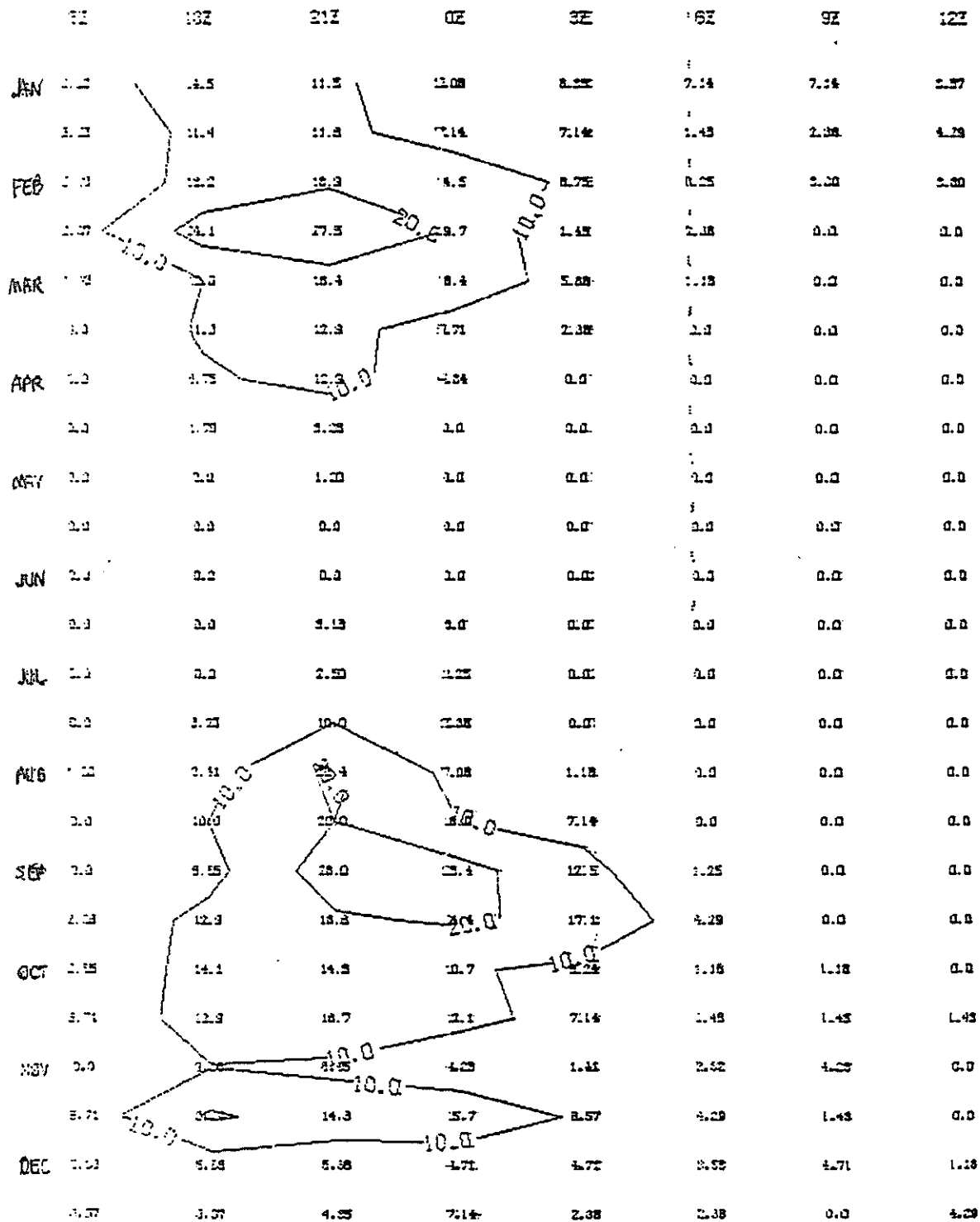


Fig. 13b

MAXWIND = 1 MAXT = 18 MINT = 8 MAXHUM = 90

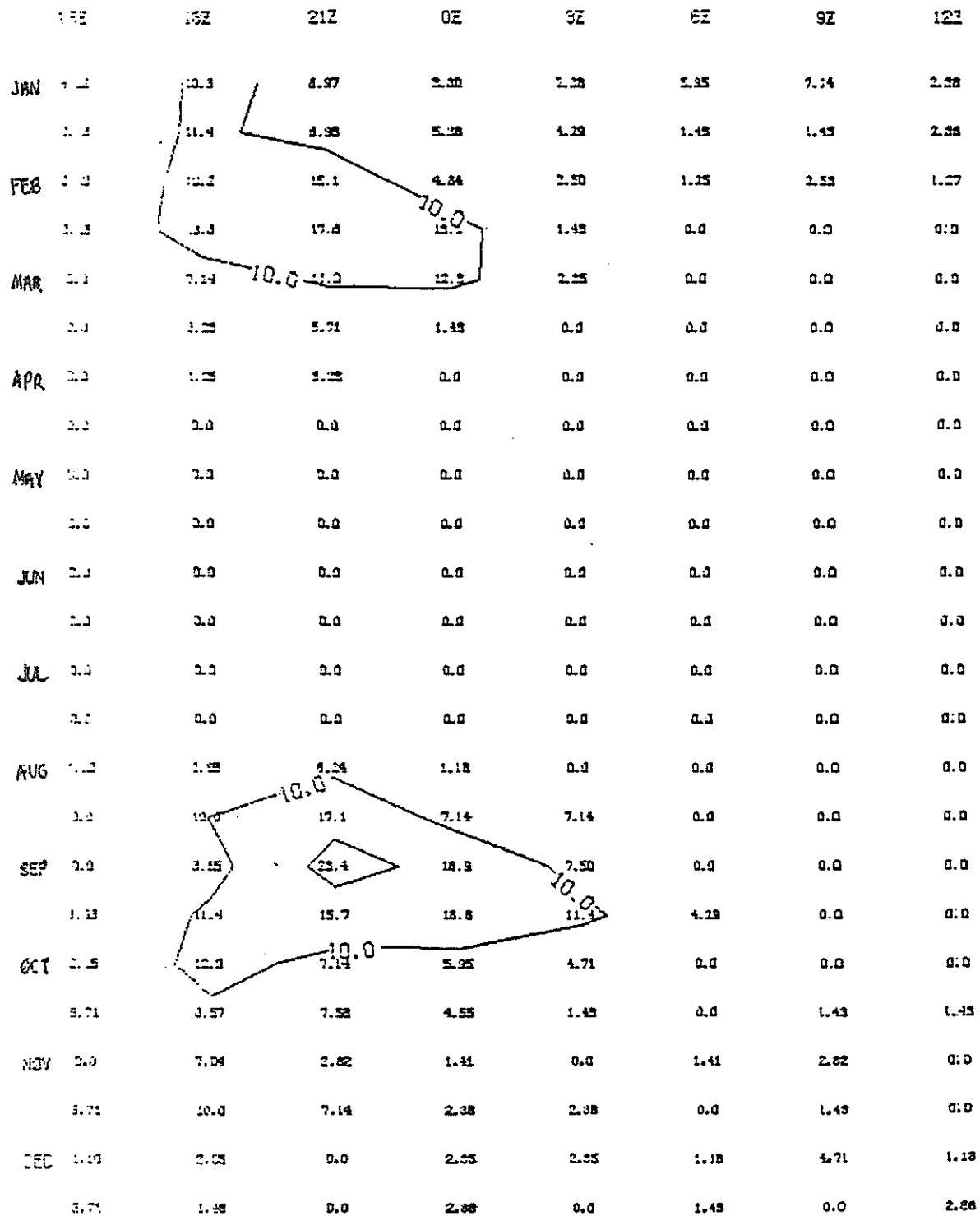


Fig. 13c

MAXWIND = 1 MAXT = 25 MINT = 8 MAXHUM = 95

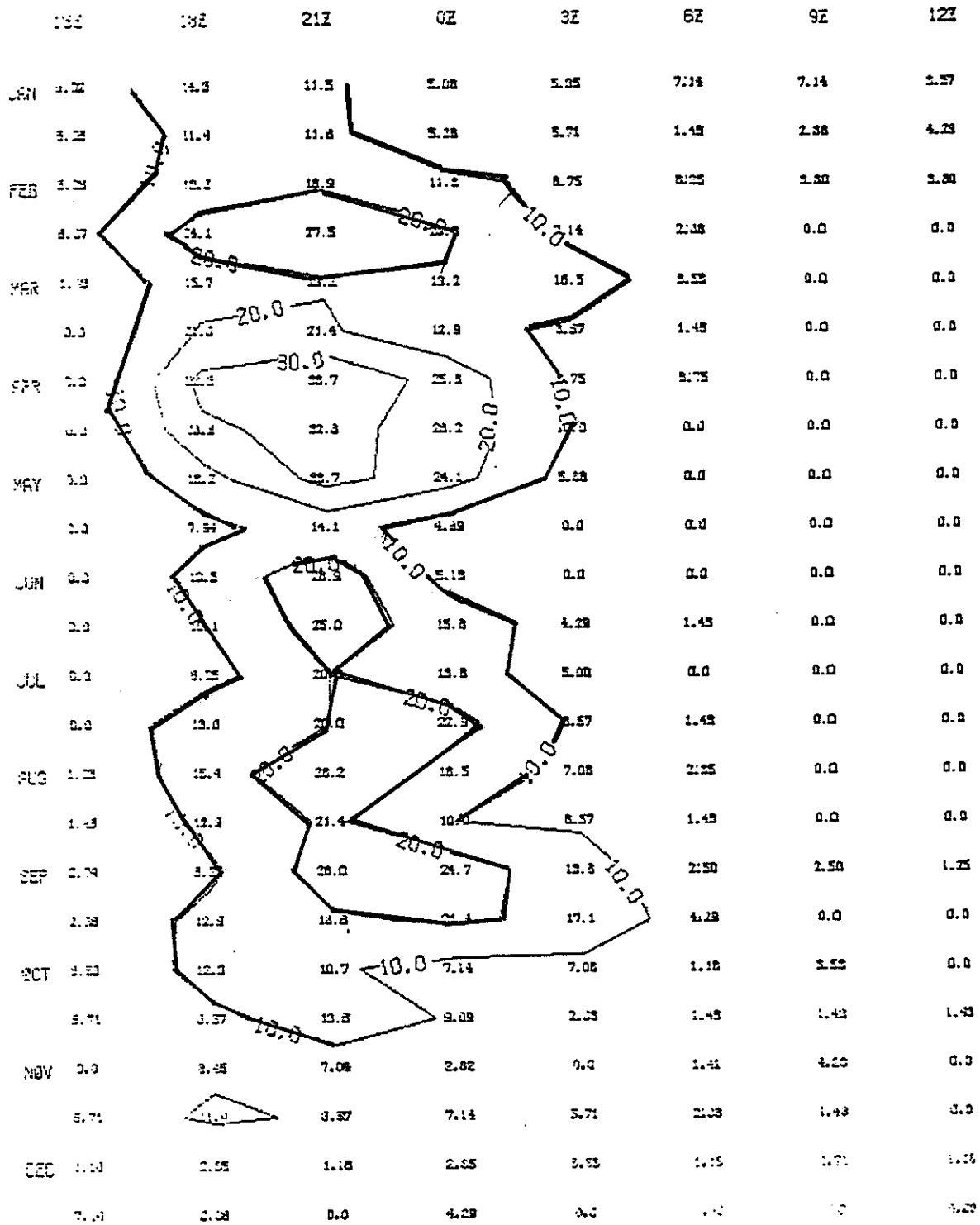


Fig. 13d

MAXWIND = 1

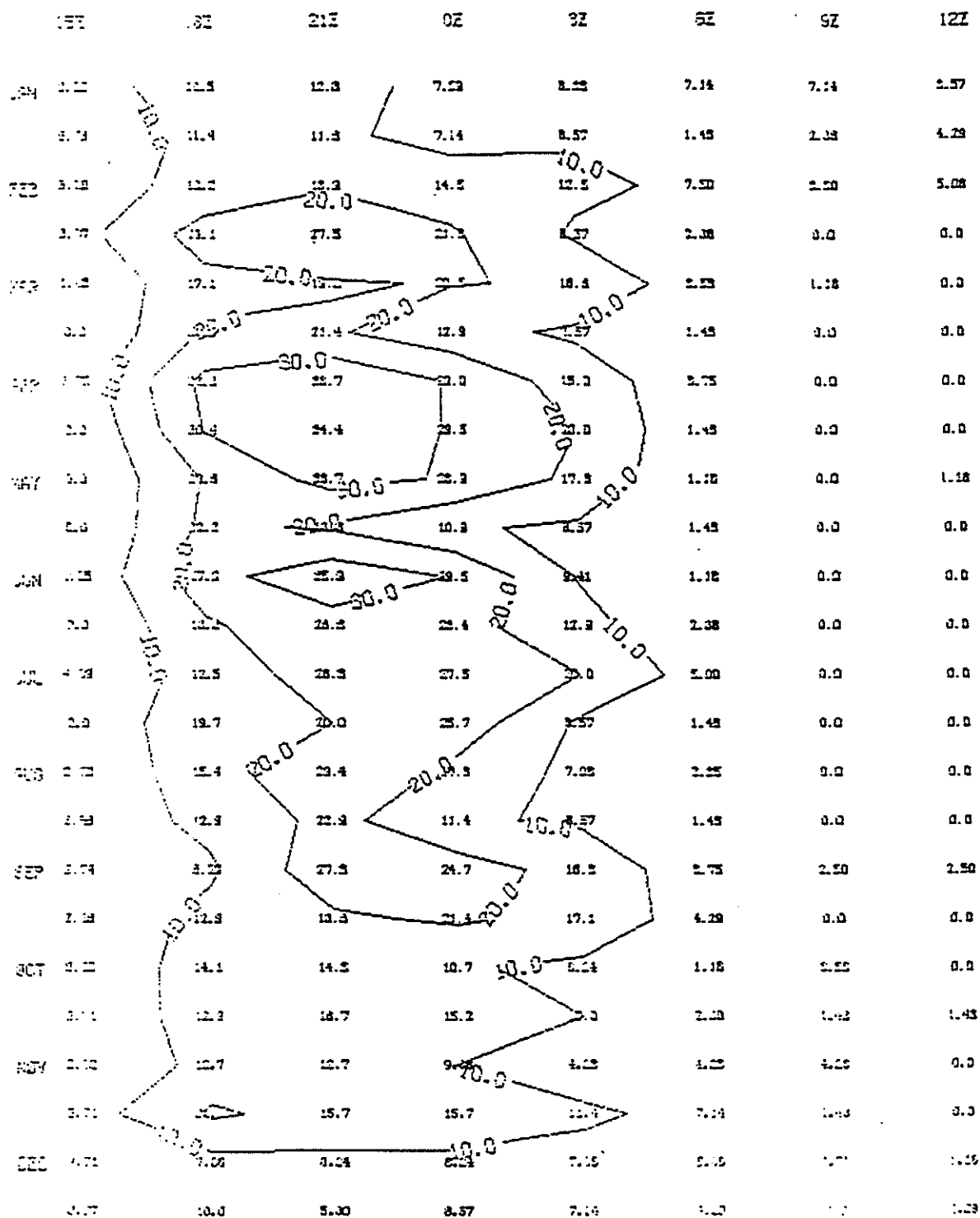


Fig. 13 As in figure 12, for six hour period

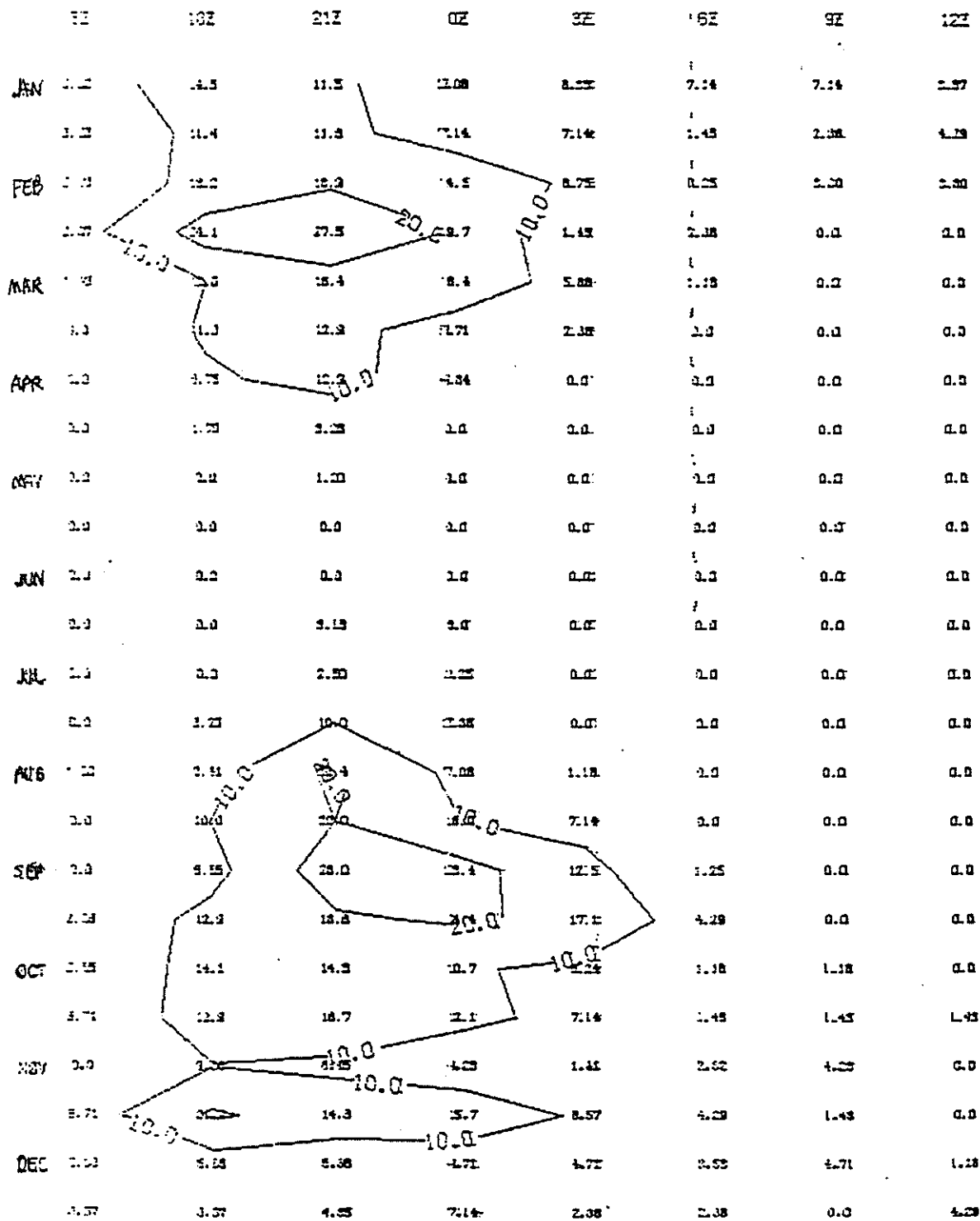


Fig. 13b



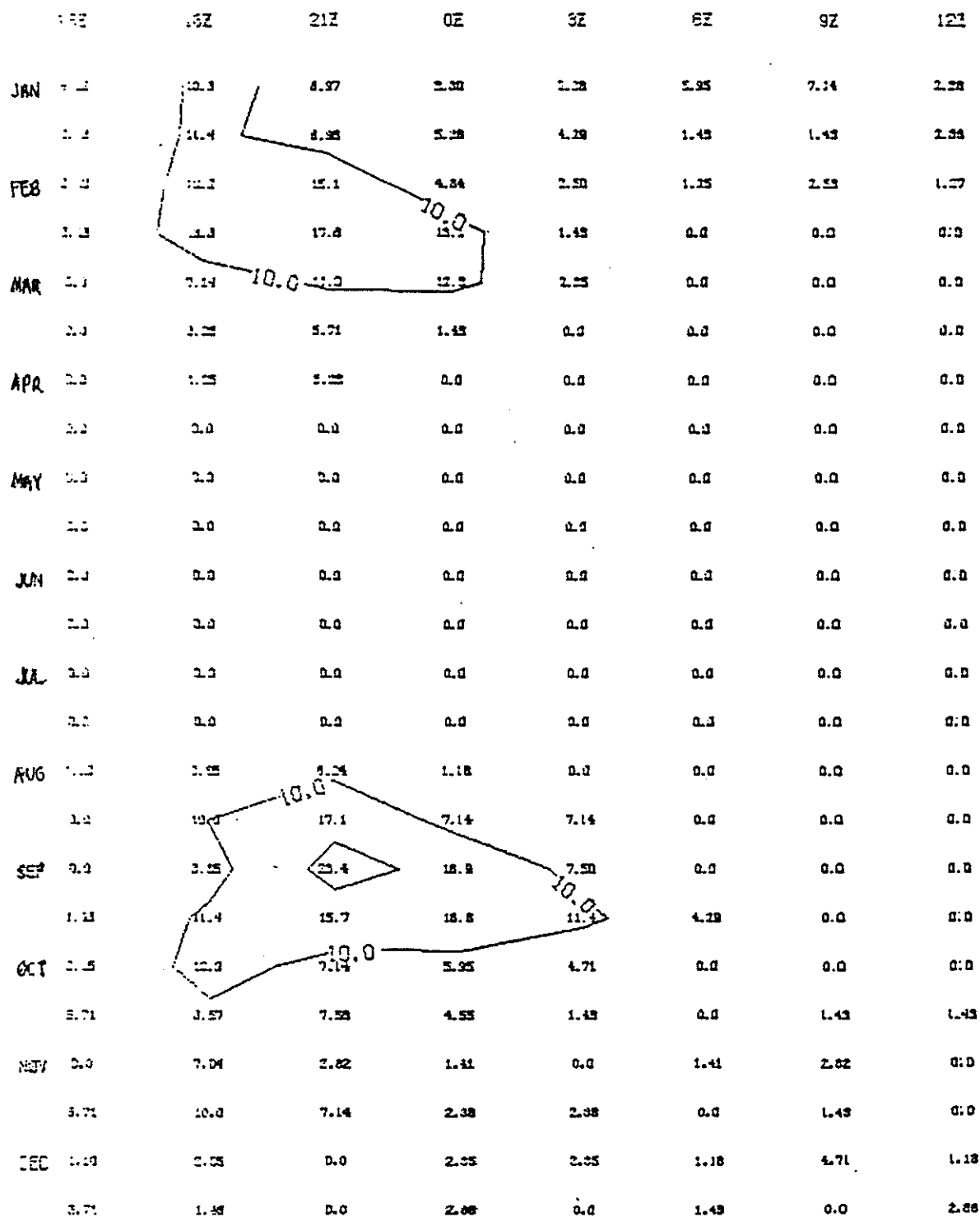


Fig. 13c

MAXWIND = 1 MAXT = 25 MINT = 8 MAXHUM = 95

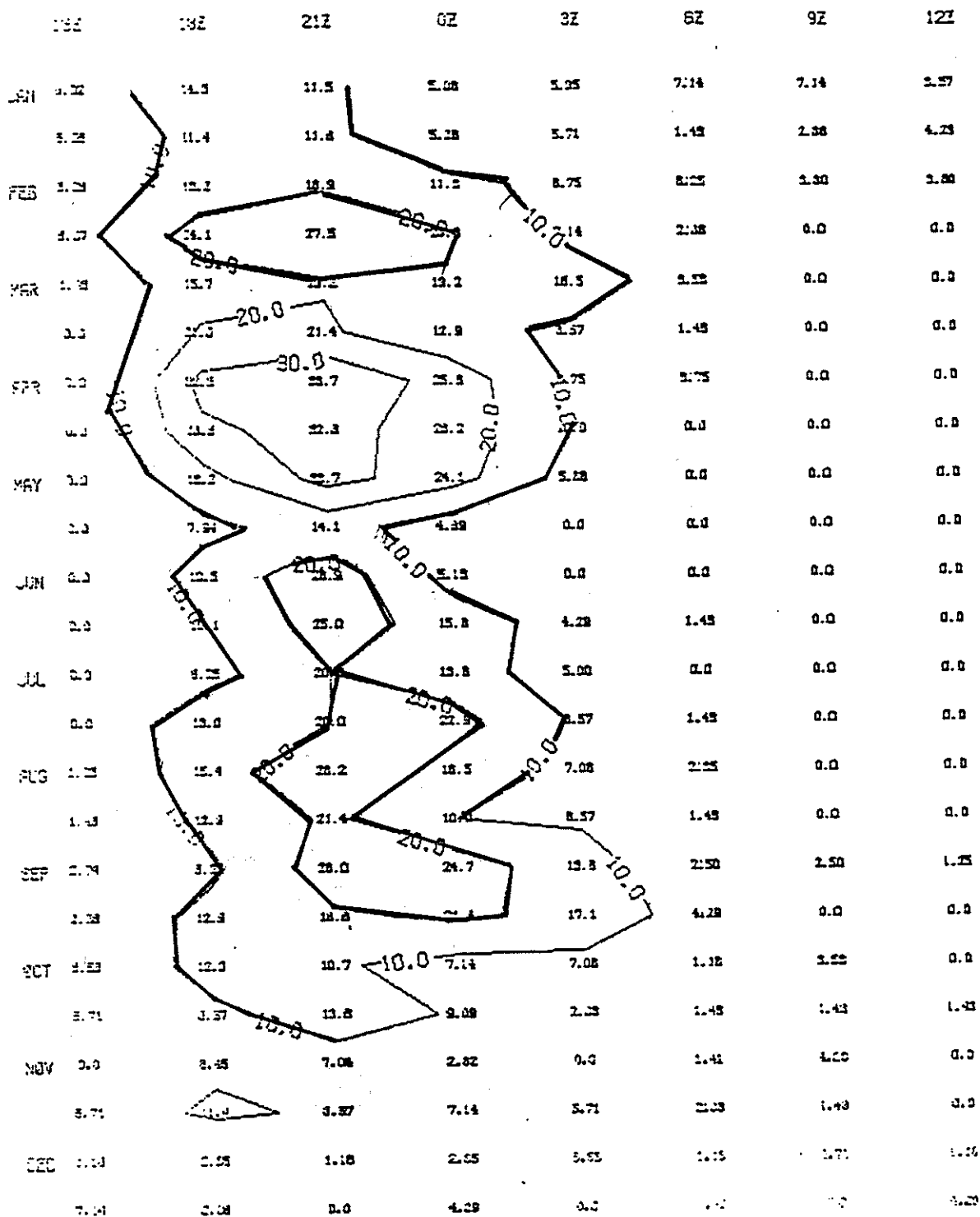


Fig. 13d

18 February 1986

MIT 54-1711

Dear John:

I am not sure whether you have completed the write-up on the meteorology for the Daedalus report, but Steve Bussolari asked me to send along these analyses.


These contour plots represent the probability of occurrence of extended calm periods, given the observation of calm conditions at a particular time and place. In essence, these are conditional probabilities, and the frequencies may be viewed as a measure of the success of forecasting a calm period extending over the next several hours, based on the observation of calm at the time indicated.

The series of five plots refer to separate analyses for the years 1979-1982, where the probabilities indicated are those for the occurrence of a three hour calm period (or longer) at Kithira, given the observation of calm at the hour indicated. There is considerable interannual variability, but the gross features are consistent from year to year. Maxima occur, in all years, in the spring (March-April); and in the Fall (approximately in September); the peak which occurs in the summer months is of course of no use to us, because of the temperature constraint. These plots are reassuring in that they are well correlated with the non-conditional plots presented in the report. The spring and fall window periods contain predictably calm periods suitable for the flight.

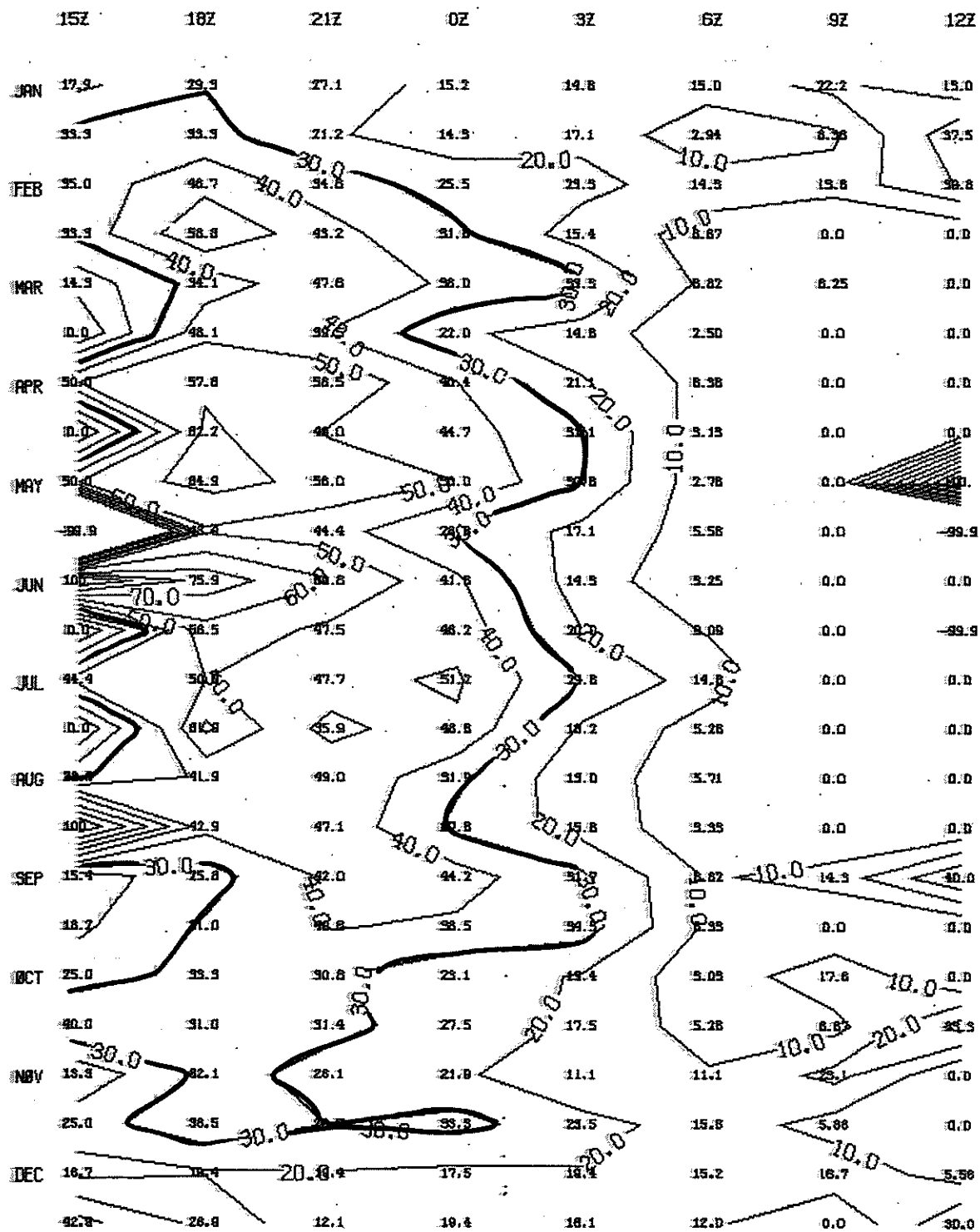
The single plot is based on a composite of all five years, and answers the following question: 'what is the probability that, given that the wind is calm at Souda at a given hour, it will be calm at Kithira six hours later (and during the intervening period)?' Again, early April and early September are characterized by extended periods of calm weather.

All things considered, the period from early March to mid-April still seems to be the most propitious. Beyond that however, there is no way of accurately forecasting when the one or two-week period of ideal weather will arrive. The month of September also looks pretty good still.

The next thing is to wait for the data from the remote stations. In the mean time I am following the day to day weather in the region on the synoptic maps in order to get a feel for the way the systems move in the Mediterranean. Let me know if you have any further questions.

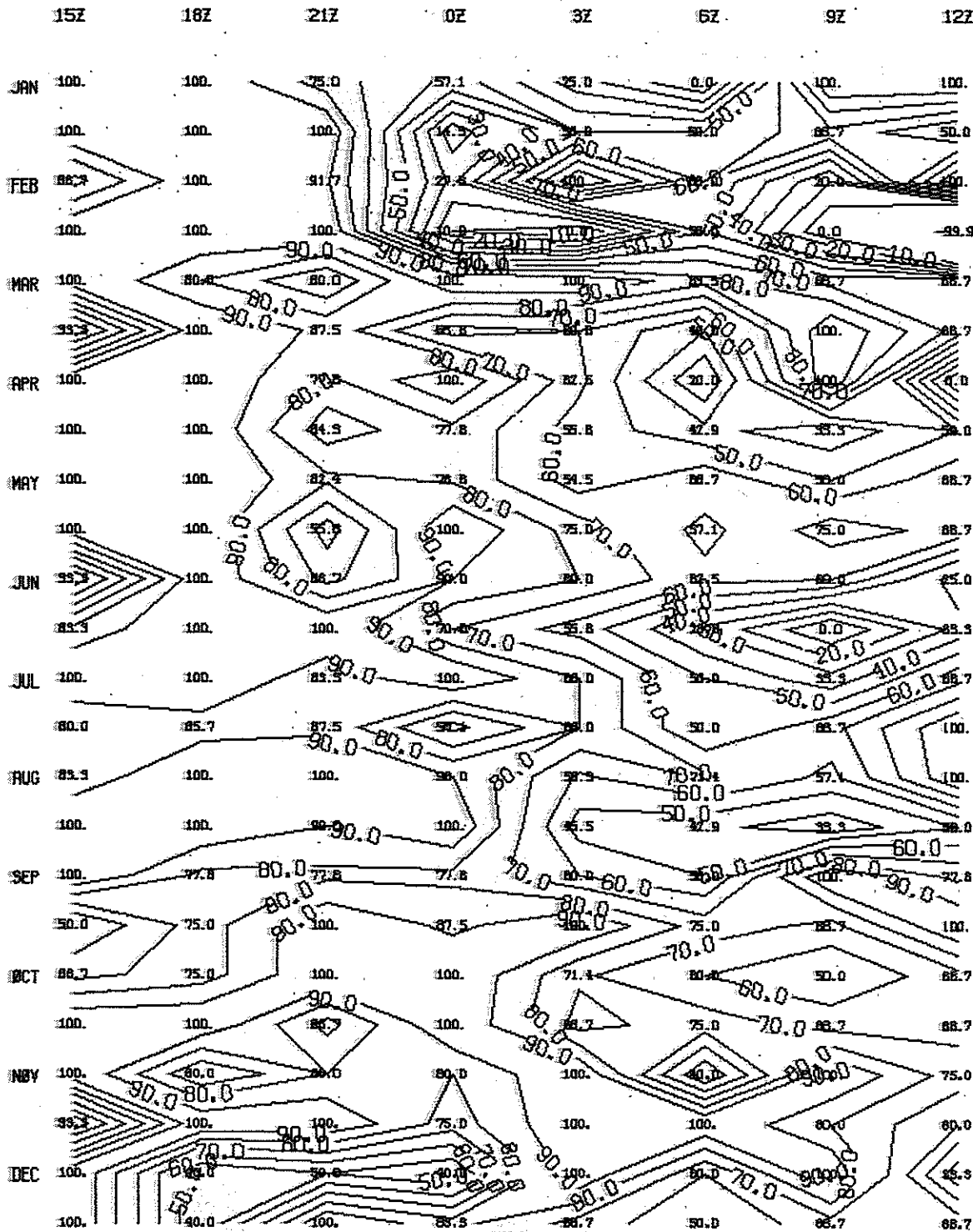
  
Jonathan Wyss

# PERSISTENCE FORECAST (6HRS/500DA)



1/2 MAR  
NOV

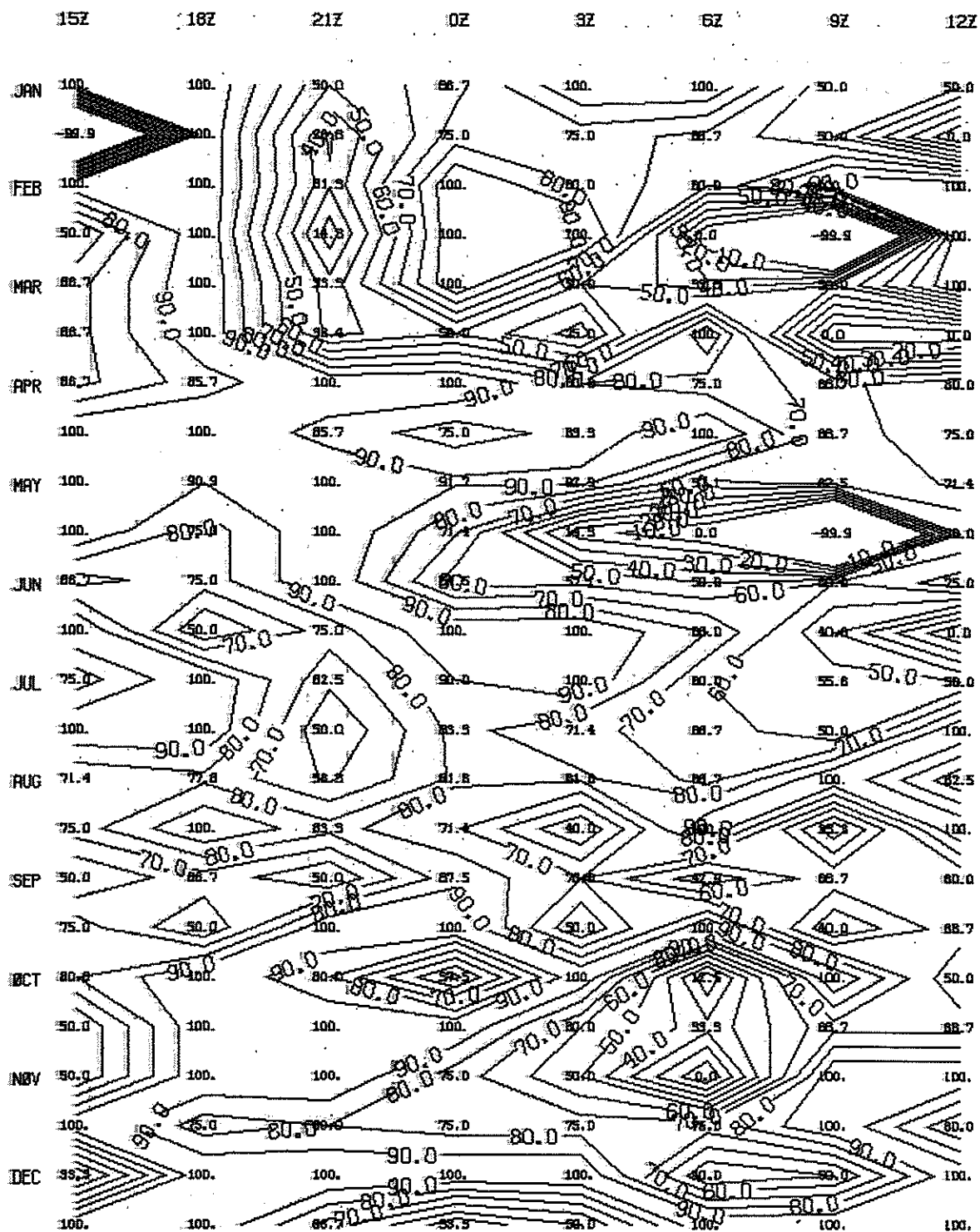
3 1983



$\frac{1}{2}$  OCT

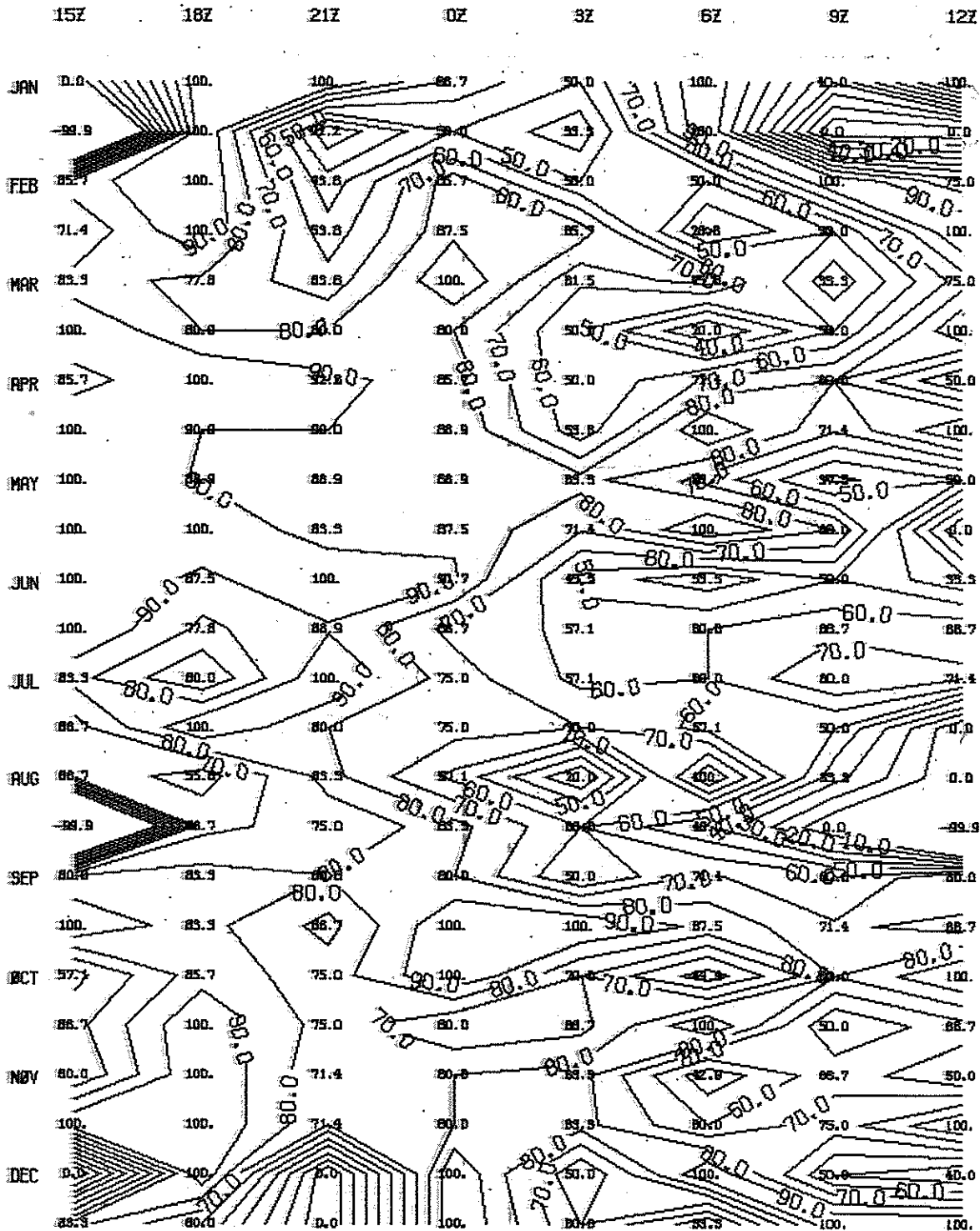
3

1982



$\frac{1}{2}$  MAY  
SEP-OCT

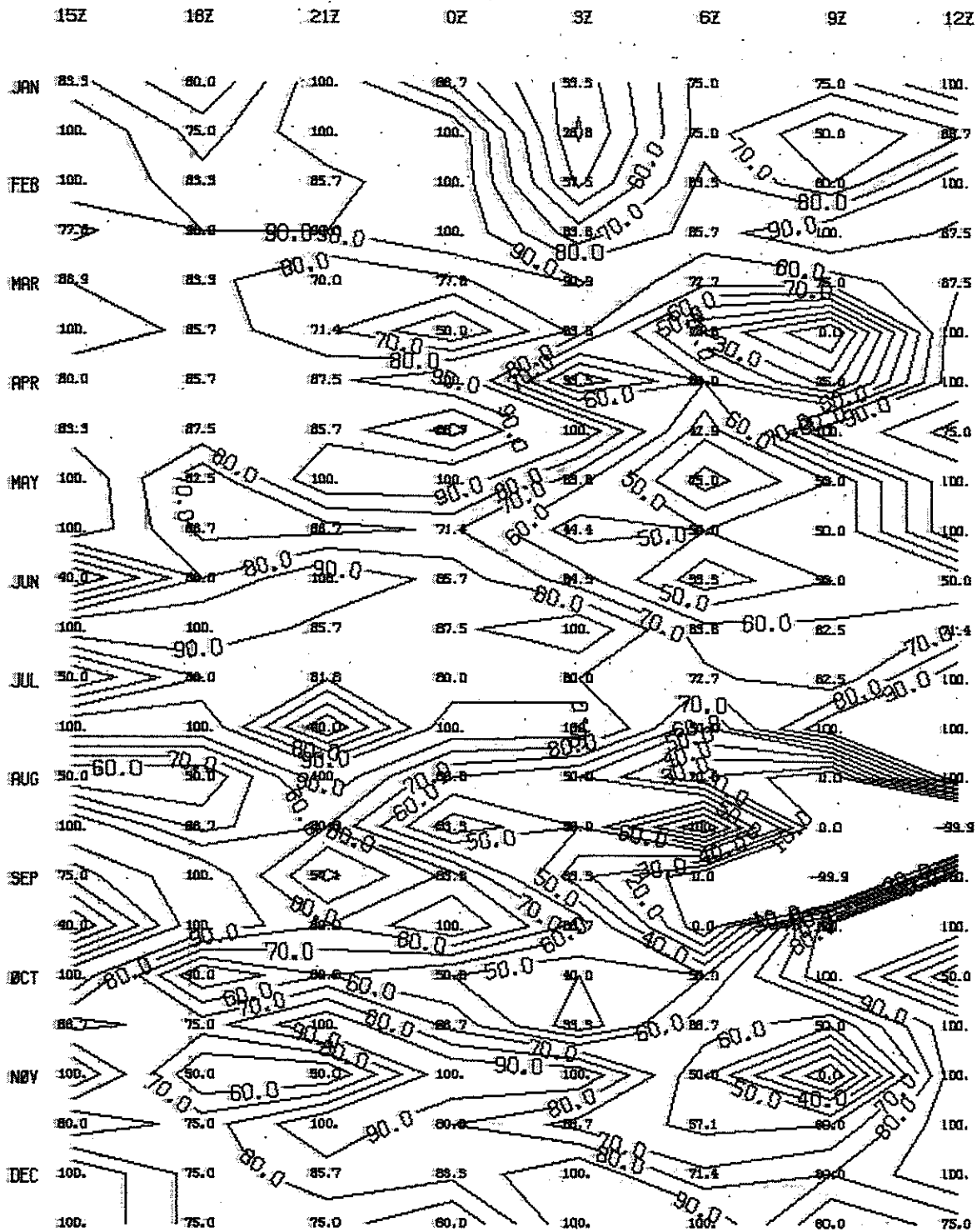
3 1981



1/2 MAR

3

1980





2 MAR

3

1979

